OUKA
The University of Osaka
Institutional Knowledge Archive

Title	NMR study of biomolecular localization in cells by the paramagnetic relaxation
Author(s)	Sakol, Nat
Citation	大阪大学, 2019, 博士論文
Version Type	VoR
URL	https://doi.org/10.18910/72662
rights	
Note	

The University of Osaka Institutional Knowledge Archive : OUKA

https://ir.library.osaka-u.ac.jp/

The University of Osaka

Doctoral Thesis

NMR study of localization of biomolecules in cells by paramagnetic relaxation

Author:
Nat Sakol

Supervisor:
Prof. Dr. Toshimichi Fujiwara

A thesis submitted in fulfilment of the requirements for the doctoral degree in Chemistry

of

Special Integrated Science Course
Graduate School of Science

Osaka University

March 2019

Declaration of Authorship

I, Nat Sakol, declare that this thesis titled ‘NMR study of localization of biomolecules in cells by paramagnetic relaxation’ is my own. I confirm that where I have quoted from the work of others, the citation is always clarified.

Nat Sakol

February 4th, 2019

Abstract

NMR study of localization of biomolecules in cells by paramagnetic relaxation

Nat SAKOL

Laboratory of Molecular Biophysics,
Institute for Protein Research, Osaka University
3-2 Yamadaoka, Suita, Osaka, 565-0871, Japan

Introduction: The information of the locations of macromolecules inside the cell is crucial for understanding the function of macromolecules and biological processes inside the cell. This research introduces a new developed in-cell solid-state NMR technique for investigating this important issue in vivo environment of *Escherichia coli* cells by employing paramagnetism of gadolinium complexes to enhance magnetic relaxation rate of cellular proton. The spin diffusion of protons spreads out the effect of gadolinium ion and generates the locational dependence of relaxation rate. The appropriate gadolinium agent and concentration were studied. The locations of macromolecules were interpreted from the relaxation rates of macromolecules.

Materials and methods: The distributions and toxicities of aqua gadolinium and Gd-DOTA complexes were studied by monitoring the water ^{1}H relaxation rate in non-labelled *E.coli* cell solution containing these paramagnetic agents.

To study the location dependence of relaxation rate by solid-state NMR, ^{13}C labeled cell sample was treated with the appropriate gadolinium agent and frozen. The relaxation ordered spectroscopy (ROSY) is the method for resolving the solid-state ^{13}C-NMR spectrum based on the ^{1}H relaxation rate. The relaxation rate of frozen cells was detected by ROSY pulse. The proton magnetization is saturated first and relaxes to the thermal equilibrium polarization along $\boldsymbol{B}_{o}$ during recovery time τ_{rec}. Cross polarization pulse then transfers the ^{1}H magnetization to the ^{13}C magnetization. Therefore, the ^{1}H relaxation process is monitored as a function of τ_{rec} via high-resolution ^{13}C NMR spectra of biomolecules under magic-angle spinning.

The signals were assigned by comparing the experimental one-dimensional ^{13}C NMR spectrum with the simulated cellular NMR spectrum and cross peaks of two-dimensional ^{13}C NMR spectrum. The locational dependence was analyzed by spin diffusion model.

Results and discussion: The proton buildup curves of *E. coli* solutions at 0°C could be analyzed with a double exponential relaxation equation. This shows that most of gadolinium complexes were distributed in extracellular part of the sample. The gadolinium solution at 150 mM was high enough to distinguish between the intracellular and extracellular relaxation rate and provided good reproducible experimental results. Aqua gadolinium complex was shown to have weak permeability to cell membrane and binding to cellular components with a dissociation constant K_d of 1.0 mM, leading to cytotoxicity. Despite of the similar cell permeability of Gd-DOTA complexes, this agent exhibited much weaker binding to cell components leading to viability of the cells over a long experimental time of days.

The buildup curve for overall proton signal of the cell sample treated with 150 mM Gd-DOTA solution showed two relaxation times of 108 ms and 393 ms for extracellular and intracellular proton, respectively, at −60°C. The contributions of proton magnetization diffusing from intracellular and extracellular parts of the cell causes the locational dependence of proton relaxation rates of phospholipid, sugar and nucleotide molecules. The proton magnetization of lipids which compose the cell membranes relaxed quickly because of strong paramagnetic effect from the extracellular part, while that of nucleotide which are located deeply inside the cell relaxed slowly due to small contribution of fast-relaxing magnetization diffusing from the extracellular part. The spin diffusion model computed using spin diffusivity of 0.8 nm^2/ms revealed that the Gd-DOTA cannot pass though the inner cell membrane. Therefore, this model could be used to analyze the relaxation rate of macromolecules locating within a 20 nm of the centre of inner cell membrane.

Conclusion: This thesis showed high-resolution solid-state NMR provided the *E. coli* cellular site information semiquantitatively for biological macromolecules by using paramagnetism of Gd-DOTA as a relaxation contrast agent. Thus this methodology enables solid-state NMR spectroscopy to study cellular structure as well as biomolecular structure.

Acknowledgements

I would like thank the number of people and institutes below for insightful help.

- Thank Dr. Ayako Egawa, Assoc. Prof. Yoh Matsuki and
  Prof. Dr. Toshimichi Fujiwara for useful advice, discussion and assistance with NMR signal acquisition.
- Thank second readers of this thesis, Prof. Dr. Yasuhisa Mizutani and
  Prof. Dr. Yasuhiro Funahashi
- Thank Laboratory of Molecular Biophysics and Institute for Protein Research, Osaka University for experimental facilities.
- Thank Ministry of Education, Culture, Sports, Science and Technology (MEXT) of Japan for scholarship.
- Thank Japan Society for the Promotion of Science for research fund

Contents

Declaration of Authorship ii

Abstract iii

Acknowledgements v

Contents vii

Introduction 1

1.1 NMR as a method for studying biological systems 1

1.2 Paramagnetic Relaxation Enhancement (PRE) 3

1.3 Gd^{3+} paramagnetism and Gd^{3+} contrast agent for MRI 4

1.4 In-cell NMR 6

1.5 Purpose of the study 7

Materials and Methods 10

2.1 Distribution of gadolinium complexes in *E. coli* sample studied by NMR 10

2.1.1 Sample preparation 10

2.1.2 NMR experiment 11

2.1.3 Data analysis for the longitudinal relaxation of wet *E. coli* sample 12

2.1.4 ^{13}C solid-state NMR experiment 14

2.1.5 Viability of E. coli cell in the sample containing gadolinium solution 14

2.2 Localization of biomolecules in *E. coli* cells as studied by ^{13}C-NMR observation of ^{1}H paramagnetic relaxation 15

2.2.1 Sample preparation 15

2.2.2 Solid-state NMR experiment 15

2.2.3 Signal assignment 17

2.2.4 Data analysis 18

Results 27

3.1 Calculation of water proton T_1 without paramagnetic agent 27

3.2 Amount of water and glycerol in *E. coli* samples 29
3.3 Validation of parameters for calculating the relaxivity 29
3.4 Calculation of the relaxivity of Gd-complex solutions in wet cell samples 31
3.5 Distribution of gadolinium complexes in *E. coli* sample studied by NMR 31
3.5.1 NMR experiment of *E. coli* sample without gadolinium solution 31
3.5.2 PRE for aqua Gd and Gd-DOTA solutions 34
3.5.3 Solid-state ^{13}C NMR spectra 39
3.5.4 Viability of *E. coli* cells and PRE effect on the cellular ^{1}H resonance in the agents 41
3.6 Localization of biomolecules in *E. coli* cells as studied by ^{13}C-NMR observation of ^{1}H paramagnetic relaxation 43
3.6.1 Assignment of ^{13}C-NMR signals of cellular macromolecules 43
3.6.2 Predicted proton relaxation rate of the frozen cell sample containing Gd-DOTA solution 47
3.6.3 Experimental proton relaxation rate of cellular macromolecules 47
3.6.4 Paramagnetic relaxation in model *E. coli* systems under proton spin diffusion 53

Discussion 56
4.1 Gd complex concentration-dependence of ^{1}H-NMR relaxation rates 56
4.2 Interaction of Gd complexes with cells 57
4.3 The effect of water exchange across the cell membranes 59
4.4 Penetration of Gd complexes into the cell 60
4.5 Location-dependence of relaxation rate in solid-state NMR 60

Conclusion 65

References 67

Appendix 81
A.1 Statistical data of *E. coli* 81

A.1.1 General properties of *E. coli* 81

A.1.2 Amounts of macromolecules in *E. coli* 82

A.1.3 Amounts of small molecules and ions in *E. coli* 83

A.1.4 Amounts of small amino acids required for producing protein in 1 g of dried cell 84

A.2 Fortran code for analyzing paramagnetic relaxation in model *E. coli* systems under proton spin diffusion 86

Chapter 1

Introduction

1.1 NMR as a method for studying biological systems

Nuclear Magnetic Resonance (NMR) spectroscopy is the study of magnetic properties of nuclear spins under strong magnetic fields. Those nuclei respond to both the main magnetic field and weak magnetic field of their neighbor nuclei. This allows the observation of characteristic properties of each nucleus such as resonance frequency, relaxation time, interactions between nuclei. The analysis of these properties can provide structural information of molecules including three-dimensional structures, dynamic behavior and interaction topology. This technique is therefore useful for several scientific fields such as chemistry, physics biology, and medical science.

NMR spectroscopy has become a powerful tool for biological study since 1957 when Saunders *et al* recorded the spectra of biological molecules such as bovine pancreatic ribonuclease and amino acids for the first time in history [1-2]. The applications of NMR in biochemical science expands continuously along the advance of magnetic technology. The state-of-the-art technologies allow many scientists to exploit NMR spectroscopy to investigate

three-dimensional structures of larger macromolecules with higher resolution and their complicated behaviors in solution, in solid forms and even in living cells.

NMR spectroscopy has some advantages over the other structural biological techniques. While X-ray crystallography could monitor the structure of crystallized biological macromolecules, solution NMR spectroscopy could investigate the structure of those macromolecules in the natural forms without crystallization process. Thus, solution NMR could provide structural information of some proteins which difficult to crystallize (e.g. unstructured protein) or study by X-ray crystallography. This technique could also determine dynamic behavior of macromolecule which hardly investigate by X-ray crystallography [3]. NMR spectroscopy is also beneficial tool for drug screening as it could also give information of macromolecule-macromolecule and macromolecule-ligand interactions such as binding sites and biding mechanism. Drug screening by NMR spectroscopy could give the dissociation constant of the complexes of interest which are not amenable to X-ray crystallography [4-5]. In addition to solution NMR, solid-state NMR permits studying structural information of solid-state samples of biological macromolecules. This is an invaluable method for exploring information of membrane proteins or biological macromolecules which is hardly amendable by solution state NMR or X-ray crystallography because protein solution and single crystals are not necessary [6].

Microscope is the other important tool for visualizing structure of macromolecule in biological system. The optical microscope could be used for indicating the biding site of protein complex using fluorescence but this data has lower resolution than structure analyzed by NMR spectroscopy [7]. The rapid evolution of Cryo-electron microscopy (Cryo-EM) in the recent years makes microscope technique more powerful choice for elucidating three-dimensional structure of biological macromolecule in its native state. However, this technique still requires high technological cost even for recording near-atomic-resolution structure in comparison with NMR spectroscopy. Moreover, the conventional Cryro-EM is only applicable to giant macromolecules larger than 100 kDa in molecular mass [8-10]. On the other hand, solid-state NMR spectroscopy can provide structural information of macromolecules in various molecular sizes in higher resolution.

Fluorescence spectroscopy is one of the tools that widely used in structural biochemistry. Fluorescence resonance energy transfer (FRET) microscopy or FRET spectroscopy is an alternative method for studying structure and folding mechanism of

disordered protein. However, the residual structure in unfolded proteins is more sensitively detected by NMR spectroscopy [11].

1.2 Paramagnetic Relaxation Enhancement (PRE)

Relaxation in NMR spectroscopy is the process in which the excited nuclei arrange themselves to return to their equilibrium state. The external radio frequency pulse applied to NMR sample could excite nuclear spin state on resonance and distort the orientation of nuclei spins from the direction of the applied static magnetic field ($\mathbf{B_0}$). In the relaxation process, nuclei spins return to the orientation of nuclei spins parallel to $\mathbf{B_0}$ along the *z*-axis at the equilibrium state. This process involves two sub-processes including longitudinal relaxation and transverse relaxation. The later process is also known as spin-spin relaxation. This is affected by magnetic inhomogeneity as well and causes the magnetization of nuclei spins to dephase from each other. The transverse relaxation time, T_2, describes the decay time constant of the magnetization M on the plane perpendicular to $\mathbf{B_0}$. However, the transverse relaxation is out of scope in this study. The longitudinal relaxation or spin-lattice relaxation (hereafter shorten as relaxation) is the recovery of the *z*-magnetization component towards the direction of $\mathbf{B_0}$. The time constant of this recovery is termed as longitudinal relaxation time or T_1. Given that the magnetization at the equilibrium is M_0, T_1 could be observed by measuring the z-component of the magnetization M_z as a function of time t as [12-13];

$$\begin{aligned} M_z(t) &= M_o - M_o \exp(-t/T_1) \\ &= M_o(1 - \exp(-t/T_1)) \end{aligned} \tag{1.1}$$

The relaxation time measurement, relaxometry, is applicable to a variety field of study e.g. material science, biochemistry and medical science. Magnetic Resonance Imaging (MRI) makes use of the concept of relaxation to create image of human organ. It detects the relaxation time of water proton excited by a radiofrequency pulse under the main magnetic field. By introducing an agent to reduce the relaxation time of some specific parts of body, the distinct relaxation time in those specific organs could be recorded and processed as contrast image of relaxation time [14-15].

Paramagnetic relaxation enhancement (PRE) effect is well used as a strategy for accelerating relaxation. This phenomenon occurs due to the magnetic interaction between a nuclear spin and an unpaired electron spin. Since the strength of PRE effect depends on the distance between the nuclear and electron spins, the enhanced relaxation rate thus could provide locational information of nuclear spins inside the sample [16-19]. This advantage could be applied to studying protein-protein interaction and finding the binding site. As an example, in solid-state NMR spectroscopy, PRE effect is commonly employed to probe specific location of peptide embedded in lipid membranes [20-22]. In these cases, the solutions of paramagnetic ion were added into the sample. The paramagnetic ion concentrating outside the membrane then changed the relaxation rate of peptide in proportion to its distance from the paramagnetic ion on the membrane surface. Therefore, the enhanced relaxation rate of peptides could be interpreted in terms of the location of the peptides in the membranes.

1.3 Gd^{3+} paramagnetism and Gd^{3+} contrast agent for MRI

Lanthanide ion is an outstanding paramagnetic source for NMR due to its unpaired electrons in *f* orbitals which can cause large and varied paramagnetism. Gadolinium (III) ion, Gd^{3+}, is an isotropic paramagnetic lanthanide ion with 7 unpaired electrons. As the number of unpaired electrons of Gd^{3+} (7 unpaired electrons) is the highest among lanthanide ions, it can provide the strongest PRE effect. The isotropic magnetic susceptibility of Gd^{3+} ion enable recording NMR spectrum without pseudocontact shift (PCS) and Residual Dipolar Couplings (RDC) which cause resonance frequency changes and make the NMR spectrum of the sample containing paramagnetic ion more complicated [24]. Thus, PRE effect of Gd^{3+} can be analyzed easier than the other paramagnetic ions. Owing to its strong PRE effect, gadolinium complex is a well-known contrast agent in magnetic resonance imaging (MRI). The contrast agent is introduced into specific targets such as cancer cell, blood vessel or other specific organs. The contrast of image occurs because of the different level of PRE in the different compartments. In 1980s, gadolinium diethylenetriamine penta-acetate or Gd-DTPA complex was introduced as the first contrast agent to improve the contrast of MRI [25]. Moreover, the Gd^{3+} is also used as a complementary tool to study structure and properties of biomacromolecule. For example, the gadolinium complex has an advantage over paramagnetic copper complex for enhancing the sensitivity of ssNMR spectroscopy [26-29]. By doping membrane protein with the gadolinium complex, the sensitivity of ssNMR is enhanced remarkably [29].

In aqueous solution, the Gd^{3+} ion forms an aqua complex with 8 coordinated water molecules. The free Gd^{3+} ion is harmful to a creature due to the fact that its ionic radius (0.99 Å) is close to that of calcium ion. Hence, it can cause trouble in biological processes that involve Ca^{2+} such as Ca^{2+} binding enzymes[30]. To apply to human, the gadolinium ion has to be restricted in a proper chelate or ligand. In MRI, the gadolinium complexes are used to reduce selectively the signal of water near the complex and raise the contrast relaxation rate. They are classified as a T_1 agent which enhances the longitudinal relaxation roughly the same amount as the transverse relaxation [31]. The water molecules surround Gd (III) ion are classified into three groups. The water molecules which coordinate directly to Gd (III) are called inner-sphere waters. A second-sphere water means the slow diffusing water molecules enclosure the inner-sphere water. The other water molecules outside the second-sphere are outer-sphere water molecules. These three categories of water unequally have their effects on the relaxation of water proton [32]. The relaxation rate per concentration of relaxation agent or relaxivity of any gadolinium complex depends on its water exchange rate, the number of coordinated water molecules, its rotational diffusion and an electronics spin relaxation rate. The water exchange rate between inner sphere and surrounding waters for a commercial MRI agent is about 200 times slower than that for the aqua gadolinium complex, $Gd(H_2O)_8^{3+}$[30]. The relaxivity of the commercial gadolinium MRI agents are about 4-5 mM s^{-1} [32]. The commercial gadolinium agents can be used effectively when its concentration is higher than 0.1 mM. Nevertheless, these agents should not be used over its clinical dose. The safety dose of gadolinium agents are usually in the level of hundreds micromolality. For instance, the safety clinical dose of Magnevist, $[Gd(DTPA)(H_2O)]^{2-}$, is 300 μmol kg^{-1} [31] and gadolinium tetraazacyclododecanetetraacetate or Gd-DOTA complex is 100 μmol kg^{-1} [33].

1.4 In-cell NMR

In-cell NMR is a newly developed nuclear magnetic resonance spectroscopy that enables characterization of structures and functions of biological macromolecules in living cells. Although these invaluable data could be retrieved by conventional NMR spectroscopy or the other well-developed technique like X-ray crystallography, there is a controversy that

information investigated by these conventional methods cannot revealed the *in vivo* biological phenomena of macromolecules in their native cellular environment. In-cell NMR is thus the promising technique that could provide the most accurate information and the revolution of this technique triggers a development in drug discovery and cell biology.

The first in-cell NMR is the spectrum of the small domain of the Tn501 mercuric ion reductase (MerA) recoded directly in living *Escherichia coli* (*E. coli*) by Serber *et al* in 2001 [34]. This pioneering experiment was performed for cultured *E. coli* cells and expressed MerA in two steps including 1) the first culture in non-labeled medium without protein expression and 2) the culture and protein expression in minimal medium containing labeled isotopes. The success of detecting the NMR spectrum in bacterial cell initiated the invention of in-cell NMR spectroscopy for eukaryotic and mammalian cells to elucidate structure of macromolecule of higher animal in similar environment. In 2006, Sakai et al and Selenko et al. introduced the technique for detecting NMR spectrum in living *Xenopus laevis* oocytes by injecting isotope labeled protein into oocytes [35-36]. This approach provided the spectra of the injected protein with small background signals. The first success in in-cell NMR in human cells was reported in 2009. Inomata *et al* linked their labeled protein of interest with cell-penetrating peptide (CPP). This linked protein could penetrate across cell membranes and accumulate in HeLa cells. The disulfide bonds by which linked their protein of interest was then cleavaged in the reducing intracellular environment and released free target protein [37]. In the same year, Ogino *et al* also demonstrated an alternative strategy for introducing the protein of interest into haman cell. In this approach, human cells were treated with a streptococcal pore-forming toxin to make pores on plasma cell which large enough for their protein to influx into the cell. The pores on the membrane then resealed by treatment of the sample with Ca^{2+} solution [38]. In 2016, Selenko and his team reported their new method for delivering protein of interest to human cell. They employed cell electroporation concept to force their protein target to permeate the cell membrane while applying electric field to the cell sample [39-40]. In additional foregoing delivery method, the protein of interest could be expressed directly inside human cell. The procedure has been developed by Jones and coworkers since 2006. This method is suitable for preparing proteins which are sensitive to redox environment [41-44].

A breakthrough of in-cell NMR in ss (solid-state) NMR spectroscopy came in 2012, when Reckel and coworkers reported the ssNMR of protein frozen *E. coli* cells. The degradation of cells can be suppressed under low temperatures, which enables informative multidimensional NMR experiments that need long experimental time. The difficulty in

developing in-cell ssNMR is the lower sensitivity and higher background level in comparison to solution NMR [45]. The sensitivity of in-cell NMR can be promoted by recording the sample containing dynamic nuclear polarization (DNP) or paramagnetic agents [46-47].

Like conventional NMR spectroscopy, recently, in-cell NMR spectroscopy can be used for studying various biochemical aspects of macromolecule such as thermodynamic activity of protein folding, protein-protein interaction, electrochemical reaction of metalloprotein, protein post-translational modification, protein-maturation, protein aggregation process [48-49].

1.5 Purpose of the study

Although, there were several progresses in in-cell NMR spectroscopy in the last decade, many advanced methods in conventional NMR spectroscopy are still not applicable in this newly developed area. For example, in solid-state NMR spectroscopy, PRE effect is commonly employed to probe specific location of peptide embedded in lipid membrane [20-23]. In these cases, the solutions of paramagnetic ion were added to the sample. The paramagnetic ion concentrating outside the membrane then allowed the relaxation rate of peptide to change as a function of its distance from paramagnetic ion on the membrane surface. The enhanced relaxation rate of peptide then could be interpreted to be the location of peptide in the membrane. The information of the location of protein is crucial for studying topology and function of protein [51]. However, there is still no report about this application in solid-state in-cell NMR. This study therefore aims to develop the ssNMR spectroscopy for probing specific location of macromolecule in living cell. The strategy for investigating this novel information was tested with living *E. coli* cells.

To apply the concept of the above case study to in-cell solid-state NMR, the paramagnetic agent for treating living cell sample has to be in nontoxic form. Moreover, it has to be distributed only in some part of the cell sample to contrast the locations depending on the relaxation rates of nuclei. MRI agents are the example of the stable paramagnetic complexes. Gd-DOTA complex, which is one of the famous clinical contrast agents for MRI, should be safe agent for enhance relaxation rates of the cell sample. Thus, this complex is employed as paramagnetic agents for determining distance information of macromolecule in *E.coli* cells in this study. Nevertheless, there are some researchers reporting that this complex also could little internalize into the cell. Therefore, the permeability of Gd-DOTA complex and aqua

gadolinium ion [30, 52] into *E. coli* cells were tested in this study by considering the relaxation rate of intracellular and extracellular proton. The toxicities and effects of the both gadolinium complexes on the ^{13}C NMR spectra were also checked in order to use these complexes as PRE agent for solid-state NMR spectroscopy.

In solid-state NMR, the diffusion of nuclear spin states through strong ^{1}H-^{1}H dipole-dipole interaction, spin diffusion, can spread PRE effect from the paramagnetic center to the remote site farther than in solution state NMR. In this study, the cell samples were treated with Gd DOTA (figure 1.1). This PRE agent is supposed to be too large and hydrophilic to penetrate into the cell across the hydrophobic biomembranes, and enhances the relaxation rate of extracellular nuclei more efficiently than intracellular nuclei. By combining spin diffusion with PRE effect, the fast-relaxing spin state from extracellular part of the sample could propagate to the intracellular part and allow detecting the faster relaxation rate of intracellular macromolecule. The enhanced relaxation rate of intracellular macromolecule then could be interpreted as its location or distance from extracellular Gd-DOTA complex. This information for the localization of molecules could help to promote the understanding of the function of macromolecule in biological processes.

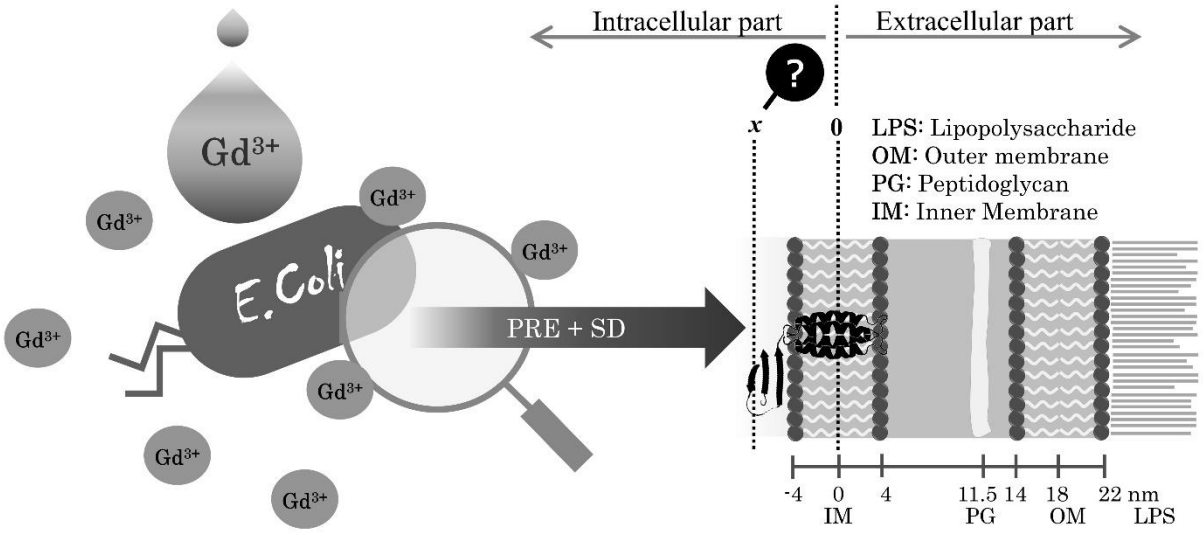

Figure 1.1: Graphic shows the purpose of this thesis. Solution containing Gd^{3+} was employed as a contrast agent in this study. The Gd^{3+} complex resides mostly outside the cells causes the extracellular protons to experience PRE effect more efficiently than intracellular protons. The fast relaxing extracellular magnetization propagates into the cell via ^{1}H-^{1}H spin diffusion. The relaxation rate of intracellular macromolecule therefore depends on their location inside the cell. This study aims to develop the technique to interpret the relaxation rates of cellular macromolecules to their specific location inside the cell.

Chapter 2

Materials and Methods

2.1 Distribution of gadolinium complexes in *E. coli* sample studied by NMR

2.1.1 Sample preparation

To study the distribution of aqua gadolinium and Gd-DOTA complexes in *E. coli* samples, the proton relaxation rate of the cell samples containing these paramagnetic agents was measured. The *E. coli* strain used in this study was BL21 Star^{TM} (DE3). The cells were cultured in 120 ml of 20 g/l LB medium containing 50 μg/ml ampicilin at 37 °C. The culture was harvested when OD_{600} reached 0.7-0.8 by centrifuging at 2000 g for 20 min at 4°C. The suspension was washed twice by dissolving in 140 mM NaCl solution and centrifuging at 3300 g at 4°C for 15 and 5 min for first and second washing respectively. The 99.0 % (mass/mass) glycerol purchased from Wako Pure Chemical Ind. (Lot No LAE4314) was added to the suspension to be the final concentration of 20% w/w. The paramagnetic agents, aqua gadolinium and Gd-DOTA solutions, were then finally added to the sample in the ratio of 1:4. The $GdCl_3.H_2O$ complex was purchased Wako Pure Chemical Ind. (Lot. DCG6787, CAS. 13450-84-5) and dissolved in Milli-Q water to be 0.00, 12.48, 24.97, 99.97, 149.02, 199.92, and 249.63 mM solution. The Gd-DOTA solutions were prepared by dissolving Gd-DOTA powder synthesized by BOC Sci. (Lot B13Z0925) in Milli-Q to be concentration of 0.00,

12.48, 24.97, 99.97, 149.02, 199.92, 249.63 mM. The *E.coli*-glycerol mixtures were mixed with the paramagnetic agents 20 min before NMR experiment.

20 μl of cell sample containing gadolinium complex was pipetted into a NORELL^{TM} glass tube (Lot No. P051809BTR) which cut to match the size of the solid-state NMR probe and closed with Parafilm® (figure 2.1).

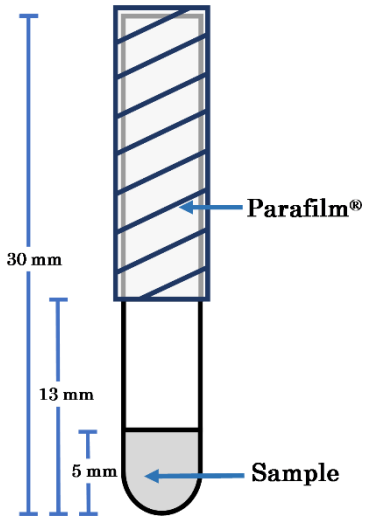

Figure 2.1: Modified NMR tube for measuring relaxation time of wet *E. coli* sample

2.1.2 NMR experiment

The proton relaxation time was measured via a 700 MHz NMR spectrometer (JEOL, Japan) equipped with a Triple Balun probe (Varian, USA) for a 4.0 mm rotor using saturation pulse followed by an excitation pulse at 0°C (figure 2.2). The experiment was completed within 40 min after adding gadolinium agent into cell sample.

In order to track the relaxation rate change as a function of time, the mixture of glycerol and *E. coli* was added with 250 mM Gd-DOTA and 249.6 mM $GdCl_3$ solutions and their relaxation time was measured repeatedly several times. The NMR tube and sample

volume were the same as the sample described above. The samples were kept in refrigerator at 4°C after finishing each measurement.

The relaxation rate was analyzed by fitting the buildup curve of the integral area of whole spectra with multiple exponential relaxation equation. However, the equation containing more than two exponential components have proved here in this study that did not improve the fitting result. Therefore, the data were analyzed by fitting only with the double exponential relaxation equation as

$$M(t) = M_{o,\,ex}\,(1-\exp(-t/T_{1,\,ex})) + M_{o,\,in}(1-\exp(-t/T_{1,\,in})) + c \qquad (2.1)$$

where the subscripts 'in' and 'ex' mean intracellular and extracellular parts, respectively.

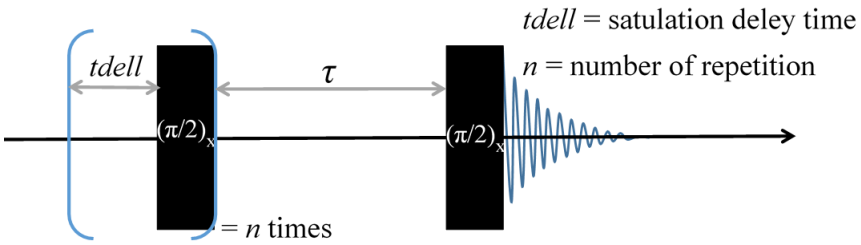

Figure 2.2: Saturation recovery pulse for measuring relaxation time of wet *E. coli* sample

2.1.3 Data analysis for the longitudinal relaxation of wet *E. coli* sample

Under high magnetic fields, the dipole-dipole interactions between nuclear spins and unpaired electron spins in an aqueous solution containing paramagnetic agent mainly cause PRE effect [53-54]. The relaxation rate due to this interaction depends on proton-electron spin distance (r), correlation time (τ_c), water exchange rate and number of water molecules in coordination sphere of PRE complex as described by Solomon-Bloembergen-Morgan equation as [55-57]:

$$\frac{1}{T_{1m}} = \frac{2}{15}\left(\frac{\mu_B \gamma_H \gamma_e \hbar}{r^3}\right)^2 S(S+1)\left\{\frac{3\tau_c}{1+\omega_H^2\tau_c^2} + \frac{7\tau_c}{1+4\omega_S^2\tau_c^2}\right\} \quad (2.2)$$

$$\frac{1}{\tau_c} = \frac{1}{T_{1e}} + \frac{1}{\tau_r} + \frac{1}{\tau_m} \quad (2.3)$$

where, γ_H is proton gyromagnetic ratio, μ_B is the permeability of vacuum, γ_e is the electron gyromagnetic ratio, S is the spin quantum number of paramagnetic ion, r is the proton-electron distance, ω_S is Larmor frequency of the electron, ω_H is Larmor frequency of proton, τ_C is correlation time of paramagnetic complex and τ_r is rotational correlation time of PRE complex. The relaxivity (R_{1p}) of PRE agent, the relaxation rate of the sample enhanced by 1 unit of concentration of PRE agent, is calculated from T_{1m} and τ_m. The function for calculating R_{1p} was derived by Luz and Meiboom and Swift and Connick as [56-59];

$$R_{1p} = \frac{q}{[H_2O]}\left(\frac{1}{T_{1m} + \tau_m}\right) \quad (2.4)$$

where q is the number of water molecules in the inner coordination sphere of PRE complex. Alternatively, R_{1p} could also be predicted from a function of R_1 and concentration of PRE agent and:

$$R_{1p} = \frac{R_1' - R_1^0}{[\text{PRE agent}]} \quad (2.5)$$

where R_1^0 and R_1' are the relaxation rates of the sample with and without the PRE agent respectively.

However, the effect of T_{1e} on R_1 of water proton could be neglected in equation (2.3) under magnetic fields higher than 3 T [31, 60]. The τ_m also affects R_1 of water proton only if the time scale of rotational diffusing and electronic relaxation is comparable to the water

exchange. Under the experimental condition in this study, the electron relaxation and the rotational diffusion are much faster than the exchange rate of water molecule between the outer sphere and the inner sphere of paramagnetic complexes. For example, at temperature of 298 K, τ_m of aqua gadolinium complex and Gd-DOTA complex are 1.20×10^{-9} and 2×10^{-7} s while τ_r are 2.9×10^{-11} and 9.0×10^{-11} s respectively [61-63]. At this temperature, T_{1e} is approximately 1.35×10^{-7} and 2.01×10^{-6} s for aqua gadolinium complex and Gd-DOTA complex respectively [33, 64-65]. Thus, R_{1p} of this agent can be calculated without considering τ_r and T_{1e} because of the large difference among τ_m , τ_r and T_{1e}. In other word, PRE effect of gadolinium complex under high magnetic fields is independence of the effect of water exchange and electron relaxation. As a consequence, $1/\tau_c$ in equation (2.3) approximately equals to $1/\tau_r$ and $T_{1m} - \tau_m$ in equation (2.4) can be rewritten as T_{1m}.

2.1.4 ^{13}C solid-state NMR experiment

80 µl of the glycerol-*E.coli* mixture was added with 20 µl 140 mM NaCl, 149 mM aqua gadolinium, and 150 mM Gd-DOTA solutions. The samples were loaded into a 4.0 mm solid-state NMR rotor and frozen in liquid nitrogen. The ^{13}C NMR spectra at 125 MHz were obtained via cross polarization pulse with mixing time of 2 ms and single 90˚ (3.8 µs) pulse on a JEOL ECAII NMR spectrometer equipped with a MAS T3 triple-resonance probe for a 4.0 mm rotor under MAS frequency of 12 kHz at -55°C. The relaxation delays for all samples were set at 7 s. The CP/MAS ^{13}C NMR spectrum of the sample containing 149 mM aqua gadolinium solution was recorded at the resonance frequency of 175 MHz and MAS frequency of 12 kHz under temperature of -55°C.

2.1.5 Viability of *E. coli* cell in the sample containing gadolinium solution

80 µl living *E. coli*-glycerol mixture was added with 20 µl 149 mM aqua gadolinium and 150 mM Gd-DOTA solutions. The samples were stored in ice bath before serial dilution. After incubation, the samples were diluted in 140 mM NaCl solution. The diluted sample was then cultured on LB agar plate at 37°C in order to count the number of living *E. coli* cells which could form colonies. As a control sample, 40 µl living *E. coli*-glycerol mixture was also added with 10 µl 150 mM NaCl solution. This sample was diluted quickly after mixing. The sample was then cultured on a LB plate similarly to the sample containing gadolinium solution. The

numbers of colony on a LB plate of the sample containing gadolinium agents were normalized with the number of colony formed by the control sample.

2.2 Localization of biomolecules in *E. coli* cells as studied by ^{13}C-NMR observation of ^{1}H paramagnetic relaxation

2.2.1 Sample preparation

E. coli used in this study was BL21 Star^{TM} (DE3), the strain which has no flagellum [66] grown in M9 medium containing [U-^{13}C] glucose, $^{14}NH_4Cl$, nonlabeled nucleosides and 50 μg/ml Ampicilin at 37 °C until OD_{600} reached the value about 0.7-0.8. The [U-^{13}C] glucose and $^{14}NH_4Cl$ were purchased from Chlrella Industry (Lot No 3052) and Wako Pure Chemical Industries (Lot No AWQ4809) respectively. The culture was harvested by centrifuging at 2000 g at 4 °C for 20 min. The suspension was then washed twice with 0.14 M NaCl solution and centrifuged again at 3300 g at 4°C for 15 and 5 min respectively. The suspension was mixed with 99.0% (w/w) glycerol. The final concentration of glycerol in the sample was 20% w/w. The glycerol was purchased from Wako Pure Chemical Industries (Lot No LAE4314). It was added in order to keep this water rich sample in homogenous form even at low temperature. 20.00 μl of 150 mM Gd-DOTA solution were then added into 80.00 μl *E. coli*-glycerol mixture. As a control sample, 20.00 μl of 140 mM NaCl solution was added instead of Gd-DOTA solution. Gd-DOTA was synthesized by BOC Sciences (Lot No. B13Z0925). Before NMR experiments, the sample was transferred into a 4.0 mm NMR rotor and frozen by putting the rotor into liquid nitrogen.

2.2.2 Solid-state NMR experiment

The relaxation rate of cellular proton signal was monitored through ^{13}C NMR signal. The series of ^{13}C NMR signals were detected by the relaxation ordered spectroscopy (ROSY) pulse [67]. ROSY pulse is basically the pulse for separating components of a ssNMR spectrum based on the proton relaxation rate. This pulse could provide the relaxation rate and spectrum of each cellular macromolecule. The magnetization of ^{1}H is saturated by a series of 90° pulse, saturation pulse, on the *xy* plane before recovering back to the *z*-axis along B_0 during recovery time τ_{rec}. Cross Polarization (CP) pulse then transfers ^{1}H magnetization to ^{13}C magnetization

(Figure 2.3). By varying τ_{rec} and recording ^{13}C NMR spectra after CP pulse, the experimental data has two dimensions of τ_{rec} and NMR signal recorded at each $\tau_{rec.}$ The time domain of this experimental data, S_{td}, could be expressed as equation 2.6;

$$S_{td}(t, \tau_{rec}) = \iint d\upsilon d T_1 I(\upsilon, T_1) \exp(i\upsilon T_1) [1 - \exp(-\tau_{rec}/T_1)] \quad (2.6)$$

where t is acquisition time, υ is frequency of ^{13}C. The spectrum of sample relaxes at specific T_1 could be separated by applying an Inverse Laplace Transform (ILT) to the term $\exp(-\tau_{rec}/T_1)$. However, the cellular ssNMR spectrum is too complicate to separate the relaxation rates of all compositions by ROSY pulse. This study applied ROSY to recording NMR spectra as function of τ_{rec} only. The spectrum recorded at each τ_{rec} was decomposed by fitting with the simulated NMR spectra of cellular components. The relaxation rate of each cellular component was finally analyzed by fitting with the double exponential relaxation equation.

The series of ^{13}C NMR spectra were recorded by ROSY pulse via a 500 MHz JEOL spectrometer equipped with a 4.0 mm probe at temperature around -55°C. The MAS spinning rate was set to 11 kHz. The proton magnetization was transferred to carbon by cross polarization pulse which is a part of ROSY pulse with a contact time of 2 ms. The detection was repeated with delays of 5 and 3 s for the sample in absence and presence of Gd-DOTA solution respectively. The spectra were then processed via JEOL Delta version 5.0.4.3. The 1D ^{13}C NMR signals were primarily detected with 4 scans via the single pulse and cross polarization pulse to select parameters that give CP NMR spectrum most similar to the single pulse spectrum. By mean of this method, the ^{1}H field strength was set at 50 kHz and ^{13}C field strength was matched with +1 sideband (61 Hz). The 2D Proton-Driven Spin Diffusion (PDSD) [68] NMR spectra were also detected via a 500 MHz JEOL spectrometer equipped with a 4.0 mm probe at temperature around −55 °C. Unless otherwise noted, time delay and contact time were the same as in 1D ^{13}C NMR experiment. The mixing time was 100 ms. This mixing time was long enough to give complete cross peak patterns of glucose monomer of polysaccharide and intra-residue cross peaks of proteins [69-70].

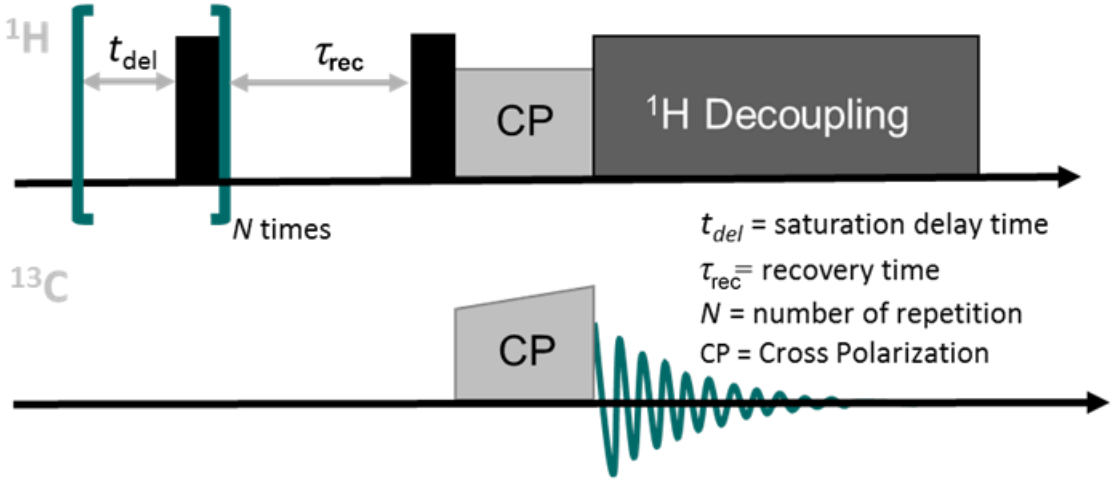

Figure 2.3: Relaxation ordered spectroscopy (ROSY) pulse modified for measuring the ^{1}H relaxation time of cellular macromolecules through high-resolution ^{13}C spectra under proton decoupling and magic-angle spinning.

2.2.3 Signal assignment

As a reference for the assignment, the ^{13}C NMR spectrum of *E. coli* cell was simulated. The chemical shifts of all cellular components were predicted by ChemBioDraw Ultra 14.0 Software. Unless the otherwise noted, the resonance lines were extended to be in Gaussian shape with a width at half height of 3 ppm. The spectra of all components were combined to be the spectrum of whole *E. coli* cell based on the ratio calculated from statistical amount of each cellular component (Table 2.1) [71-72], amount of each amino acid, RNA and DNA building block [73] and amount of each metabolite [74]. This simulation assumed that fraction of carbon in each cellular compositions gave the signal intensity by the number of atoms. The structure of lipopolysaccharide was downloaded from PubChem database (Code: SID625489). The chains of all lipid molecules were supposed to be in saturated form. The spectrum of peptidoglycan was simulated from its monomer reported elsewhere [75] as well as the spectrum of glycogen which simulated from the monomer available on PubChem database (Code: CID439177). In addition to the simulated spectrum, the assignments were also confirmed by considering correlations of NMR peaks in the 2D PDSD ^{13}C NMR spectrum.

Table 1. Percent of cellular volume occupied by each cellular component [19]

Cellular components	Percent of volume	Number of molecules
water	70	-
protein	17	-
RNA	6	222,000
DNA	1	-
lipid	3	25,000,000
Lipopolysaccharide	1	-
Peptidoglycan	1	-
glycogen	1	-
small organics	1	-

2.2.4 Data analysis

2.2.4.1 Theory of PRE in solid-state NMR spectroscopy

The relaxation behavior of nuclear spins in the presence of paramagnetic ions in solid states is somewhat difference from that in solution states. Although the nuclear spins nearby paramagnetic ion relax in the same manner for the two states, the process that propagate PRE effect is different. In other word, the relaxation behavior of the nuclear spin close to paramagnetic center experience the same PRE effect, termed in this thesis as actual PRE effect. In solution, PRE effect could spread from the paramagnetic center through water exchange mechanism in which the water molecule in the coordination sphere of the paramagnetic ion can exchange with the bulk water in the sphere outside. Therefore, the average relaxation rate of water proton depends on the exchange rate and the number of the coordinated water molecule. In contrast, the restricted motion of water molecules in solid states obstructs water exchange to spread PRE effect from the paramagnetic center. The strong dipole-dipole interaction of protons in solid samples alternatively allows PRE effect to spread farther through the spin diffusion. Here, this relaxation process is named as PRE due to spin diffusion. In our ssNMR experiments for cells, we selected temperature and the concentration of paramagnetic compounds so that the proton relaxation time is primarily determined by the paramatnetic relaxation and not by the thermal motion of molecules.

In this thesis, the theoretical descriptions of PRE effects in solid-state NMR reported elsewhere were summarized as below. Here, the nuclear magnetization at the time t and position r is given as $M(r, t)$. This term could be written as the combination of the relaxation enhancement due to spin diffusion and direct PRE effect and written as [76];

$$\left[\frac{\partial M(r,t)}{\partial t}\right]_{total} = \left[\frac{\partial M(r,t)}{\partial t}\right]_{ACT} + \left[\frac{\partial M(r,t)}{\partial t}\right]_{SD} \tag{2.7}$$

where the subscript ACT and SD mean the direct paramagnetic relaxation enhancement and spin diffusion respectively. The equation (2.7) can be expressed as;

$$\frac{\partial \mathfrak{m}(r,t)}{\partial t} = D\,\nabla^2 \mathfrak{m}(r,t) - \mathfrak{m}(r,t)\frac{C}{r^6} \tag{2.8}$$

where $\mathfrak{m}(r,t) = M_0 - M(r,t)$, D is spin diffusivity and C is the coefficient of paramagnetic ion defined as;

$$C = \frac{2}{5} S(S+1)\gamma_n^2\gamma_p^2\hbar^2 \left\{\frac{\tau_c}{1+\omega_0^2\tau_c^2} + \frac{7\tau_c}{3(1+\omega_e^2\tau_c^2)}\right\}. \tag{2.9}$$

in which γ_p and γ_n are the gyromagnetic ratios of paramagnetic ion and nuclear spin respectively, S is the spin quantum number of paramagnetic ion, ω_e and ω_0 are Larmor frequencies of electron and nuclear spins and τ_c is the correlation time of paramagnetic ion. Therefore, the first term of equation (2.8) contributes the effect of spin diffusion while the second term is PRE effect of paramagnetic agent on the relaxation process. In solid samples containing Gd^{3+} ion, τ_c can be approximated from the relation [77];

$$\tau_c = 3.7 \times 10^{-8}/T \tag{2.10}$$

and C could be calculated from the relation [77];

$$C = 1.55 \times 10^{-30} \tau_c. \quad (2.11)$$

Since the relaxation rate of the sample containing paramagnetic agent depends on the distance between the paramagnetic ion and nuclear spin, PRE effect on the sample is divided into three cases according to the difference of relaxation behavior in each site. The inner region close to the paramagnetic ion is the site where the strong local magnetic field is induced by the electron spin. Thus, Larmor frequencies of the nuclear spins in this site are considerably different by more than dipolar couplings from those of the other spins in the outer area. The spin diffusion from this inner site to the other sites is consequently quenched. The boundary of this inner site is defined as the radius of *b* [78-79];

$$b = a\left(\frac{\mu_p}{\mu_n}\right)^{1/3} \quad (2.12)$$

where *a* is the distance between adjacent nuclei, μ_p is the magnetic moment of paramagnetic electron and μ_n is the magnetic moment of nuclei. Furthermore, the strong PRE effect broadens the signal of the nuclei spin and makes it unobservable. In other word, within the radius of *b* from the paramagnetic ion, the nuclear spins are unable to contribute their signals in the NMR spectrum and spin diffusion is suppressed.

Next to the inner site, the region within boundary *b* and β is the region where nuclei is affected by the PRE effect (Figure 2.4 and 2.5). In this site, the relaxation enhancement due to spin diffusion competes with the direct PRE effect. Since the magnitude of the direct PRE effect decreases rapidly as a function of r^{-6} (equation (2.8)), only the spin diffusion dominates the relaxation of the nuclear spins outside the boundary. The boundary β could be estimated from the coefficient *C* in equation (2.11) and spin diffusivity *D* as [78];

$$\beta = 0.68\left(\frac{C}{D}\right)^{1/4}. \quad (2.13)$$

For a rigid solid sample like polystyrene investigated at the temperature lower than its glass transition temperature, Cai *et al* suggested the diffusivity should be in the range of 0.5-0.8 nm^2 ms^{-1} [80].

The relaxation rate of the nuclei neighboring the paramagnetic center could alternatively be estimated using the simplified mathematical equations explained later in this section. The difference in concentration of the paramagnetic ion and spin diffusivity causes the mathematical description described previously could be simplified in three different ways including a) relaxation without spin diffusion regime, b) relaxation with limited spin diffusion regime and c) relaxation with rapid spin diffusion regime. These simplifications are based on the assumption that the distance between the neighboring paramagnetic ions is infinite or the concentration of paramagnetic ion in the sample is low so that the electron-electron spin diffusion is ignored. The relation between the concentration of paramagnetic ion (N_p) and the distance between the neighboring ions (R) could be calculated from;

$$R = \left(\frac{3}{4\pi N_p}\right)^{1/3} . \tag{2.14}$$

a) Relaxation without spin diffusion regime

In this regime, the spin diffusivity is considerably slow and the area within the boundary β of the sample is significant large enough to fulfill the requirement $\beta \approx R \gg b$ (Figure 2.4a). Thus, the direct PRE effect is the dominant effect that drives the relaxation of nuclear spin surrounding paramagnetic ion. Blumberg proposed the equation for calculating nuclear magnetization of nuclear spins at the time t in this case as following equations.

$$M = M_0 (1 - e^{-Ct/r^6}) \; ; \text{for small } t \tag{2.15}$$

$$\mathfrak{M}_z (t) \cong \frac{4\pi^{3/2} N_p (Ct)^{1/2}}{3} \quad ; t > \frac{b^6}{C} \tag{2.16}$$

$\mathfrak{M}_z (t)$ is the total magnetization defined by;

$$\mathfrak{M}_z(t) = \int M\, d^3 r. \tag{2.17}$$

b) Relaxation with limited spin diffusion regime

When the spin diffusion is effective enough and reaches the requirement that $R \gg \beta \gg b$ (Figure 2.4b), the relaxation behavior of nuclear spin is under the condition of limited spin diffusion. Within the boundary β in which the direct PRE effect competes with the effect of spin diffusion, the nuclear magnetization propagate in proportion to the square root of time. The relaxation equation can be generalized and yields the equation for estimating relaxation time as [81];

$$T_1 = \frac{1}{4\pi N_p \beta D}\ . \tag{2.18}$$

c) Relaxation with rapid spin diffusion regime

Under the condition that the dipolar coupling between nuclear spin is strong enough that $R > b \gg \beta$ (Figure 2.4c and 2.5), the rapid-spin diffusion regime will be applied to analyzing the relaxation rate. The influence of PRE is limited to relative small area inside β which is much smaller than the radius b. Thus, the relaxation of nuclear spins within this area can be neglected. The average relaxation time can be estimated from the relation [78, 81];

$$\begin{aligned} \frac{1}{T_1} &\approx \frac{\int_\beta^R Cr^6 4\pi r^2 dr}{\int_\beta^R 4\pi r^2 dr} \\ &\approx \frac{4\pi N_p C}{3\beta^3} \\ &\approx N_p \beta D\ . \end{aligned} \tag{2.19}$$

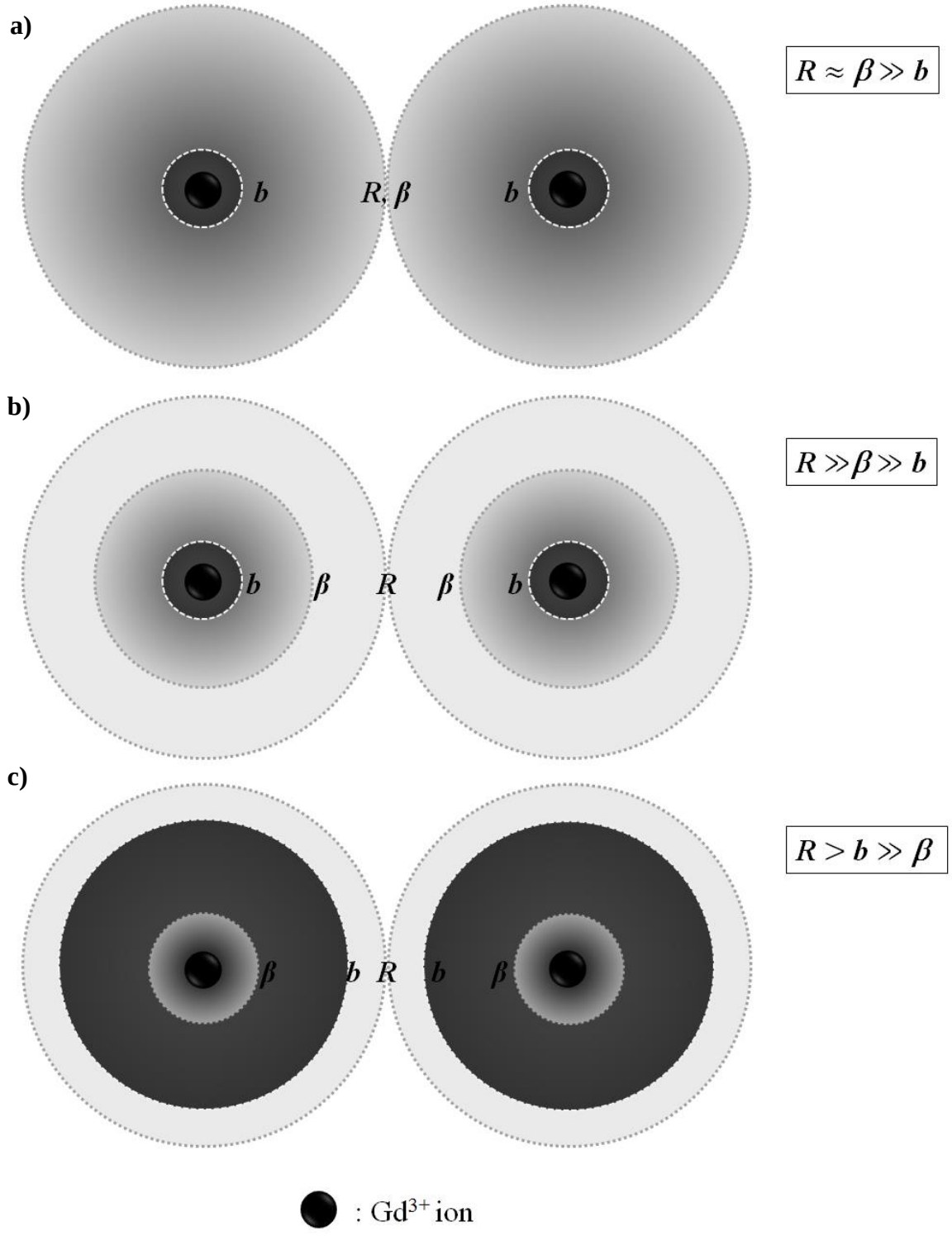

Figure 2.4: Graphics demonstrate boundary R, β and b of a) relaxation without spin diffusion regime, b) relaxation with limited spin diffusion regime and c) relaxation with rapid spin diffusion regime.

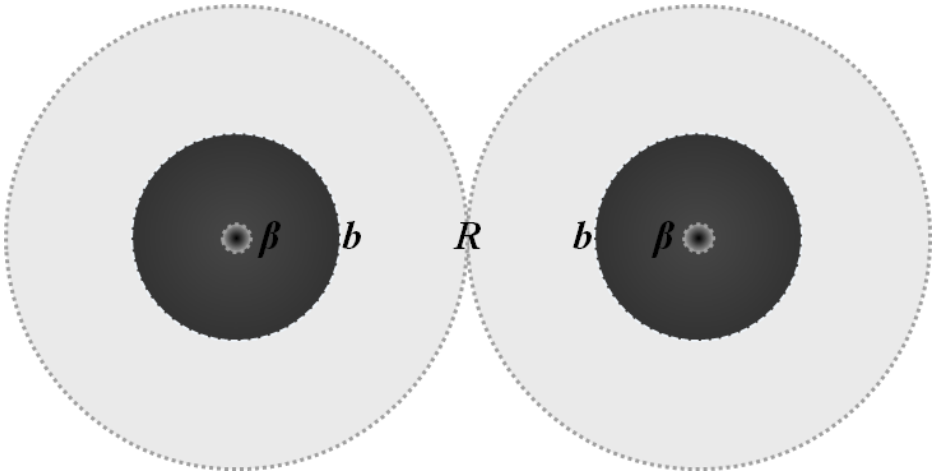

Figure 2.5: Graphic shows boundaries R, β and b of intracellular part of 40 µl *E. coli*-glycerol mixture added with 10 µl 150 mM Gd-DOTA solution are close to rapid spin diffusion regime. R = 38 Å, b =22 Å, β = 6.5 Å. (see calculation details in Appendix)

2.2.4.2 Data analysis for the longitudinal relaxation of frozen *E. coli* sample

The series of NMR spectra of the sample containing Gd-DOTA solution recorded via the ROSY pulse as a function of recovery time, $S_{total}(\delta, \tau_{rec})$, was fitted with simulated NMR spectra of cellular components as;

$$S_{total}(\delta,\tau_{rec}) = \sum_{i}\left\{S_i(\delta)\left[(A_{i,\,fast}(1 - e^{-\frac{\tau_{rec}}{T_{1,\,fast}}}))\right] + \left[(A_{i,\;slow}(1 - e^{-\frac{\tau_{rec}}{T_{1,\,slow}}}))\right]\right\} \qquad (2.20)$$

where δ is chemical shift, τ_{rec} is recovery time and i is cellular component including lipid, sugar, protein and nucleotide. The initial relaxation times, $T_{1,\,fast}$ and $T_{1,\,slow}$, were estimated by fitting the buildup curve of integral area under ROSY spectra with double exponential relaxation function;

$$I_{total}(\tau) = \left[(I_{fast}(1 - e^{-\frac{\tau_{rec}}{T_{1,\,fast}}}))\right] + \left[(I_{slow}(1 - e^{-\frac{\tau_{rec}}{T_{1,\,slow}}}))\right] \qquad (2.21)$$

where *I* is signal intensity. The analysis using two relaxation time constants has been proved to well explain the relaxation behavior of water proton in the cell sample containing PRE agent [82-83].

The simulated NMR spectra of cellular components were modified by changing chemical shift and half width of some peaks in order to improve the similarity to the experimental spectra. (figure 2.6) Since small amount of lipopolysaccharide, peptidoglycan and glycogen causes difficulty getting reliable fitting results, these macromolecules were group together as sugar.

To estimate the initial value of A_i, the modified spectra were compared with the experimental spectrum which recorded using τ of 7 s.

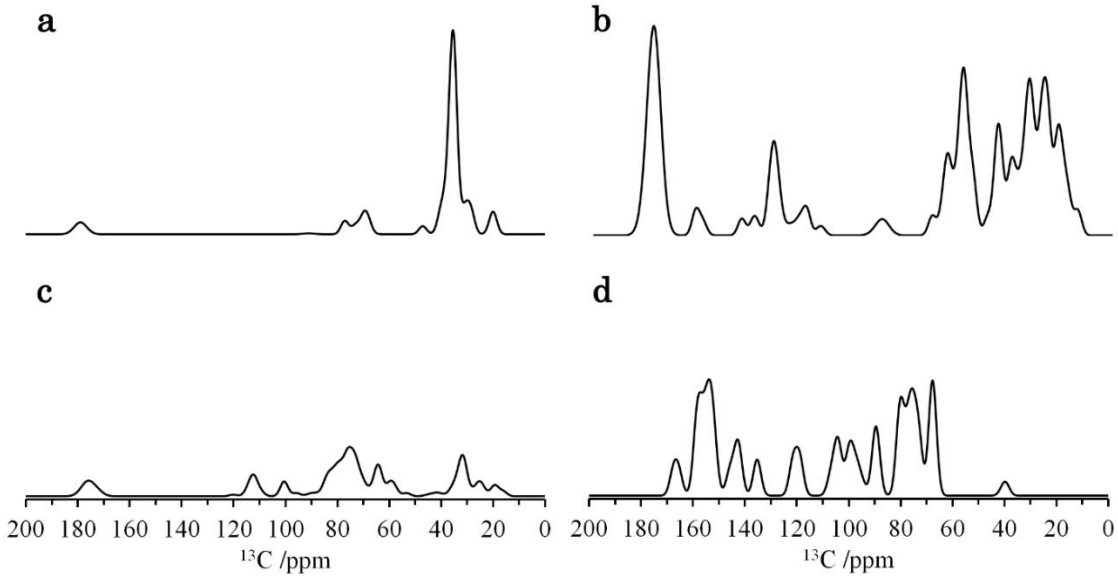

Figure 2.6: Simulated ^{13}C NMR spectra of components of *E. coli* cell including lipid (a), protein (b), sugar (c), and nucleotide (d).

2.2.4.3 Model of spin diffusion across cell membrane

In an attempt to describe the location dependence of the relaxation rate, the spin diffusion throughout the sample was modeled mathematically. This model simulated the magnetization diffuses from the extracellular part into intracellular part and exchanges with the magnetization diffuses from intracellular part to extracellular part simultaneously. This model could be described as;

$$M(\tau_{rec}) = \sum_{y=a}^{y=b}\sum_{x=a}^{x=d}\left\{G\,(y, x; \tau_{rec}, \Delta\tau)\left[M(x, \tau_{rec} - \Delta\tau_{rec}) + \frac{M_{o,\,in} - M(x, \tau_{rec} - \Delta\tau_{rec})}{T_{1,\,in}}\right]\right\}$$

$$+\sum_{x=a}^{x=d}\left\{G\,(0; \tau_{rec}, \Delta\tau_{rec})\left[\mathrm{M}(x, \tau_{rec}-\Delta\tau_{rec}) + \frac{M_{o,\,intf} - M(\tau_{rec}, \tau_{rec} - \Delta\tau_{rec})}{T_{1,\,intf}}\right]\right\}$$

$$+\sum_{y=c}^{y=d}\sum_{x=a}^{x=d}\left\{G\,(y, x; \tau_{rec}, \Delta\tau_{rec})\left[M(x, \tau_{rec} - \Delta\tau_{rec}) + \frac{M_{o,ex} - M(x, \tau_{rec} - \Delta\tau)}{T_{1,ex}}\right]\right\} \quad (2.22)$$

where the subscripts ‘in’, ‘intf’ ‘ex’ mean the intracellular part, interface and extracellular part respectively. The barriers of the intracellular and extracellular parts are noted as a, b, c, and d as illustrated in figure 2.7. The $G\,(y, x; \tau, \Delta\tau)$ function is a green function for expressing the diffusional process [84] that used for simulating the magnetization diffuses from y point at the time τ to any x point after the time $\Delta\tau$ elapses.

$$G\,(y,x\,;\tau_{rec}, \Delta\tau_{rec}) = \frac{1}{\sqrt{4D\pi\Delta t}}\,\exp\left\{-\frac{(x-y)^2}{4D\Delta\tau_{rec}}\right\} \quad (2.23)$$

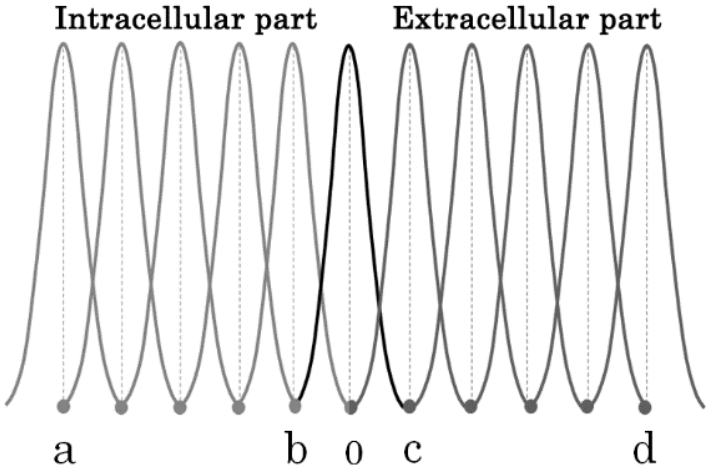

Figure 2.7: Illustration shows the model of spin diffusion in *E. coli* sample, diffusion of the magnetizations from one point to another point, barriers of intracellular (a, b) extracellular (c, d) parts and interface between these two parts (0).

Chapter 3

Results

3.1 Calculation of water proton T_1 without paramagnetic agent

In the absence of paramagnetic agent, the relaxation time T_1 of water proton can be calculated as

$$\frac{1}{T_1} = C\left\{\frac{\tau_r}{1+\omega_H^2\tau_r^2} + \frac{2\tau_r}{1+4\omega_H^2\tau_r^2}\right\} \quad (3.1)$$

where ω_H is ^1H Larmor frequency. The coefficient C was obtained empirically by fitting T_1 reported by Hindman *et al* [85] to the above function. The correlation time τ_r was expressed by the equation:

$$\tau_r = \frac{4\pi\eta A^3}{3kT} \quad (3.2)$$

with viscosity η and a radius of molecule A = 1.4 Å [86]. The viscosity was estimated from the equation proposed by Fogel'son *et al* [87] as

$$\eta = \eta_0 e^{(E/k(T+T_0))} \tag{3.3}$$

where η_0 = 2.4152 x10^{-5} Pa s, E = 4.7428 kJ mol^{-1} and T_0 = –139.86 K.

This approximation gave the coefficient C of 3.69 × 10^{10} s^{-2}. This coefficient was used for simulating the temperature dependent T_1 (Figure 3.1). Figure 3.1 shows the agreement between the experimental and calculated values at the ^{1}H resonance frequency of 500 MHz. The experimental T_1 was slightly shorter than the prediction, which would be due to paramagnetism of O_2 in the water.

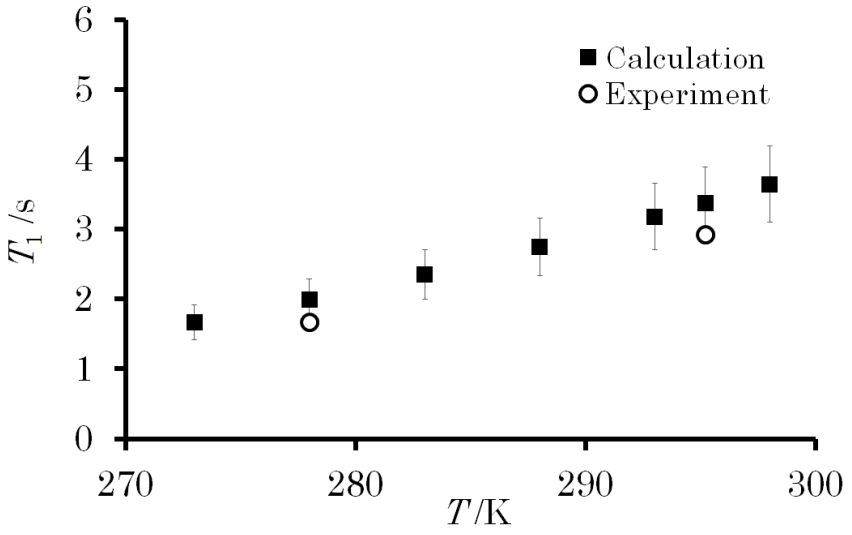

Figure 3.1: Relaxation time of water proton magnetization obtained experimentally (open circle) and theoretically (closed square) from the Bloembergen-Purcell-Pound equation with an empirical parameter plotted against temperature.

3.2 Amount of water and glycerol in *E. coli* samples

To validate NMR experimental result, it is important to estimate amount of water and glycerol in cell sample. *E. coli* sample without glycerol was lyophilized overnight. The dry weight of this *E. coli* pellet was measured. The amount of intracellular water was calculated from this weight of dried cells so that 70% of the cellular weight was water [71]. The amount of extracellular water was obtained by subtracting the amount of intracellular water from the total amount of water in the sample. This method showed that the intracellular and extracellular water weight in the *E. coli* sample was 22 ± 2% and 68 ± 2% of the sample weight, respectively. These values were used for calculating the amount of water and glycerol in the sample after mixing *E. coli* cells with glycerol and gadolinium solutions. For example, *E. coli* sample of 80.00 mg was composed of 18.67 mg of intracellular water and 53.33 mg of extracellular water. This sample was mixed with 20.00 mg of 99.0% glycerol. Given that the density of glycerol and *E. coli* cell was 1.26 and 1.11 g/ml [88-89], respectively, the total density of this *E. coli*-glycerol mixture was 1.05 g/ml, and the composition ratio of intracellular water, extracellular water and glycerol was 19.7, 56.4 and 16.5% of the sample volume, respectively. 10.00 μl NaCl or Gd solution was added to 40.00 μl of this mixture. This addition of the solution increased the fraction of extracellular water from 56.4 to 65.1% of the sample volume and decreased that of glycerol from 16.5 to 13.2%.

3.3 Validation of parameters for calculating the relaxivity

The parameters for estimating the relaxivity were validated by comparing the calculated relaxivity with the experimental results of aqua Gd solution. The relaxivity R_{1p} of gadolinium solution was calculated from equations 2.2 – 2.4. Distance r in equation 3.1 was set at 3.2 Å [90]. The correlation time τ_r was calculated for the radius of aqua Gd complex 3.87 Å [91]. The experimental results (Figure 3.2) showed that the relaxivity of aqua Gd solution at 295 K and $\omega_H/2\pi$ = 500 MHz was 11.4 ± 0.2 s^{-1} mM^{-1} which is close to the predicted value 11.9 s^{-1} mM^{-1} given in table 3.1. The experimental relaxivity was obtained from equation 3.4. The agreement between the experimental and predicted relaxivity indicates that equations 3.1 – 3.4 are applicable to analyzing the experimental results in this study.

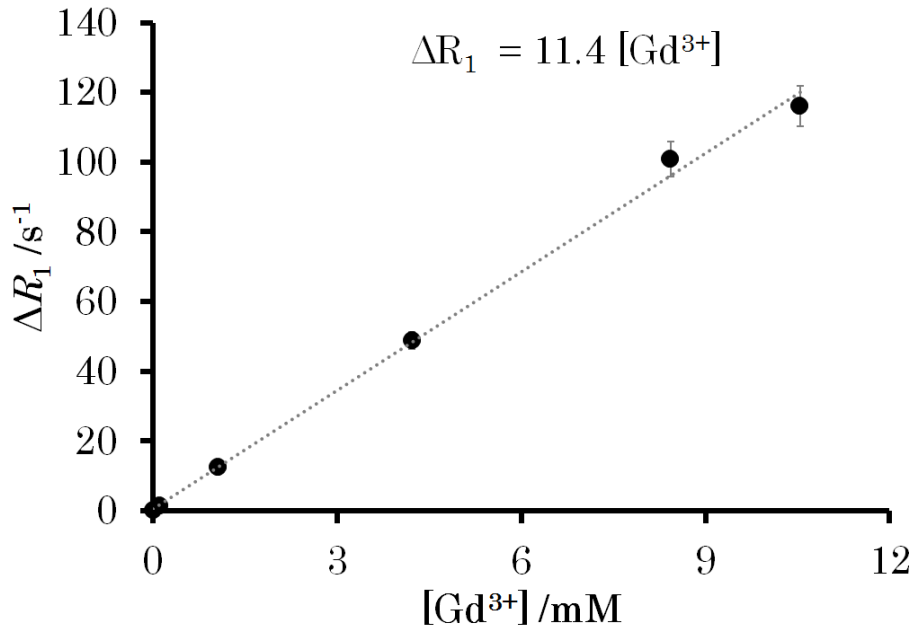

Figure 3.2: Proton relaxation rate of aqua Gd^{3+} solution due to PRE effect plotted against the concentration of aqua Gd, showing a relaxivity of $11.4 \pm 0.2 s^{-1} mM^{-1}$.

Table 3.1: Calculated relaxivity of aqua Gd complex as a function of correlation time τ_r and viscosity η.

T (K)	η (Pa s)	τ_r (ns)	$\frac{3\tau_r}{1+\omega_H^2\tau_r^2}+\frac{7\tau_r}{1+4\omega_S^2\tau_r^2}$ (10^{-10})	T_{1m} (μs)	R_{1p} (s^{-1} mM^{-1})
278	0.001501	94.94	2.849	7.274	19.797
283	0.001299	80.73	2.426	8.541	16.861
288	0.001136	69.35	2.087	9.927	14.506
293	0.001002	60.11	1.812	11.432	12.596
295	**0.000955**	**56.90**	**1.717**	**12.067**	**11.933**
298	0.00089	52.54	1.587	13.054	11.031
303	0.000797	46.26	1.401	14.789	9.737
308	0.000718	41.02	1.246	16.634	8.657
313	0.000651	36.59	1.115	18.583	7.749

3.4 Calculation of the relaxivity of Gd-complex solutions in wet cell samples

The relaxivity of extracellular aqua Gd solution was calculated with equations 3.1 - 3.3. The correlation time of aqua Gd complex was computed with a radius of the complex of 3.87 Å [90] and the viscosity reported in section 1 for eight water molecules in the inner coordination sphere. This calculation gave a relaxivity of 34.5 s^{-1} mM^{-1}. The intracellular relaxivity was also calculated in the same way. Since the intracellular water is composed of the bulk and the first hydration sphere water, the relaxivity in intracellular water was averaged as equation 3.4. This calculation gave a relaxivity of the intracellular aqua Gd complex solution of 25.4 s^{-1} mM^{-1}.

The extracellular and intracellular relaxivity of Gd-DOTA complex was also calculated by the above method. The radius of the complex was set at 4.0 Å [92]. Consequently, the relaxivity was 4.81 and 3.50 s^{-1} mM^{-1} for the extracellular and intracellular Gd-DOTA solutions, respectively.

3.5 Distribution of gadolinium complexes in *E. coli* sample studied by NMR

3.5.1 NMR experiment of *E. coli* sample without gadolinium solution

Since water generally accounts for 70% of an *E. coli* cell [71], the largest signal in the ^{1}H NMR spectra of *E. coli*-glycerol samples is due to hydroxyl proton of water and glycerol (Figure 3.3). The water proton exchanges with the hydroxyl proton of glycerol at a rate much faster than the longitudinal relaxation rate. The smaller signal beside the hydroxyl peak was assigned to the methylene and methine protons of glycerol. The signals for the other cellular components did not appear noticeably. This is because those components have large chemical shift dispersion with the concentrations much lower than water and glycerol. Large rigid cellular components should give broad resonances due to strong ^{1}H–^{1}H dipolar interactions.

The experimental ^{1}H relaxation rate of *E. coli* samples in the absence of paramagnetic ions was 1.51 $\pm$ 0.31 and 0.887 $\pm$ 0.035 s^{-1} for intracellular and extracellular water, respectively, at 273 K and ^{1}H resonance frequency of 700 MHz. These relaxation rates were used to calculate the rotational correlation time and viscosity from equation 3.1. Given the coefficient $C = 3.39 \times 10^{-10}$ s^{-2} as in the previous section, the extracellular relaxation rate of 0.887 s^{-1} provided τ_r = 8.06 ps and the viscosity of 2.64 mPa.s from equation 3.2.

The rotational correlation time and viscosity of intracellular water were also calculated based on the same theory. Here, the intracellular water consists of the bulk water and the first hydration layer water surrounding macromolecules with the composition of 85% and 15%, respectively, according to the model developed by Persson and Halle [93-94]. Thus, the relaxation rate of the intracellular water is expressed as the sum of the relaxation rates of the bulk water and the first hydration sphere water:

$$R_{1,\text{intra}} = 0.85\, R_{1,\text{bulk}} + 0.15\, R_{1,\text{hyd}} \qquad (3.4)$$

where subscripts 'intra', 'bulk' and 'hyd' stand for the intracellular, bulk and first hydration layer water, respectively.

The correlation rate of the first hydration water is 15.6 time longer than bulk water in the model. By using equation 3.4,

$$\frac{1}{T_1} = 0.85\mathrm{C}\left\{\frac{\tau_{\text{r,bulk}}}{1+\omega^2\tau_{\text{r,bulk}}^2}+\frac{2\tau_{\text{bulk}}}{1+4\omega^2\tau_{\text{bulk}}^2}\right\}+0.15\mathrm{C}\left\{\frac{15.6\tau_{\text{r,bulk}}}{1+\omega^2(15.6\tau_{\text{bulk}})^2}+\frac{2\times15.6\tau_{\text{bulk}}}{1+4\omega^2(15.6\tau_{\text{bulk}})^2}\right\} \qquad (3.5)$$

equation 3.5 gave $\tau_{\text{r,bulk}}$ = 5.36 ps and $\tau_{\text{r,hyd}}$ = 83.6 ps (= 15.6 × $\tau_{\text{r,bulk}}$). Consequently, the viscosity was 1.76 and 27.4 mPa.s for the intracellular bulk water and the first hydration water, respectively. The obtained τ_c of the intracellular bulk water, 5.36 ps, agrees with τ_c predicted from empirical parameters for the bulk water, 5.26 ps. This agreement supports the assignment of the relaxation component with R_1 of 1.51 s^{-1} to the intracellular water.

.

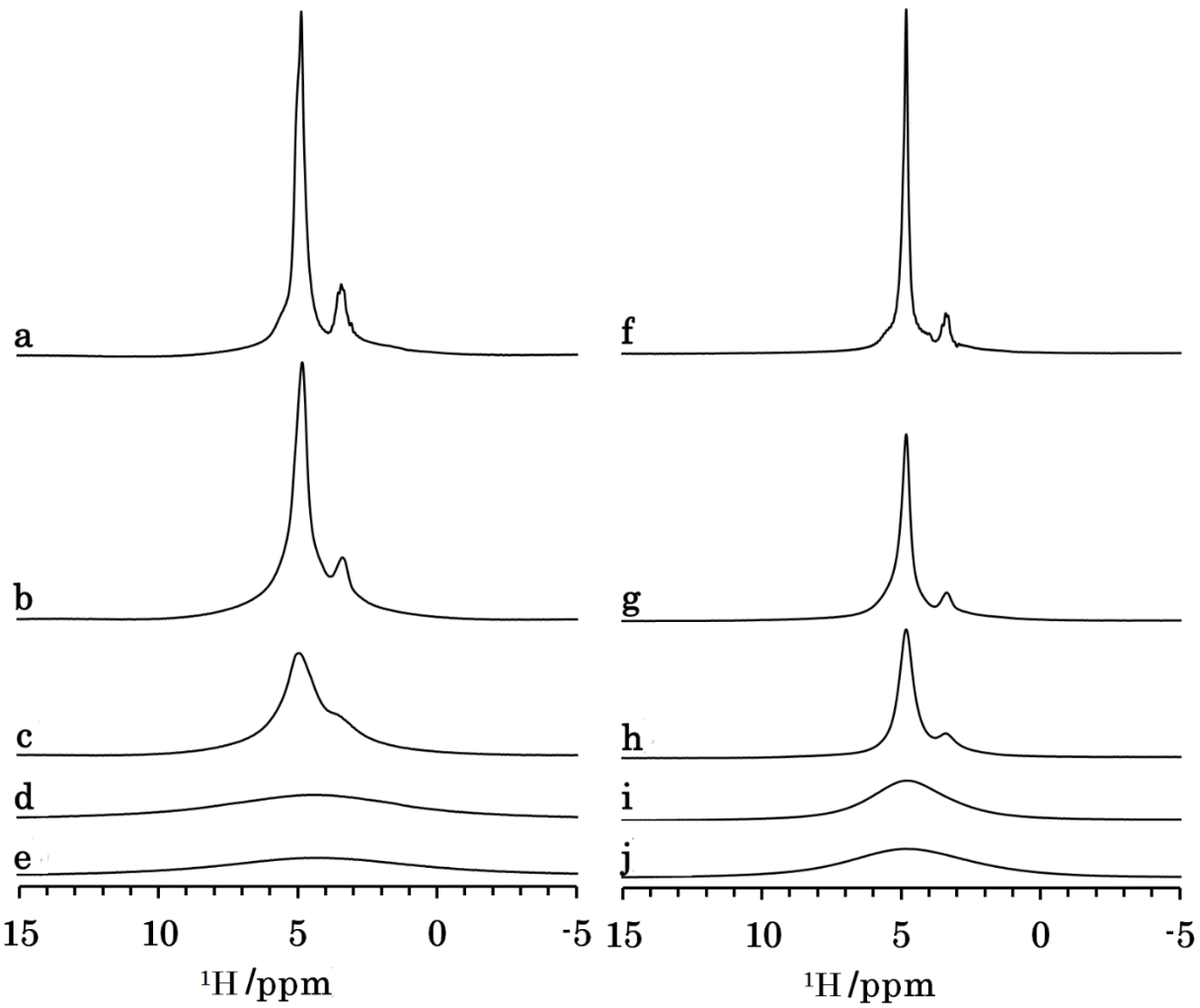

Figure 3.3: ^{1}H-NMR spectra of glycerol-*E. coli* solutions with aqua Gd (a-e) and Gd-DOTA (f-j) recorded at 273 K and a ^{1}H resonance frequency of 700 MHz. Solutions with 40 μl of glycerol-*E. coli* were mixed with 10 μl of 0 (a), 12 (b), 25 (c) 149 (d) and 250 mM (e) aqua Gd solutions. Solutions with 40 μl of glycerol-*E. coli* was mixed with 10 μl of 0 (f), 15 (g), 25 (h), 150 (i), and 250 mM (j) Gd-DOTA solutions.

To estimate the concentration of glycerol in the extracellular part from R_1, R_1 of water proton in a solution at a known glycerol concentration of 20% *v/v* was measured. This glycerol solution with an experimental R_1 of 0.98 s^{-1} gave τ_c of 9.43 ps and η of 3.09 mPa.s. The experimental R_1 of the extracellular water was converted to τ_c of 8.06 ps with η of 2.64 mPa.s.The extracellular water η relative to η of the 20% *v/v* glycerol solution provided a glycerol extracellular concentration of about 17%. This concentration agrees with the concentration of glycerol in the extracellular solution 16.9 - 22.7% *v/v* obtained from the added amount of glycerol under the assumption that the glycerol did not penetrate into the cytoplasm

(section 3.2). This agreement also supports the assignment of the relaxation component with R_1 of 0.887 s^{-1} to the extracellular water.

3.5.2 PRE for aqua Gd and Gd-DOTA solutions

The *E. coli* solutions with aqua Gd gave ^{1}H-NMR spectra similar to the spectra of those with Gd-DOTA (Figure 3.3). The methylene and methine signals broadened and disappeared owing to the transverse PRE with the increase in the concentration of the gadolinium complexes.

The relaxation rate of water protons in the cellular samples increased with the added amount of Gd complexes (Figure 3.4). The Gd complex concentration of the intracellular and extracellular parts given by the vertical axes on the right of figure 3.4 c,d was obtained by using the relaxivity. The relaxivity of Gd complexes were calculated from the viscosities obtained in the analysis for *E. coli* samples without Gd. The relaxivity of aqua Gd complex was 25.4 and 34.5 s^{-1} mM^{-1} for the intracellular and extracellular solutions and that of Gd-DOTA complex was 3.50 and 4.81 s^{-1} mM^{-1}, respectively. This relaxivity was calculated for the proton-Gd ion distance of 3.2 Å in the complexes as given in section 3.3 and 3.4. Though the relaxivity of aqua Gd complex for extracellular water was higher than that for intracellular water only by a factor about 1.4, R_1 of extracellular water was more than 3-fold faster than the intracellular water at every addition of Gd complex solutions with different Gd amount. This indicates that the concentration of aqua Gd complex in the extracellular part was higher than that in the intracellular part significantly. The extracellular R_1 increased non-linearly with the amount of added aqua Gd complex as shown in figure 3.4 c.

Table 3.2: Extracellular and intracellular amplitudes and relaxation rates of 40 µl of *E. coli*-glycerol sample mixed with 10 µl aqua gadolinium and Gd-DOTA solution.

Agent	[Agent]	Extracellular solution		Intracellular solution	
	(mM)	Amplitude (%)	R_1 (s^{-1})	Amplitude (%)	R_1 (s^{-1})
-	0	68 ± 25	0.89 ± 0.03	32 ± 25	1.5 ± 0.3
$[Gd(H_2O)_8]^{3+}$	12	25 ± 3	14 ± 3	75 ± 3	1.7 ± 0.2
	25	35 ± 10	36 ± 21	65 ± 10	3.6 ± 2.3
	100	62 ± 3	77 ± 2	38 ± 3	10 ± 1
	149	55 ± 16	170 ± 26	44 ± 16	37 ± 11
	200	74 ± 6	744 ± 124	26 ± 6	47 ± 21
	250	75 ± 3	965 ± 429	25 ± 3	25 ± 7
Gd-DOTA	15	16 ± 1	34 ± 1	84 ± 1	12 ± 0
	25	37 ± 5	45 ± 1	63 ± 5	16 ± 0
	100	56 ± 0	121 ± 7	44 ± 0	16 ± 3
	150	68 ± 4	182 ± 15	32 ± 4	34 ± 6
	200	65 ± 3	223 ± 30	35 ± 3	24 ± 7
	250	73 ± 1	259 ± 32	27 ± 1	26 ± 6

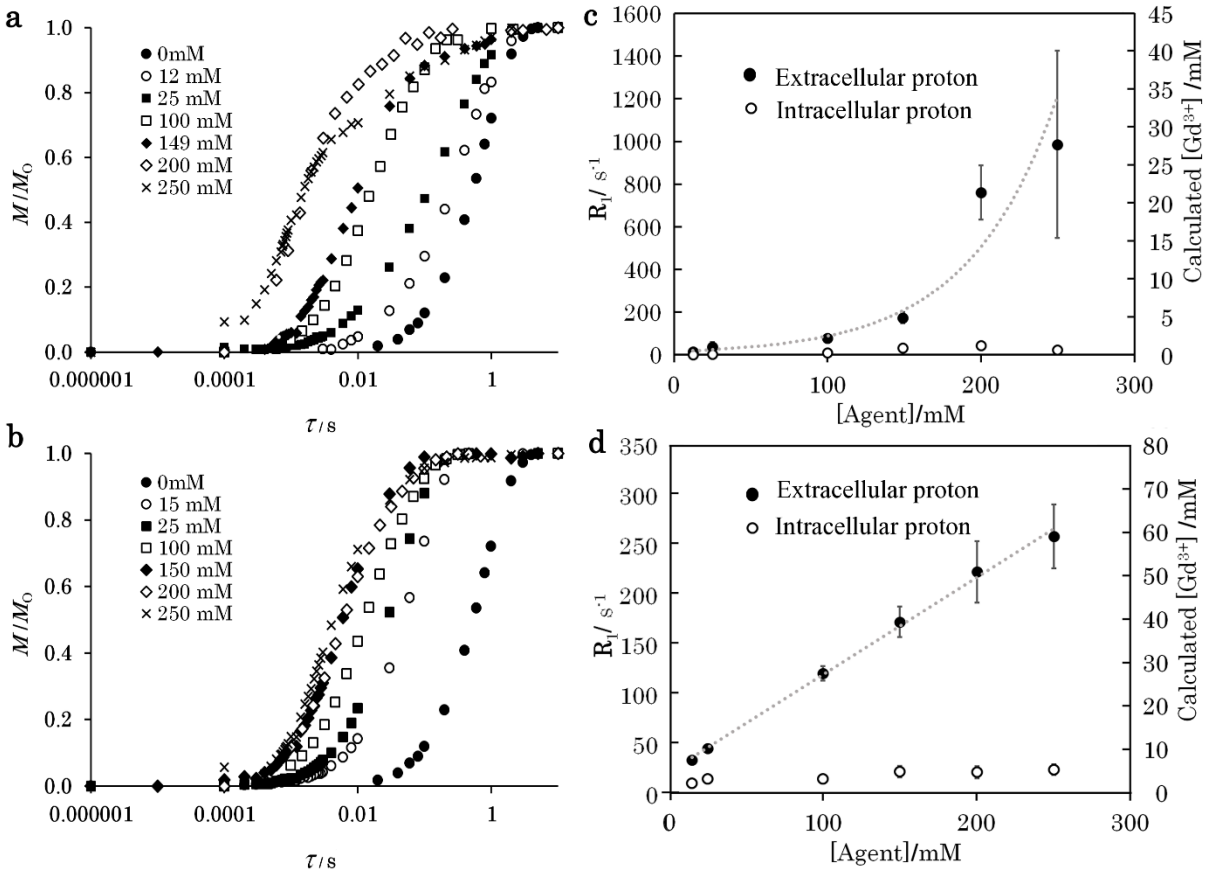

Figure 3.4: Buildup curves of the ^{1}H polarization (a, b), relaxation rate R_1 and cellular Gd complex concentration calculated from R_1 as a function of the concentration of added Gd complex solutions (c, d). These buildup curves, R_1 and cellular Gd concentrations are shown for 40 μl of glycerol-*E. coli* mixed with 10 μl of aqua Gd (a, c) or Gd-DOTA solutions (b, d). R_1 only for the intracellular water is 73% of the values given by the vertical axes on the left for Panels c and d, because the vertical axes are scaled by the relaxivity for the extracellular water.

The amount of Gd^{3+} was calculated from the intracellular and extracellular proton relaxation rates R_1. This amount relative to the total amount of Gd^{3+} added as solution with the known aqua Gd and Gd-DOTA concentrations is shown in figure 3.5. The relative Gd^{3+} amount was much lower than 100% only for aqua Gd. The reduction of this amount, the capability of Gd^{3+} for PRE, indicates that the exchangeable water molecules were prevented from accessing the unpaired electrons in Gd^{3+}.

In contrast to R_1 for aqua Gd, R_1 of the extracellular part for Gd-DOTA increased in proportion to the added amount (Figure 3.4d). Amount of Gd-DOTA calculated from R_1 relative to the total amount of Gd-DOTA was about 76-116% as in figure 3.5. Thus, this R_1 shows that Gd-DOTA was dissolved in the *E. coli* sample in contrast to aqua Gd.

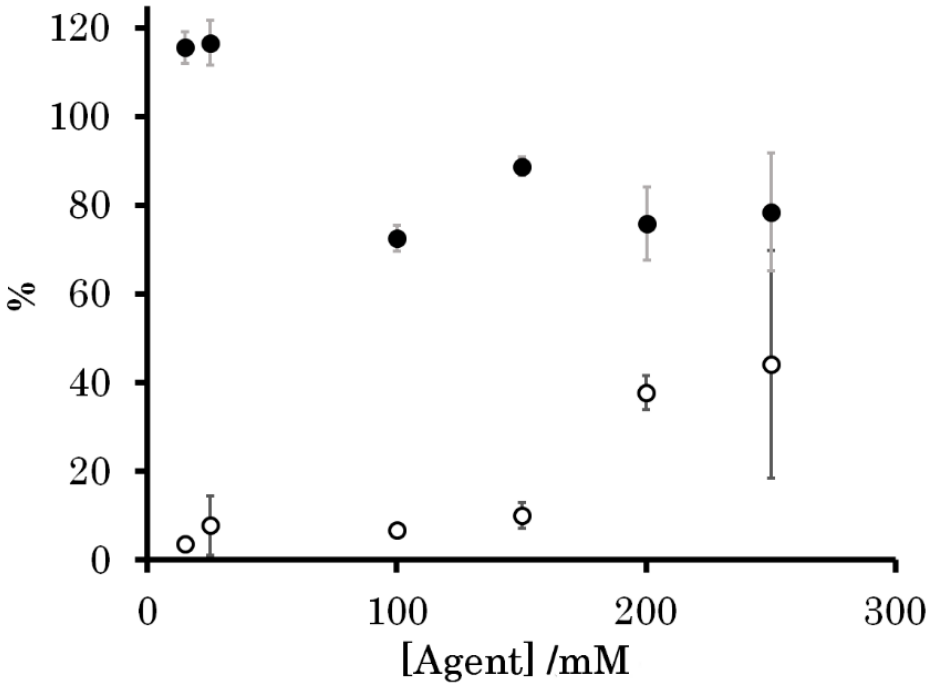

Figure 3.5: Percentage by mass of Gd^{3+} ion in solution states relative to the mass added to the samples as calculated from relaxation rate R_1 for glycerol-*E. coli* samples containing aqua Gd (open circle) and Gd-DOTA (closed circle). The horizontal axis shows the concentration of added 10 μl Gd complex solutions.

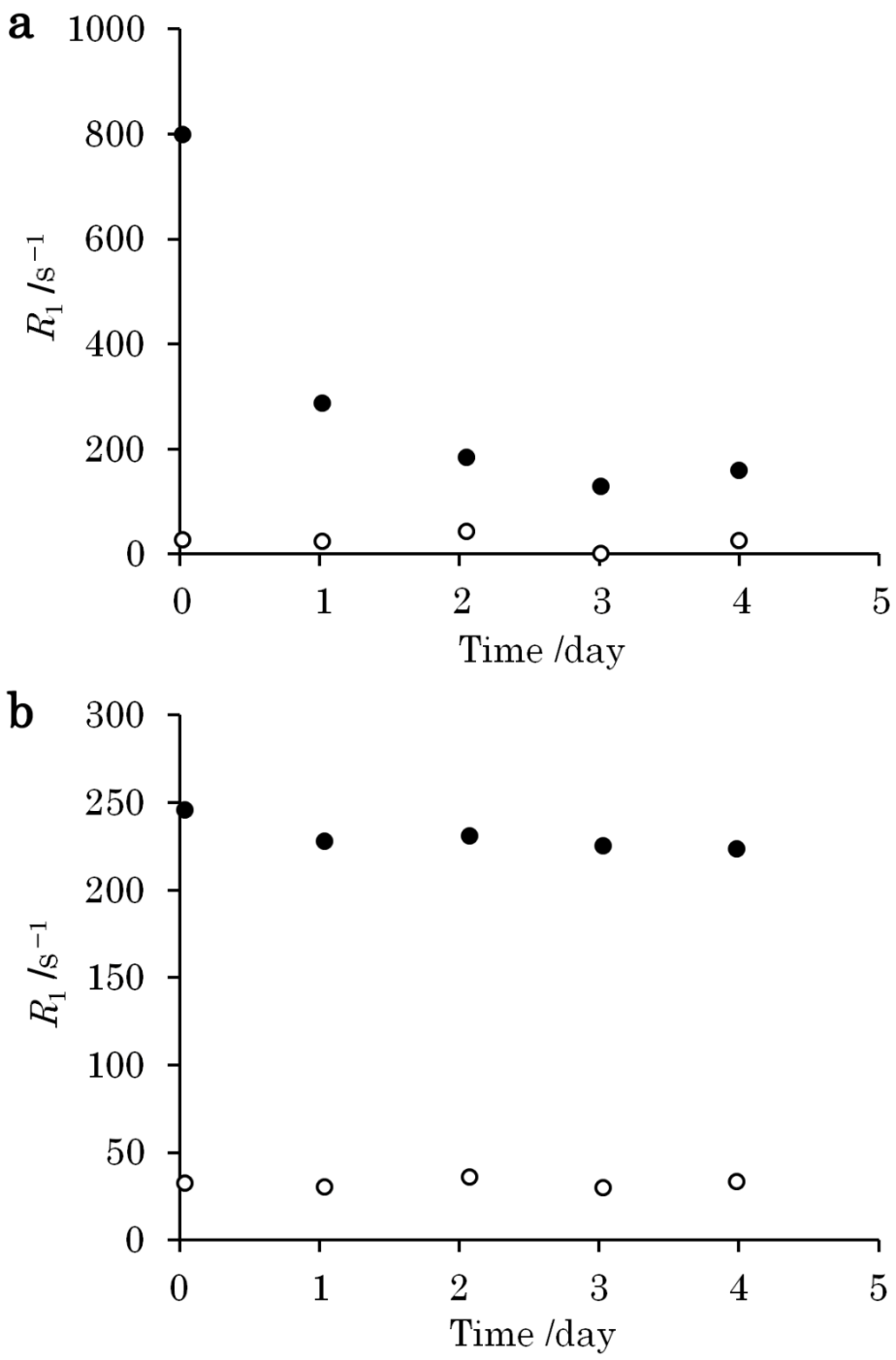

Figure 3.6: Intracellular (open circle) and extracellular (closed circle) relaxation rates plotted against the time after adding each of 10 μl of 250 mM aqua Gd (a) and 250 mM Gd-DOTA (b) solutions to a 40 μl *E. coli*-glycerol sample at 273 K.

3.5.3 Solid-state ^{13}C NMR spectra

CPMAS and single pulse experiments, respectively, provide solid-state ^{13}C-NMR spectra for only static parts and those for all the static and mobile parts of the *E. coli* cell samples. The CPMAS and single pulse experiments gave similar spectra for the *E. coli* cells without paramagnetic agents at an experimental temperature of 218 K as shown in figure 3.7 c and f. Thus, all the cellular components including biological macromolecules were in a static state at the low temperature.

The solid-state ^{13}C-NMR spectra of the *E. coli* sample with Gd-DOTA were similar to those without Gd complexes. The *E. coli* sample with the aqua Gd complex, however, gave the spectra exhibiting a conspicuous reduction of the methylene peak intensity at 35.5 ppm. This ^{13}C resonance was assigned to $^{13}CH_2$ in the acyl chains of lipids in the cell membranes [46]. Its peak had the strongest signal height in the spectra of gadolinium-free and Gd-DOTA containing samples owing to its large molecular composition of lipid 9% in *E. coli* cells [54]. This strong peak was suppressed due to PRE by Gd^{3+} only in the spectra of the sample containing aqua Gd. This specific reduction of the methylene carbon signal indicates that Gd^{3+} bound to phospholipids in the bilayer membranes [95-96]. The Gd^{3+} paramagnetic fields should suppress more than half of the lipid signal of methylene carbons which are located within about 1 nm of Gd^{3+} ions [78, 97]. The methyl carbon signal of lipid at 16.8 ppm [98-100] was not much affected by this PRE effect because the methyl carbons would be about 2 nm away from Gd^{3+} ions in the interface region of the bilayer membranes.

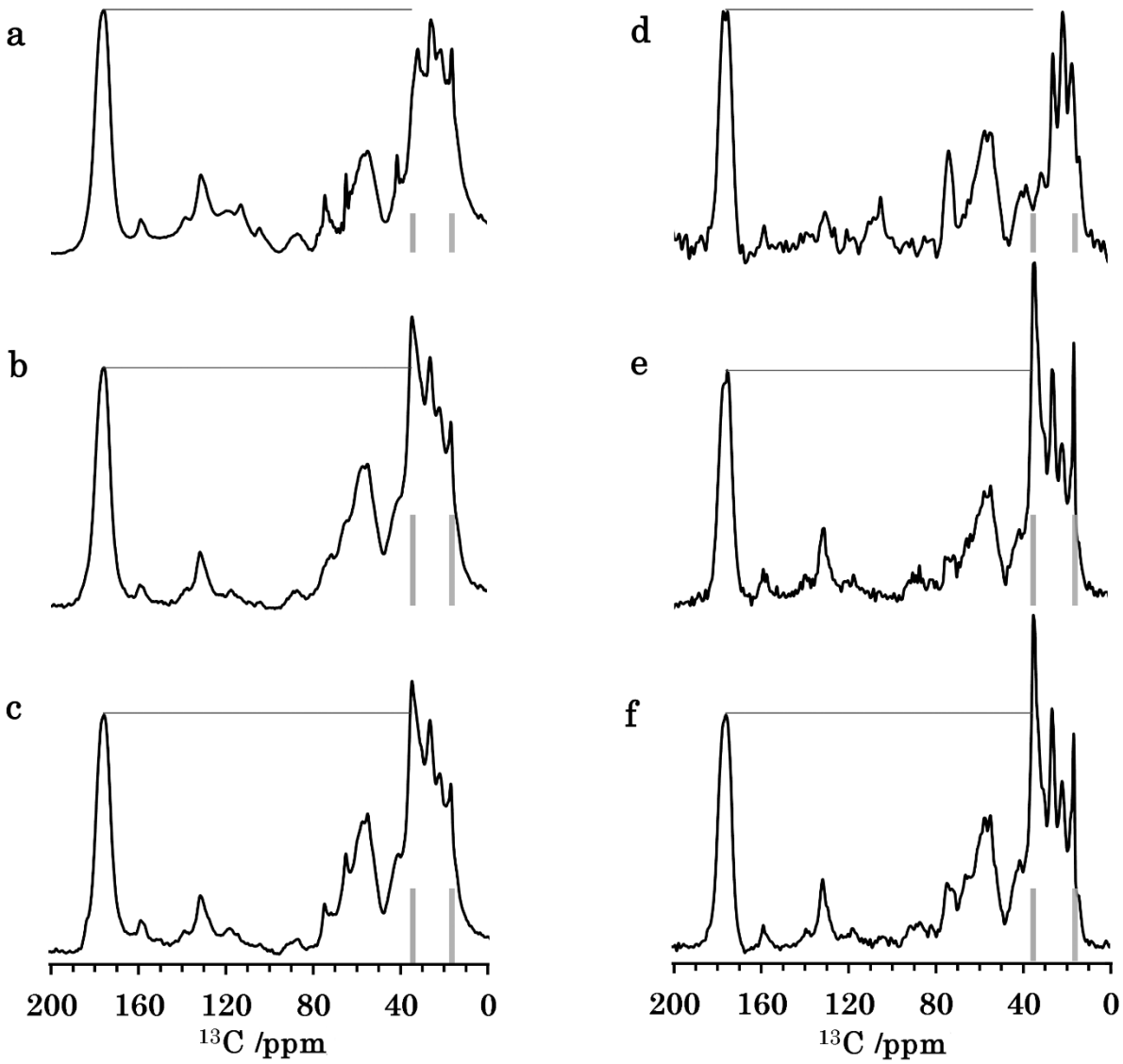

Figure 3.7: Solid-state ^{13}C-NMR spectra recorded by single 90˚ pulse (left column) and CPMAS (right column) experiments of *E. coli* samples in the presence of aqua Gd (a, d), Gd-DOTA (b, e), and NaCl (c, f) solutions. Resonances for methylene carbon (35.5 ppm) and methyl carbon (16.8 ppm) of membrane lipids and carbonyl peak height are indicated by lines to guide the eye.

3.5.4 Viability of *E. coli* cells and PRE effect on the cellular ^{1}H resonance in the agents

The viability of *E. coli* incubated after mixing with a 150 mM Gd-DOTA solution was tested by measuring the number of colony-forming unit (CFU) on LB plates [101]. The experimental results for *E. coli* samples mixed with solution at a concentration of 250 mM were not obtained with high reproducibility. Thus a 150 mM solution which gave a sample concentration close to salt concentration of the native cellular environment [102-103] was selected. The normalized CFU ratio showed that about 90% of the *E. coli* cells incubated in the Gd-DOTA solution were still alive in three hours (Figure 3.8), which can be characterized by time constant of 36 hours for an exponential decrease. R_1 measurements for the cells finished within 40 min so that the experiments provided the relaxation rates of the samples in which more than 90% of cells were alive. In contrast, the *E. coli* sample incubated with 149 mM aqua Gd solution displayed its colony formability less than 10% after the incubation for 10 min.

R_1 of the sample added with 250 mM aqua Gd solution repeatedly over several days was measured in order to examine its dependence on the time elapsed after the sample preparation. The extracellular relaxation rate dropped with the time constant of 1.09 ± 0.44 day for the exponential decrease (Figure 3.6a). Since the intracellular R_1 and the amplitudes of intracellular and extracellular proton did not change more than by 10%, the declination of extracellular R_1 should not occur owing to the cell lysis or internalization of aqua Gd complex into the cytoplasmic solution. Thus, this observation for the extracellular R_1 should reflect the adsorption of Gd^{3+} ions by the cellular components. In contrast to the effect of aqua Gd, the *E. coli* sample added with 250 mM Gd-DOTA solution gave the extracellular and intracellular relaxation rate changes by less than 10% during the period of four days (Figure 3.6b). This slow relaxation rate change can be characterized as the initial process of an exponential reduction with a time constant of 41.7 ± 6.1 day. Therefore, Gd-DOTA has an advantage over aqua Gd in the long-term stability of PRE effect on the cellular ^{1}H resonance.

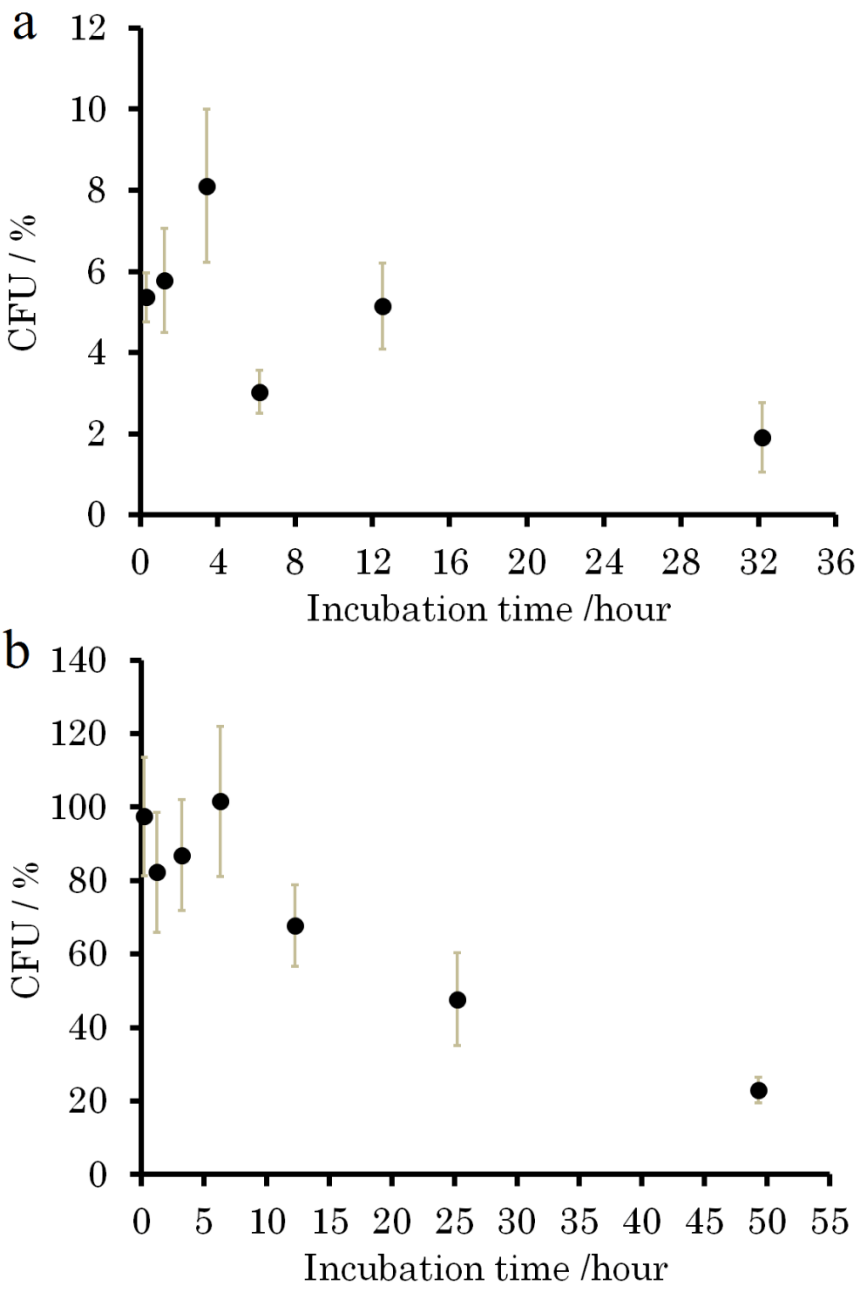

Figure 3.8: Percentage of colony-forming unit of *E. coli* cells mixed with 149 mM aqua Gd (a) and 150 mM Gd-DOTA (b) solutions relative to the control sample mixed with a 150 mM NaCl solution. The error bars show the standard deviation of the experimental results of two separate samples (n = 2).

3.6 Localization of biomolecules in *E. coli* cells as studied by ^{13}C-NMR observation of ^{1}H paramagnetic relaxation

3.6.1 Assignment of ^{13}C-NMR signals of cellular macromolecules

In order to assign the NMR peaks of cellular macromolecules, the experimental 1D and 2D PDSD ^{13}C NMR spectra of cell samples in absence of Gd-DOTA complex were compared with the simulated spectrum. The spectrum simulated without the contribution of nucleotide signal showed a good agreement with the experimental results (Figure 3.9). As *E. coli* cells were cultured in M9 medium containing 0.08 g/l non-labeled nucleoside, *E. coli* cells possibly used a non-labeled nucleoside in the medium as a substrate for their nucleotide synthesis. Thus, the signals of nucleotide did not appear evidently on the experimental NMR spectra except the small peak at 93 ppm [46].

In contrast to above sample, the cells grown in nucleoside-free medium provided the spectrum with more prominent nucleotide peaks. These nucleotide signals were still not strong enough to be analyzed their locational-dependence PRE effect (Figure 3.9). In addition to low abundance of labeled nucleotide in the cell sample, the signals for nucleotide are broader than those for the other macromolecules. Thus there is difficulty in assigning these signals [104].

The accuracy of the simulated spectrum was furthermore confirmed by considering the correspondence of its chemical shifts (Figure 3.10) with the cross peaks appeared on the experimental 2D ^{13}C-^{13}C NMR spectra (Figure 3.11). Hence, this simulated spectrum could be utilize for analyzing relaxation behavior of cellular macromolecule from ROSY spectra (Equation 2.18).

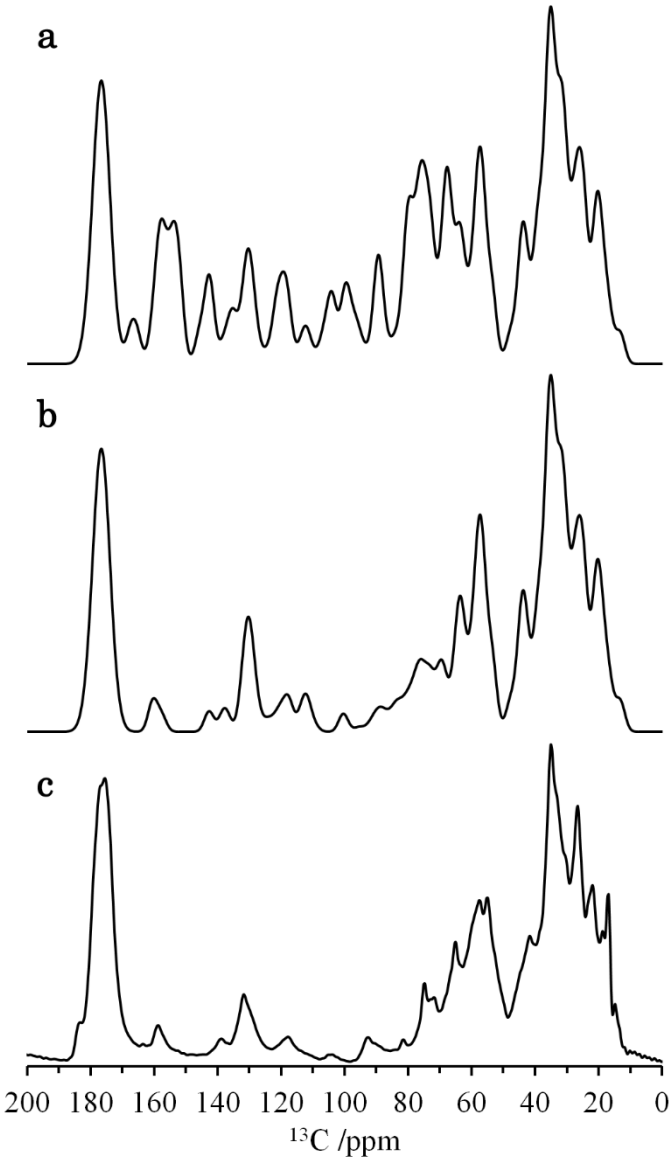

Figure 3.9: The experimental solid-state ^{13}C NMR spectra of *E. coli* sample in absence of Gd-DOTA solution recorded by 500 MHz NMR spectrometer via single 90˚ pulse (c) is more similar to the simulated spectrum excluding nucleotide signals (b) than the simulated spectrum including nucleotide signals (a). This indicates that the experimental solid-state ^{13}C NMR spectra contain only small amount of nucleotide signals.

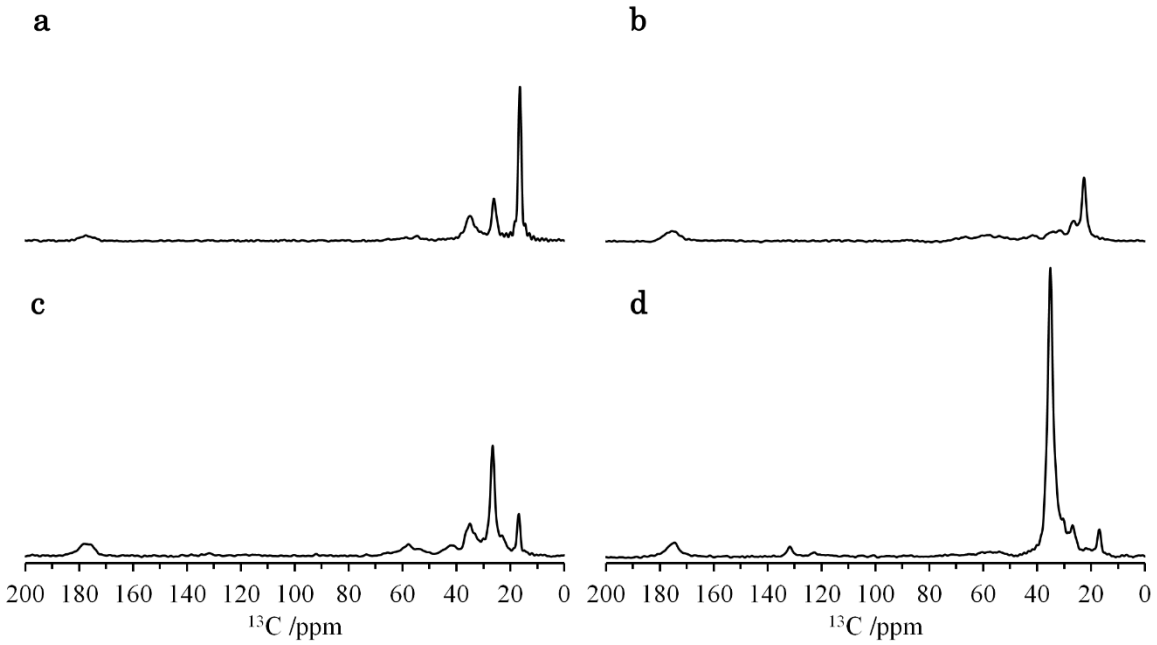

Figure 3.10: Cross sections of the proton driven ^{13}C spin diffusion 2D ^{13}C-^{13}C dipolar correlation ^{13}C NMR of *E. coli* sample without Gd-DOTA solution at a) 16.8, b) 22.7, c) 26.5 and d) 35.0 ppm shows high contribution of lipid on the peak at 16.8 and 35.1 ppm and protein signal on the peak at 22.7 ppm contains higher amount of protein.

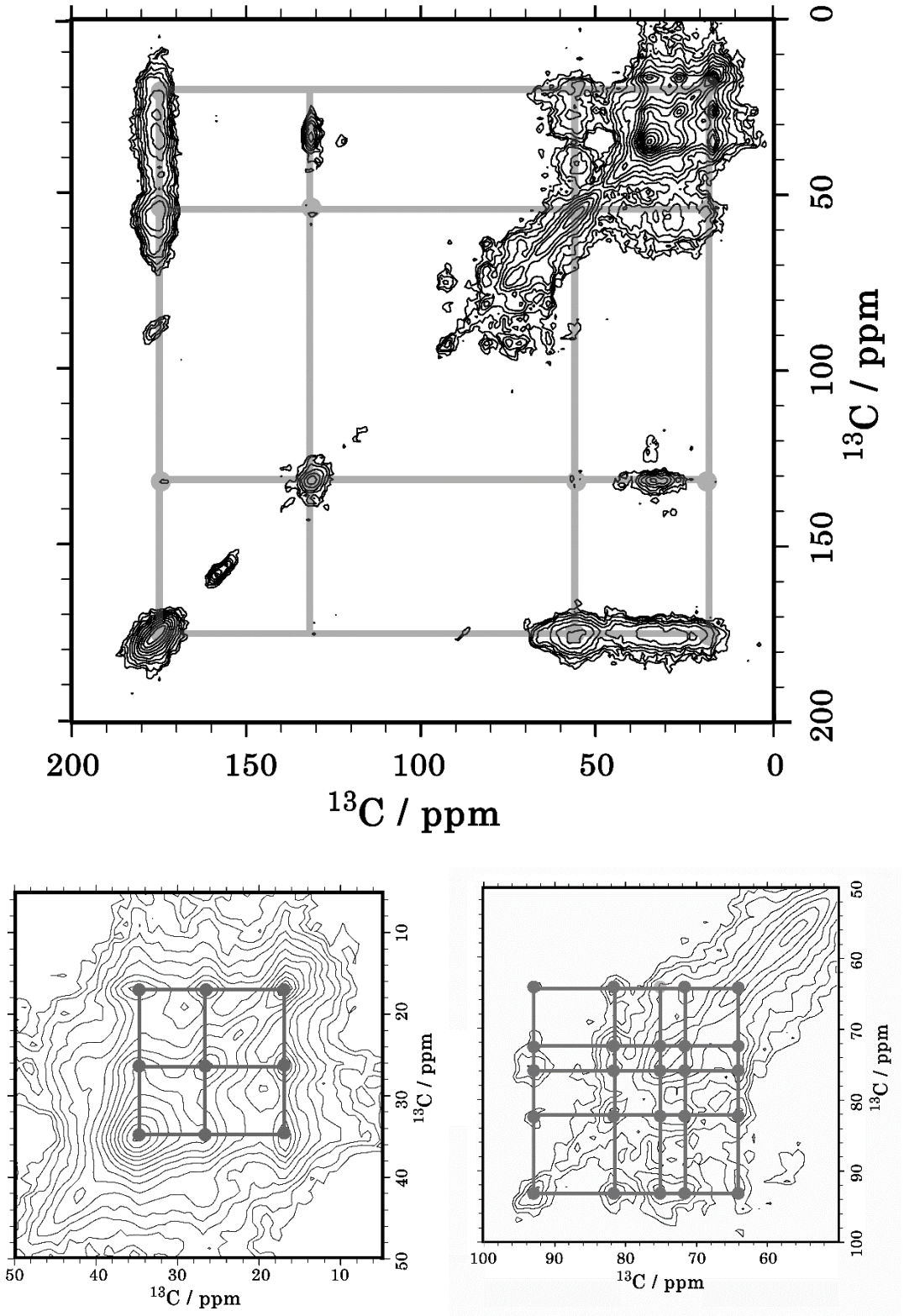

Figure 3.11: The proton driven ^{13}C spin diffusion 2D ^{13}C-^{13}C dipolar correlation spectra of an *E. coli* sample in absence of Gd-DOTA solution recorded by a 500 MHz NMR spectrometer showing the cross peak of protein (a), lipid (b) and sugar (c)

3.6.2 Predicted proton relaxation rate of the frozen cell sample containing Gd-DOTA solution

The relaxation rate of the frozen cell sample was measured by solid state NMR spectrometer. (see section 2.2.2 for more details). In ssNMR, ^{1}H-^{1}H spin diffusion effect could promote or compete with PRE of paramagnetic agent. There are three different PRE regimes in solid-sample including 1) relaxation without spin diffusion regime, 2) relaxation with limited spin diffusion regime and 3) relaxation with rapid spin diffusion regime. (see section 2.2.4.1 for more details). The boundary *b* in which spin diffusion effect is quenched could be calculated from equation 2.10. Given that a = 2.5 Å [105], $\mu_p = 9.28 \times 10^{-24}$ J.T^{-1} [106] and $\mu_n = 1.41 \times 10^{-24}$ J.T^{-6} [106], boundary *b* of gadolinium ion is 22 Å. The boundary β, where nuclei inside mainly effected by PRE, was calculated using D of 0.8 nm^2 ms^{-1}, $K = 3.7 \times 10^{-8}$/T [77] (equation 2.9) = 2.05×10^{-52} s^{-1} m^6. Equation 2.11 gives β = 6.5 Å. The boundary R distance between Gd^{3+} ions depends on concentration of Gd-DOTA complex (equation 2.12). The relaxation rates of intracellular and extracellular NMR measured by solution NMR spectroscopy suggested that the intracellular and extracellular concentrations of Gd-DOTA are 9 ± 2 and 37 ± 4 mM respectively. Thus, R = 21.5 ± 0.8 and 34.8 ± 2.6 Å for intracellular and extracellular proton. Therefore, the relaxation of intracellular and extracellular proton were most close to rapid spin diffusion regime. As consequence, the relaxation time of intracellular and extracellular proton were 375.6 ± 83.4 and 87.9 ± 9.5 ms respectively (calculated from equation 2.17).

3.6.3 Experimental proton relaxation rate of cellular macromolecules

The experimental NMR spectra were decomposed. The buildup of the signal areas under the prominent decomposed peaks were fitted with exponential relaxation function. The fitting results revealed similar relaxation times of the peaks on the spectrum of Gd-DOTA-free sample in the range from 963 to 1142 ms (Figure 3.12a). The sample in presence of Gd-DOTA, in contrast, showed a variation of the relaxation times among the peaks (Figure 3.12b). The peaks of phospholipids at 35.1 and 17.0 ppm showed short relaxation times in comparison with the other macromolecules. Since lipids are located mainly in the membranes of the cell, lipid molecules could experience PRE effect of extracellular Gd-DOTA solution stronger than the

other macromolecules. Thus, the short relaxation times of lipid peaks demonstrates its location-dependence.

The average extracellular and intracellular relaxation rates were analyzed from the buildup curve of the integral area in the ROSY spectra. The curve of the integral area against recovery time was fitted with double exponential relaxation equation (equation 2.19). The average extracellular and intracellular relaxation times analyzed by this method were 108 ± 26 ms and 393 ± 46 ms, respectively. As mention in section 3.1, the *E. coli* sample for ssNMR in this section should contain Gd-DOTA of 5 ± 1 and 39 ± 3 mM in the intracellular and extracellular parts respectively. Given the spin diffusivity of 0.8 nm^2/ms [107], the relaxation times calculated theoretically should be 376 ± 118 ms and 88 ± 13 ms for intracellular and extracellular magnetization components respectively (more details about calculation in Appendix).

The location-dependence of relaxation rate was moreover proved by the high-resolution 2D PDSD ^{13}C-NMR spectra. These spectra were obtained after applying saturation recovery pulse with recovery time of 2 s and 120 ms. The time delay and contact time for CP for these experiments were 2 sec and 1.8 ms respectively. Since the 1D NMR spectra revealed that the magnetization of all macromolecules relaxed completely at the recovery time of 2 s, the integral areas were normalized to the area under the spectrum recorded with recovery time of 2 s. On the 2D spectrum recorded with the recovery time of 120 ms, only the signal whose relaxation time is shorter than the recovery time could relax more than 50% of its equilibrium intensity. This mean only lipids could reach this level of relaxation. The PDSD 2D ^{13}C-NMR spectrum provided the results that well agreed with this approximation. The integral area of lipid peaks at 16.8 and 35.1 ppm recorded with the recovery time of 120 ms showed the magnetization intensity higher than 0.5. Under the same condition, the other peaks were lower than 0.5 in intensity (Table 3.3). This result confirms that the relaxation times of lipids which occupies only in the membranes close to the extracellular solution could experience stronger PRE effect than the other macromolecules.

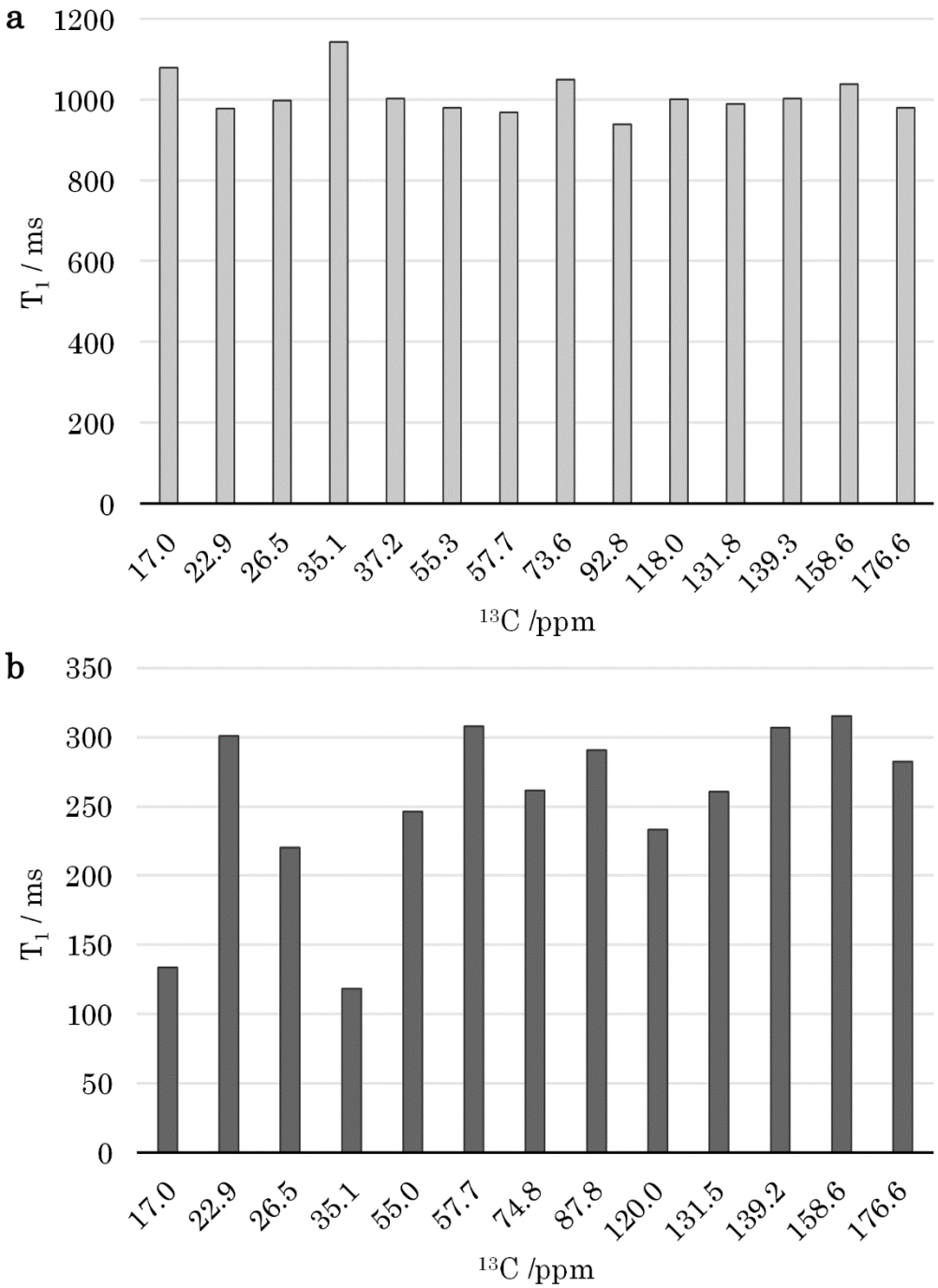

Figure 3.12: Bar graph showing similar relaxation times of the decomposed peak of ^{13}C NMR spectra of *E. coli* samples in absence of Gd-DOTA solution (a) and nonconstant relaxation times of the decomposed peaks of the spectra for the sample in presence of Gd-DOTA solution.

Table 3.3: Ratio of the integral area under the peak appear in 2D ^{13}C PDSD spectrum detected with the recovery time of 120 ms to those in the spectrum with the recovery time of 2 s.

Chemical shift (ppm)	Component	Ratio
35.1	Lipid	0.62
16.8	Lipid	0.54
75.1	Lipid, LPS, PG, Glycogen, RNA, DNA	0.33
131.9	Protein	0.28
176.6	Lipid, LPS, PG, Protein	0.38

The analysis of the buildup curve of the integral area for the ROSY spectra gave the relaxation times of the extracellular and intracellular protons of 108 and 393 ms, respectively. These relaxation times were used to fitted the ROSY spectra. The experimental spectra were fitted with the simulated spectrum and equation 2.18 in order to determine the contribution of extracellular magnetization propagating for each NMR peak (Figure 2.6).

The results of this analysis showed the mass ratios of cellular macromolecules that agree well with the statistical information (Table 3.4). It furthermore revealed the pattern of the ratio of slow and fast relaxing magnetizations contributing to the peaks of each macromolecule (Figure 3.14). The fast relaxing spins diffusing from Gd-DOTA-rich extracellular part of the cell contributed 84 % on the signal of the lipid appearing on ROSY spectra. The amplitudes of slow and fast relaxing magnetizations of sugar peaks are also related to the locations of sugar that occupies on the cell walls (peptidoglycan and lipopolysaccharide) close to extracellular solution and in the cytoplasm (glycogen). The amplitude of the fast relaxing spin in protein peaks of 27 % also corresponds with the abundance of protein (inner, out membrane and periplasmic proteins) on cell wall of 22% of all protein in the cell. This total amount of protein was calculated on an assumption that cell has no flagella and pili [108]. The signal nucleotide which occupies deeply in the cytoplasm slowly relaxed under the influence of intracellular PRE effect only.

The amplitudes of the slow and fast-relaxing magnetization components extracted from the ROSY spectra were further used to simulate the relaxation curve of each cellular macromolecules (Figure 3.15). A variety of the shapes of the buildup curves confer an advantage in predicting the location of macromolecule in *E. coli* cells.

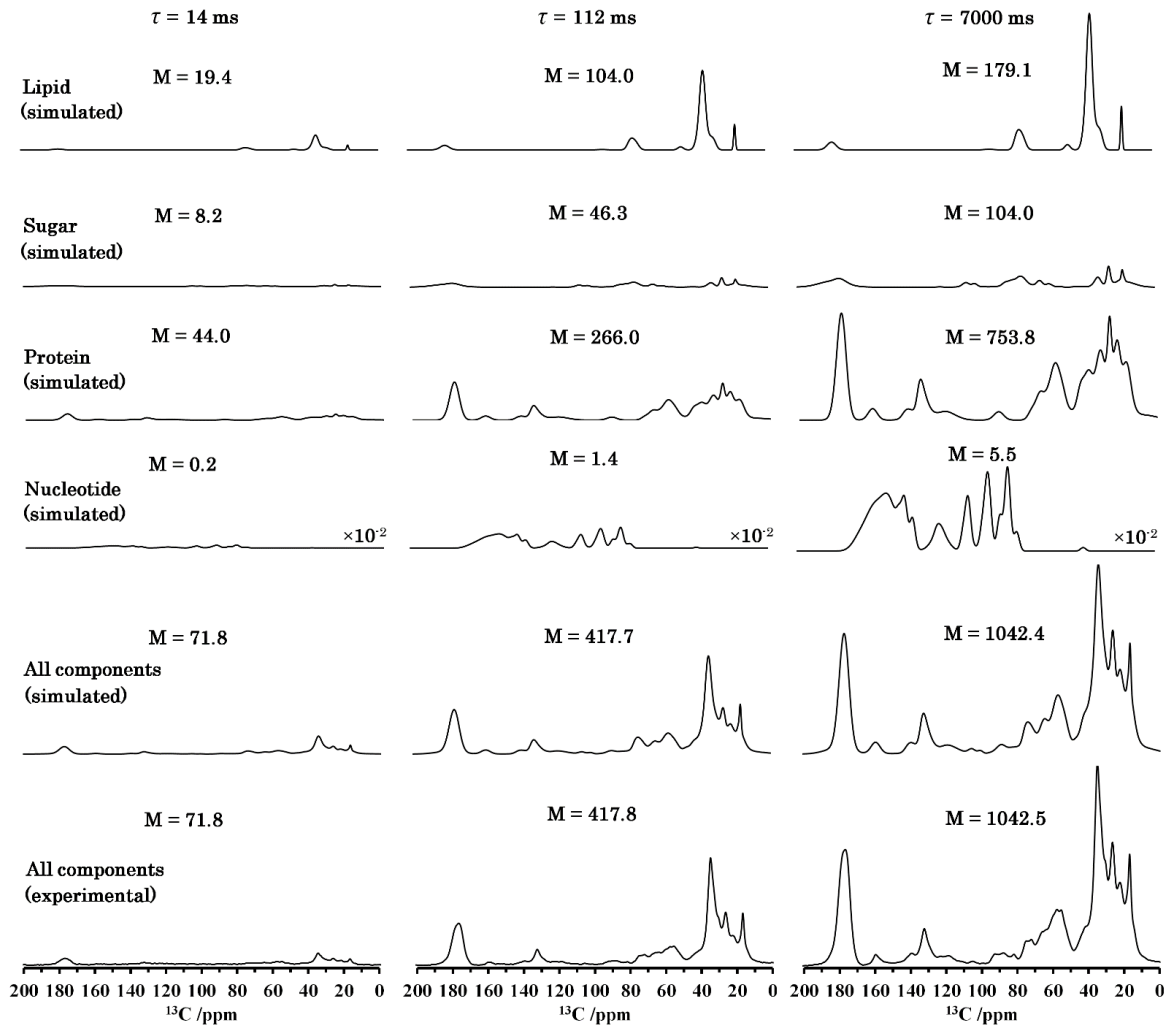

Figure 3.13: The experimental and simulated ^{13}C NMR spectra of cellular components. The simulated spectra were calculated based on the fitting result in figure 3.9 for which the relaxation rates of fast and slow-relaxing components are 108 and 393 ms, respectively.

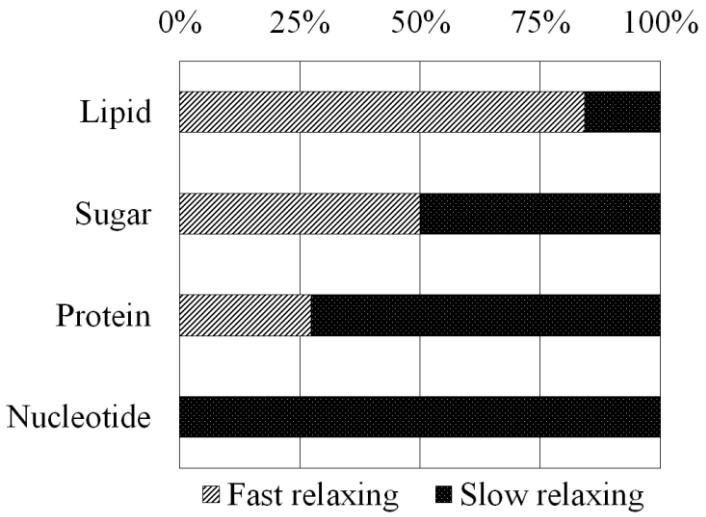

Figure 3.14: Fractions of the fast and slow-relaxing protons in cellular macromolecules analyzed by fitting the ROSY spectra of *E. coli* samples containing Gd-DOTA with the simulated spectra of the cellular components. The fast and slow-relaxing relaxation rates were given at 108 and 393 ms as analyzed from the buildup curve of the integral areas constituting the whole spectra.

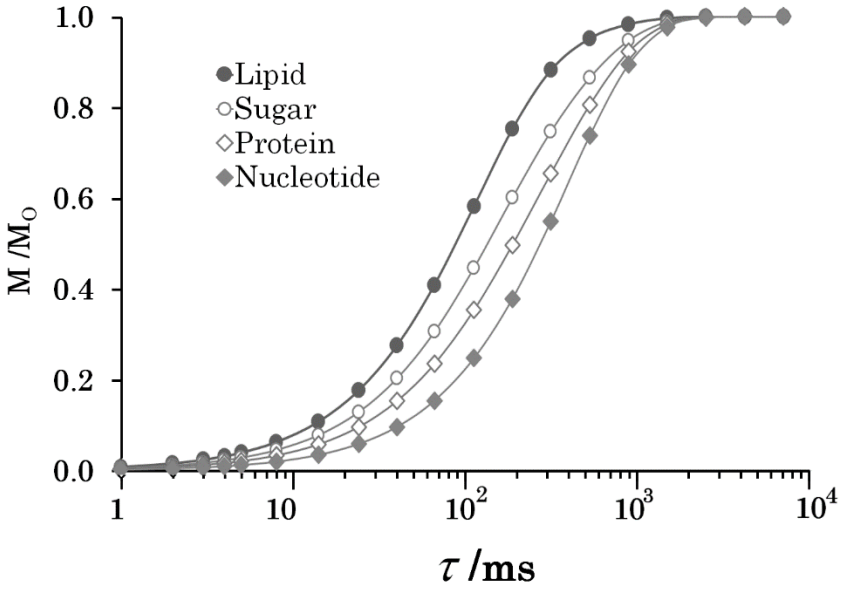

Figure 3.15: Relaxation curves of the cellular macromolecules simulated from data in Figure 3.14 showing the location dependence of the relaxation time of cellular macromolecules.

Table 3.4: Masses of cellular components fitted from ROSY spectra and statistical masses calculated with neglecting mass of nucleotide.

Cellular components	Statistical mass (%)	Fitted mass (%)
Lipid	15.9	10.0
Sugar	14.7	17.2
Protein	69.4	72.3
Nucleotide	0.0	0.5

3.6.4 Paramagnetic relaxation in model *E. coli* systems under proton spin diffusion

The diffusion of the proton magnetization through the solid cell sample was modelled on the basis previously described. The proton diffusion coefficient was set at 0.8 nm^2/ms, the intracellular and extracellular relaxation times were given as the values derived from the buildup curve of the areas for ROSY spectra (108 and 393 ms for $T_{1,ex}$ and $T_{1,in}$ respectively). The dimensions of extracellular and intracellular part were given at 850 and 400 nm as estimated from the ratio of extracellular and intracellular proton observed in the above solution state NMR experiments of cellular water protons. The relaxation study of liquid *E. coli* sample containing Gd-DOTA showed that the ratio of intracellular and extracellular proton were 32 ± 4 and 68 ± 4% respectively. By assuming that *E. coli* distributed homogenously in the sample and cell radius is 400 nm [71], the dimension of extracellular part is therefore 850 nm.

The simulation displayed the magnetization of cellular components around the interface between extracellular and intracellular parts relax with the rate between the relaxation rates of magnetization components in the two parts (Figure 3.16). In this model, the *x* position was set to 0 at the interface, increased to positive value in the extracellular part and declined along the intracellular part to negative value. The diffusion across the interface reaches its equilibrium at the recovery time of 7 s. Therefore, the magnetization density throughout the sample in this model become homogenous at 7 s. These calculation results are in good agreement with the experimental buildup curve of the decomposed ROSY peaks. This simulation also supported that the maximum recovery time of 7 s in the experiment allows proton spins of all cellular components to relax completely. The buildup curves plotted against the *x* coordinate expressed

characteristic shape in the *x* range of –20 to 20 nm (Figure 3.17). Hence, the relaxation rates of macromolecules in this range are the location-dependence. The relaxation rates of cellular components in this region could be assigned to the location inside the cells for macromolecules.

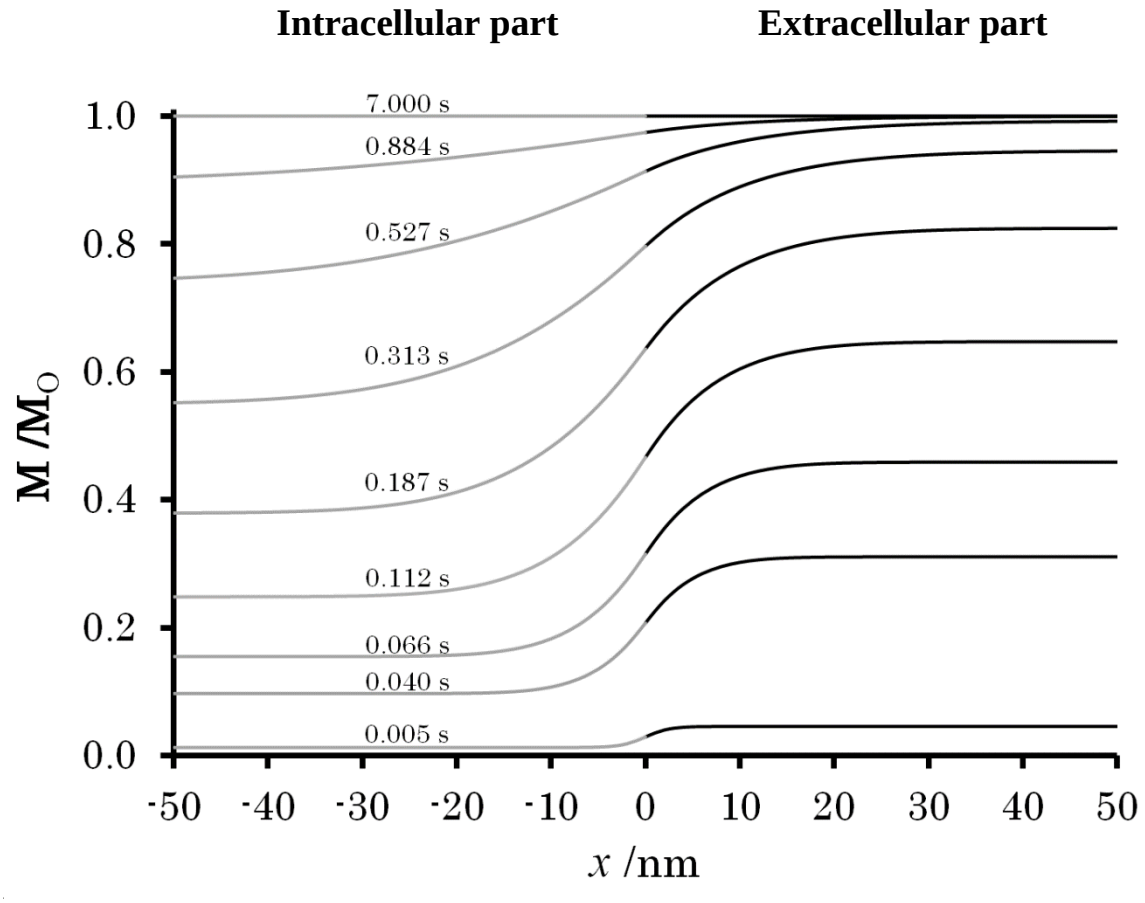

Figure 3.16: Relaxation profile of the magnetization at *x* as a function of recovery time calculated by the spin diffusion model of the cell. The fast and slow relaxation rates and spin diffusivity were given at 108 ms, 393 ms and 0.8 nm^2 ms^{-1}, respectively.

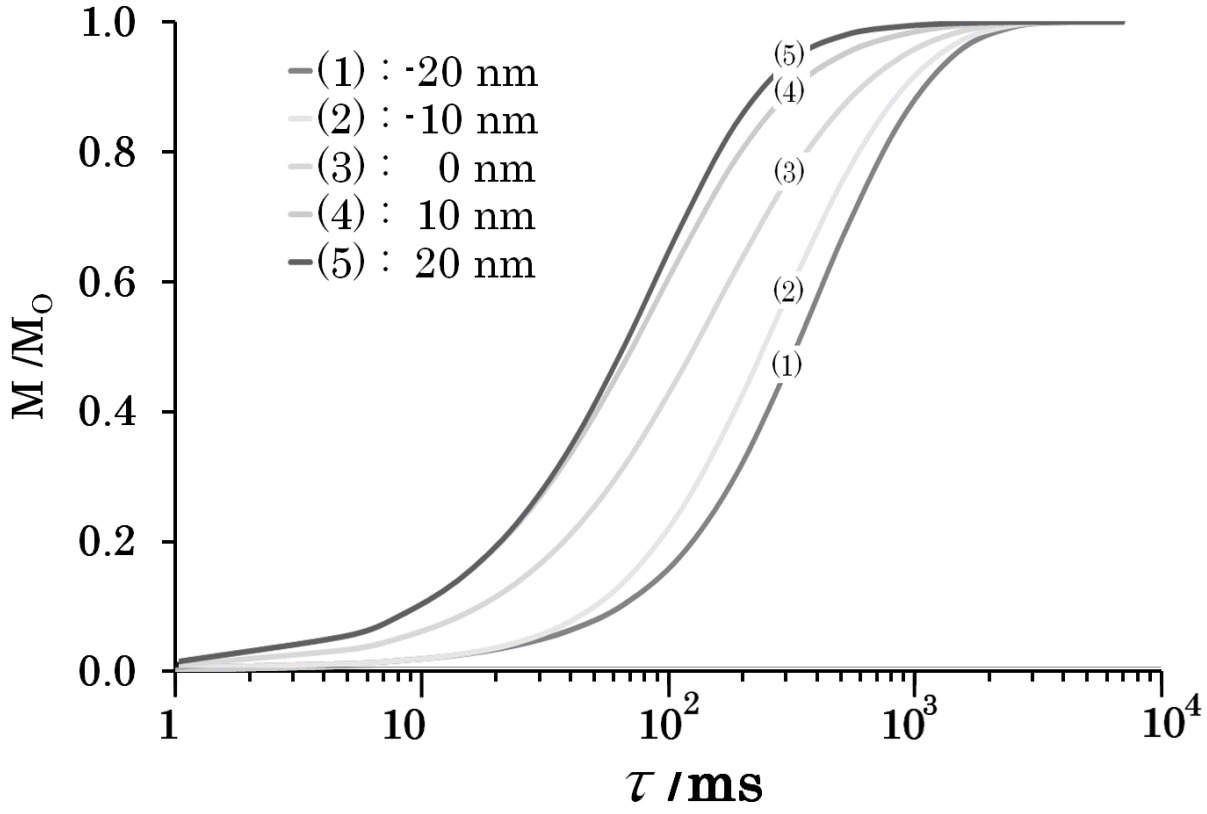

Figure 3.17: Relaxation curve of nuclear spin locating at position x = -20, -10, 0, 10, and 20 nm for the spin diffusion model of cells. The fast and slow relaxation rates and spin diffusivity were given at 108 ms, 393 ms and 0.8 nm^2 ms^{-1}. This suggests that experimental approach in this study could be applied to studying the location of macromolecule specifically locating within 20 nm from the center of the inner membrane of *E. coli* cells (from outer membrane to some part in the cytoplasm).

Chapter 4

Discussion

4.1 Gd complex concentration-dependence of ^{1}H-NMR relaxation rates

The relaxation rate of the resonance at about 4.7 ppm can be affected by protons other than water such as CH/CH_2 protons in glycerol. However those protons in glycerol should have a minor effect, less than by about 20%, on the averaged R_1. This is because 1) glycerol proton content relative to water protons was less than about 20%, and 2) R_1 for CH/CH_2 resonance was lower than that for water resonance, e.g. R_1 for CH/CH_2 and water was 66 and 200 s^{-1}, respectively, in a glycerol-water mixture at the Gd-DOTA concentration of 12 mM. As seen in the broadening of all the resonances in the spectra in figure 3.4 b, d, the CH/CH_2 resonance was affected by PRE similarly to the water resonance. This PRE effect on all the protons also reduces the discrepancy of the averaged R_1 from the water R_1. It should also be noted that the relaxation rate of intracellular proton was different from that of the extracellular proton relaxation by a factor of about 10 at the addition of 150 mM Gd-DOTA solution, which is much larger than the effect of CH/CH_2 on the measured R_1. Thus the intra- and extra-cellular spaces could be distinguished from the difference in the relaxation especially at such high Gd concentrations.

4.2 Interaction of Gd complexes with cells

The weak PRE effect in R_1 observed for the aqua Gd^{3+} titration ^{1}H-NMR experiments of the cellular system was probably due to the binding of Gd^{3+} to *E. coli* cellular components, especially at negatively charged lipids and macromolecules [95-96]. The PRE effect on the bulk water can be suppressed by sequestering Gd^{3+} from bulk exchangeable water molecules. The low R_1 values in the aqua Gd^{3+} titration were significant at the addition of Gd^{3+} solution with a concentration less than 150 mM (Figure 3.4c and 3.5). This Gd^{3+} titration experiment was characterized by a dissociation constant K_d of 1.0 mM and a total binding site concentration of 42 mM as shown in figure 4.1. In this analysis, the amount of the Gd-cell complex was obtained as a subtraction of the amount of Gd^{3+} in the extracellular solution from the total amount added to the sample. The Gd^{3+} ions should be transported to the periplasmic space through the outer-membrane porin channels. Under this assumption that Gd^{3+} bound to membranes in the periplasm and cell surface, the number of total binding sites computed from the titration experiments was converted to the membrane surface area per binding Gd^{3+} ion, about 0.4 nm^2, by using the number of the cells, the extracellular volume and cell surface area. This area 0.4 nm^2 is nearly equal to area per lipid molecule, 0.6 nm^2, [54, 109]. Only about a quarter of *E. coli* phospholipids are known to be anionic [110]. Thus Gd^{3+} ions would bind to not only head groups of anionic phospholipids [95-96] but also phosphates of neutral lipids and negatively charged biomolecules in the membranes and periplasm. This interaction mode of Gd^{3+} with *E. coli* cells is supported by the ^{13}C-NMR spectra (Figure 3.7) showing that the PRE effect of Gd^{3+} specifically reduced the intensity of the lipid methylene $^{13}CH_2$ resonance by about 80%.

Note that the cell sample aggregated after the addition of 149 or 250 mM aqua Gd solution leading to difficulty in the pipetting of the cells. Similar phenomena were not observed for the addition of Gd-DOTA. Such macroscopic difference of the cell precipitates may correlate with the electric charge state modified by Gd^{3+} binding to the cell surfaces.

The strong cytotoxicity of aqua Gd^{3+} as seen in the low CFU would be caused by its binding to phospholipids which disrupts the interaction of bilayer membranes with functional proteins by altering the electrostatic properties. Similarly, its bind to proteins should modify the protein-protein and protein-ligand interactions due to the electrostatic forces. Such alternation of biomolecular interactions should damage the cellular functions for the

metabolism and proliferation. This toxicity did not directly correlated with the cell lysis because the R_1 did not exhibit the increase of Gd^{3+} concentration in the intracellular part.

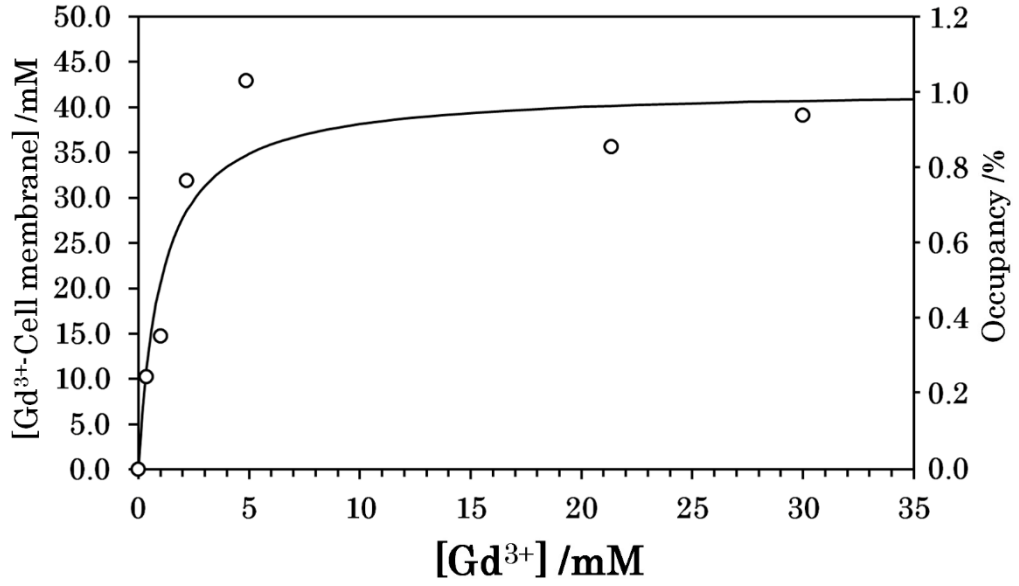

Figure 4.1: Concentration of Gd^{3+} binding with *E. coli* cells, [Gd^{3+}-Cell membrane], and the fractional occupancy of the cell Gd^{3+} binding site *Y* as a function of extracellular Gd^{3+} concentration [Gd^{3+}]. Experimental data were fitted to the equation [Gd^{3+}-Cell membrane] = *S* ([Gd^{3+}]/K_d)/(1+([Gd^{3+}]/K_d)) with the total binding site concentration *S* = [Gd^{3+}-Cell membrane]+[free cell membrane]. The percent of occupancy is [Gd^{3+}-Cell membrane]×100/*S*.

In contrast to aqua Gd, Gd-DOTA was stable in *E. coli* samples, and its Gd^{3+} ion did not strongly bind with cellular components. Thus, Gd-DOTA complex could keep its metal center accessible to water molecules. This stability led to enhancement of R_1 more efficiently than aqua Gd, even though the number of water molecule in the coordination sphere of Gd-DOTA complex was only one while that of aqua Gd complex was eight.

The toxicity of aqua Gd and Gd-DOTA was studied also by the other research groups. The toxicity of aqua Gd complex is well known [30]. In analogous to the experimental results, Fuma *et al*. found the population of *E. coli* DH5α cells in culture medium dropped suddenly when the cells were exposed to 3 mM aqua Gd solution [111]. Although Gd-DOTA is a stable complex for MRI study, this complex accumulates in the cells of an animal treated with this

agent. Taupitz *et al.* demonstrated that the Gd^{3+} ion of Gd-DOTA complex could be released under in vivo environment through transchelation process with glycosaminoglycan [33].

On the basis of data in this study, the stable Gd complex such as Gd-DOTA is a proper paramagnetic agent for NMR spectroscopy of living cells. A typical extracellular concentration of 40 mM in this study should be safe for *E. coli* because this concentration is close to the natural salt concentration in *E. coli* cells [102-103]. Although this concentration is more than one order higher than the safety clinical dose for an MRI contrast agent in human, more than 80% of the cell was alive for three hours under this condition. Since NMR experiment was completed within about one hour, cells were alive in the solution NMR experiments. It should be noted that the decreasing of extracellular relaxation rate of *E. coli* Gd-DOTA solution with time constant 41.7 days (Figure 4.2) is considerably slower than the death rate (Figure 3.8) of the cells with time constant 1.5 days. Thus, the inactive cells in terms of proliferation should have intact form in the membrane permeability to small molecules within a few days after the addition of Gd-DOTA.

4.3 The effect of water exchange across the cell membranes

The relaxation buildup curves were fitted to a double exponential function to obtain R_1 under the assumption that the water exchange between extracellular and intracellular parts was slower than the R_1. This model has been proved to be acceptable for explaining the phenomena for cellular water under the PRE effect [82-84]. Without Gd complexes, relaxation components with R_1 = 0.9 and 1.5 s^{-1} were obtained. Thus, the exchange rate should be 2 $s^{-1} \geq k_{ex}$ to distinguish the two components [82-84, 112]. This exchange rate is supported by a relaxographic study for the suspension of microorganism at 298 K which reported that the water exchange rate across the membrane of yeast was slow as 1.49 s^{-1} [113]. Taking account of the temperature-dependence of k_{ex} [114], k_{ex} of the sedimented *E. coli* suspension at 273 K was slower than 1.49 s^{-1}. Under the presence of Gd complexes, $R_1 >> 2\ s^{-1} \geq k_{ex}$, so that k_{ex} can be neglected especially at high Gd concentrations. This negligence is confirmed by the observation of two relaxation components different by a factor of 10 in R_1 as shown in Fig. 2 c and d. The Gd complex concentrations were computed from the PRE effect obtained by subtracting R_1 measured in the absence of Gd complexes from R_1 in the presence of Gd complexes. Thus effect of k_{ex} was suppressed in the calculation of the concentrations.

4.4 Penetration of Gd complexes into the cell

Stable and non-stable Gd complexes such as aqua Gd and Gd-DOTA complexes respectively are known to penetrate into eukaryotic cells in a similar amount [115-117]. This study also showed the permeability of *E. coli* cell membranes to those complexes. The aqua Gd and Gd-DOTA concentrations were about 1 and 4 mM respectively in the cells irrespective of the extracellular concentrations. The ratio of the extracellular to intracellular gadolinium complex concentrations increased with the extracellular concentration. Thus, the extracellular and intracellular water resonances could be distinguished clearly from the T_1 relaxation time.

4.5 Location-dependence of relaxation rate in solid-state NMR

According to the solid-state NMR of *E. coli*, the longitudinal relaxation rates of the protons appearing on the spectrum of gadolinium-free sample does not provide any locational information as there was no obvious distinction among these rates. The proton relaxation rates of all cellular components were averaged by fast spin diffusion due to strong proton-proton dipolar interactions in proton-rich environment in cells. In other word, the spin diffusion is generally a drawback in this condition which obstructs the utilizing of the relaxation rate for understanding molecular property such as molecular dynamics and structure. Nevertheless, the spin diffusion will be able to demonstrate the distribution or the location of macromolecule in the cell if the sample is discriminated into different parts due to their distinct local amplitude of magnetization. The contribution of molecular dynamics due to thermal energy on T_1 relaxation in each part could be suppressed by freezing samples at low temperature. Thus, PRE effect could be measured without consideration of Brownian motion. The exchange of nuclear spin between these parts through spin diffusion then causes the molecules localized in these discriminated parts to relax with different rates and give the information of the location of macromolecules in the cell.

The discrepancy between the intracellular and extracellular concentration of Gd-DOTA cause the variation in relaxation rate of protons throughout the cell sample. The PRE of paramagnetic ions in M9 medium such as $FeCl_3$ and $MnCl_2$ could be neglected because of their small amount in the level of μM. Therefore, these magnetic ions should not affect the relaxation rate of Gd-DOTA-free sample as well. The relaxation rates of all signals appearing on ss-NMR spectrum of this sample were similar regardless the location of protons in the cell.

The proton relaxation rate is location dependent in the sample containing the Gd-DOTA complex. The difference between the intracellular and extracellular concentration Gd-DOTA is enough to generate the location-dependency of the relaxation rate. The two relaxation rates analyzed for ss-NMR experimental results agreed well with the theoretically predicted values. The correspondence between the experimental and predicted relaxation rates revealed the protons in the sample containing Gd-DOTA relaxed under rapid spin diffusion regime as expected [78, 81].

The relaxation behavior of macromolecules occupying near the cell membrane gained strong effect from fast-relaxing magnetization diffusing from outside the cell. Hence, the protons of phospholipids at 35.1 and 17.0 ppm relaxed distinctively faster than the other macromolecules. On the other hand, RNA and DNA which occupying deeply in the cell far from extracellular Gd-DOTA complex insignificantly experienced PRE effect and their protons at 93 ppm in ^{13}C-NMR relaxed with the slowest rate. The buildup curve constructed from relaxation rates analyzed from ROSY spectra (Figure 3.15) emphasized the fastest and slowest proton relaxation behaviors for lipid and nucleotide respectively. The other macromolecules such as protein and sugar which were distributed throughout the cell showed their buildup curves between the curve of nucleotide and lipid.

In an attempt to demonstrate quantitatively the locational dependence of the proton relaxation, the mathematical model of the spin diffusion across the cell membrane was built using the intracellular and extracellular relaxation rates obtained from experimental ssNMR results. The model shows the variety of the buildup curves of molecules placed at x of -20 to 20 nm where x is in the interface between the extracellular and intracellular parts. On condition that the interface is at the center of inner cell membrane (Figure 4.2). The buildup curves computed from this model are in good agreement with all experimental relaxation curves (Figure 4.3). For instance, the thickness of both lipid bilayers, lipopolysaccharide, periplasm, layer and cell radius were given at 8, 7, 10 and 400 nm respectively [71, 73, 118-119]. The ratio of lipid on the inner to outer cell membrane was 13:7 estimated from data reported elsewhere [71]. The buildup curve of lipids was then constructed by averaging the buildup curves of lipids in the inner membrane and outer membrane using this ratio as weighing factor. The model reveals the good correspondence between the experimental results and the curves computed from this model (Figure 4.3). Therefore, the interface between the extracellular and intracellular parts is reasonable at the center of inner membrane layer. This suggests that Gd-DOTA complex could pass through the outer cell membrane and enter to periplasmic space but

the inner cell membrane block its internalization into cytoplasm. Gd-DOTA complex could pass into periplasm through porin pores, 7-10 Å pores on the outer cell membrane. These pores generally nonspecifically allow small hydrophobic molecule to permeate into the cell [35-38]. As the size of Gd-DOTA complex is smaller than this pore, this complex could pass into the periplasmic space through porin pores. Similarly, Gd-DOTA complex also possibly pass through a pore on peptidoglycan which has lower molecular selectivity and is larger than the porin pore in size [120-121]. In contrast, protein channels on inner membrane protein has selectivity and allows only some specific chemical to pass [36]. Thus, these channels limited the number of Gd-DOTA complex passing into cytoplasm and caused only the peptidoglycan layer, the inner leaflet of the inner membrane and the outer membranes to soak in the Gd-DOTA solution. The difference of Gd-DOTA concentration and the propagation of magnetization across the interface via spin diffusion lead macromolecules locating within a distance of 20 nm from the interface to relax with different rate as revealed by the buildup curve computed from the above mathematic model. In other word, the model under the condition that interface is at center of inner cell membrane could be utilized for analyzing the specific location of the molecule locating at x of -20 to 20 nm. The resolution of this technique is higher than 20 nm (Figure 3.17 and figure 4.2) which is better than the resolution of cell image recorded by the other techniques. X-ray spectroscopy and fluorescence spectroscopy provide lower cell image of 50-100 nm [122] and 250-600 nm [123] respectively. Although FRET spectroscopy and Cyro-EM also could provide high-resolution image (1-10 nm [124] and 0.3-0.4 nm [125] respectively), there is a difficulty in applying these techniques to small macromolecules [8-10] or unfolded proteins [11] while ssNMR could provide the signals for these macromolecules [8-11]. Thus ssNMR approach could be developed further to be a technique for determining site specificity of macromolecule on the cell wall. This promising strategy requires an advance technique to express labeled macromolecules of interest specifically on the cell membrane or introduce the labeled molecules into the cells.

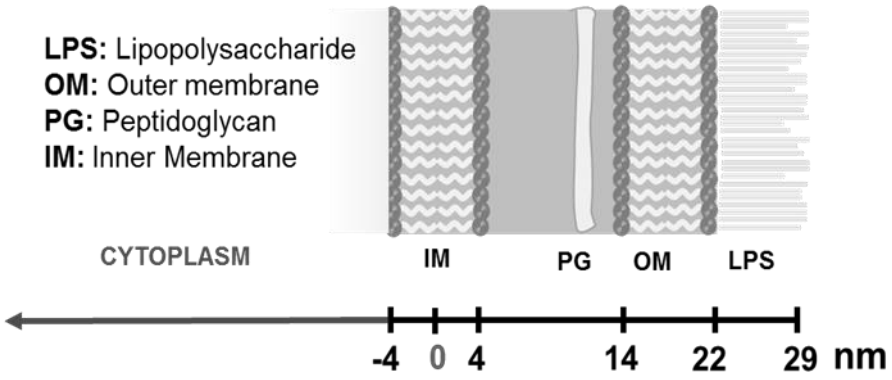

Figure 4.2: Illustration showing the *x* coordinate of the mathematical model of spin diffusion in *E. coli* sample which give the simulated relaxation curves correspond to the experimental results. The location of cellular component was arranged according to the statistical data reported [19].

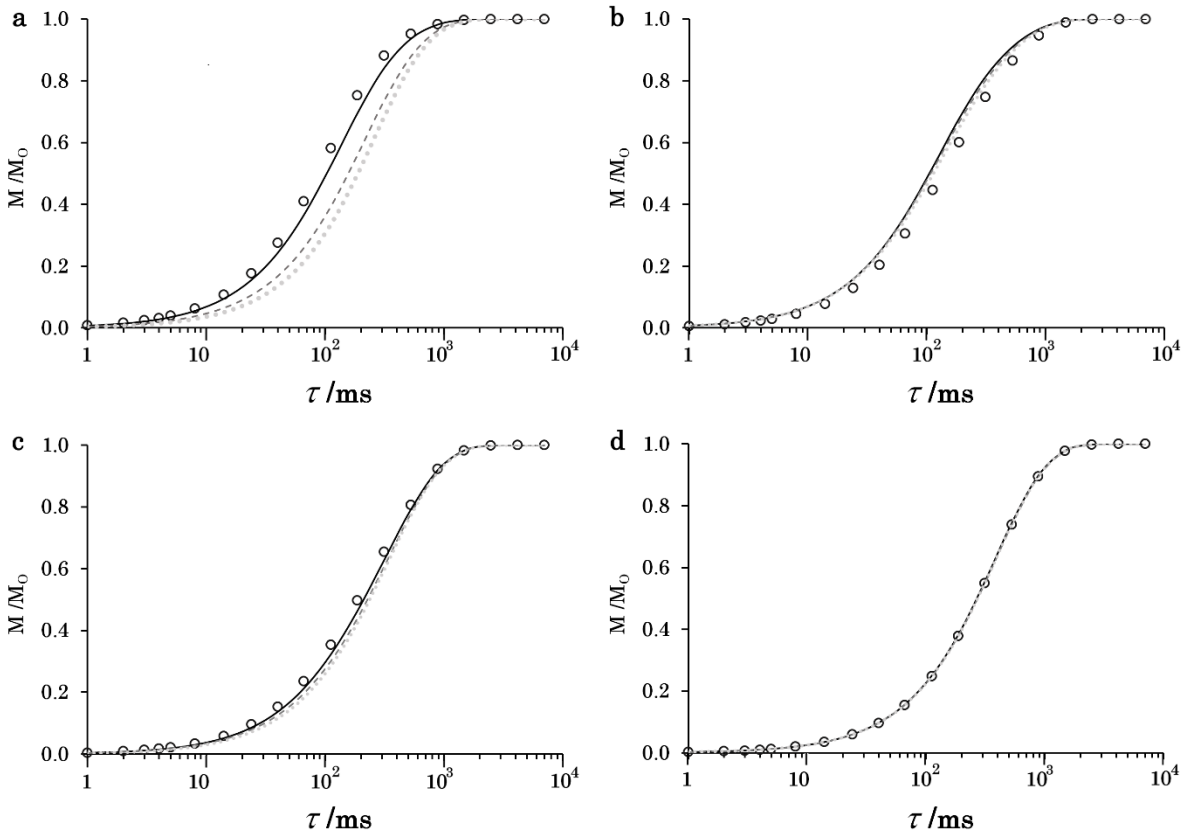

Figure 4.3: Proton relaxation curves of lipid (a), sugar (b), protein (c) and nucleotide (d) simulated from data in figure 3.13 (open circle) comparing with the relaxation curve calculated from spin diffusion models which are calculated for the interface between fast and slow-relaxing region at inner membrane (line), peptidoglycan layer (dash) and outer membrane (dot)

Chapter 5

Conclusion

Gadolinium complexes enhanced the longitudinal relaxation rate R_1 of extracellular water protons selectively owing to the low permeability of cell membranes to the agents and the low water exchange rate across the membranes. The R_1 of the extracellular part was more than ten times faster than the intracellular R_1, which allowed the discrimination between extra- and intra-cellular parts. The PRE effect in solid-state ^{13}C-NMR indicated that aqua Gd bound to lipid membranes stronger than Gd-DOTA. This binding with a dissociation constant of 1 mM should be the cause for the cytotoxicity of aqua Gd stronger than that of Gd-DOTA. As the results, Gd-DOTA was more suitable than aqua Gd as an R_1 contrast agent in cellular NMR spectroscopy: Gd-DOTA had lower cytotoxicity even at higher concentrations around 30 mM, exhibited the intense PRE effect through the exchange between ligand and bulk water molecules, and stayed in the solution phase for a period longer than four days.

The analysis of solid-state NMR results based on the spin diffusion model explained that the penetration of Gd-DOTA complex into the cell cytoplasm is limited probably by protein channels on the inner cell membrane. The sample was frozen at low temperatures to make use of slow thermal R_1 relaxation and rapid proton spin diffusion under reduced motional state. Thus the R_1 does not depend on biomolecular motion but on the concentration of unpaired electron spins. The difference in Gd-DOTA concentration across the inner cell membrane caused the different proton polarization amplitudes in the two parts during the relaxation

process from the completely saturated state. The spin diffusion allowed fast relaxing proton polarization in the extracellular part to propagate into the cell cytoplasm which led to locational dependence of relaxation rate of cellular macromolecule. This location-dependence of relaxation rate is useful for determining the specific site of macromolecule inside the cell. By using this location dependence, solid-state ^{13}C-NMR spectroscopy succeeded in providing the *E. coli* cellular site information semiquantitatively for biological macromolecules which were detected under high-resolution, magic-angle spinning condition. Thus this methodology enables solid-state NMR spectroscopy to study cellular structure as well as biomolecular structure. In combination with biomolecule specific isotope labeling technology, the biomolecular structure functioning in cells can be studied at atomic resolution by multidimensional solid-state NMR.

References

[1] Marion, D. An Introduction to Biological NMR Spectroscopy. *Mol Cell Proteomics*. **2013**, 12 (11): 3006–3025.

[2] Saunders, M.; Wishnia, A.; Kirkwood, J. G. The nuclear magnetic resonance spectrum of ribonuclease. *J. Am. Chem. Soc*. **1957**, 79: 3289–3290.

[3] Mittermaier, A. K.; Kay, L. E. Observing biological dynamics at atomic resolution using NMR. *Trends Biochem Sci*. **2009**, 34(12):601-11.

[4] Pellecchia, M.; Bertini, I.; Cowburn, D.; Dalvit, C.; Giralt, E.; Jahnke, W.; James, T. L.; Homans, S. W.; Kessler, H.; Luchinat, C.; Meyer, B.; Oschkinat, H.; Peng, J.; Schwalbe, H.; Siegal, G. Perspectives on NMR in drug discovery: a technique comes of age. *Nat Rev Drug Discov*. **2008**, 7(9):738-45.

[5] Geist, L.; Mayer, M.; Cockcroft, X.; Wolkerstorfer, B.; Kessler, D.; Engelhardt, H.; McConnell, D. B.; Konrat, R. Direct NMR Probing of Hydration Shells of Protein Ligand Interfaces and Its Application to Drug Design. *J. Med. Chem.* 2017, 60(21): 8708–8715.

[6] Fenwick, R. B.; Bedem, H. V. D.; Fraser, J. S.; Wright, P. E. Integrated description of protein dynamics from room-temperature X-ray crystallography and NMR. *Proc. Natl. Acad. Sci. USA.* 2014, 111(4): E445-E454.

[7] Weisenburger, S.; Boening, D.; Schomburg, B.; Giller, K.; Becker, S.; Griesinger, C.; Sandoghdar, V. Cryogenic optical localization provides 3D protein structure data with Angstrom resolution. *Nature Methods* 2017, 14: 141–144.

[8] Cheng, Y. Single-particle cryo-EM—How did it get here and where will it go. *Science*. 2018, 361(6405): 876-880.

[9] Murata, K.; Wolf, M. Cryo-electron microscopy for structural analysis of dynamic biological macromolecules. *Biochim. Biophys. Acta, Gen. Subj.* 2018, 1862(2): 324-334.

[10] Shoemaker, S. C.; Ando, N. X-rays in the Cryo-EM Era: Structural Biology's Dynamic Future. *Biochemistry*. 2018, 57(3): 277–285.

[11] Aznauryan, M.; Delgado, L.; Soranno, A.; Nettels, D.; Huang, J. R.; Labhardt, A. M.; Grzesiek, S.; Schuler, B. Comprehensive structural and dynamical view of an unfolded protein from the combination of single-molecule FRET, NMR, and SAXS. *Proc. Natl. Acad. Sci. USA.* 2016, 113(37): E5389-98.

[12] Levitt, M. H. *Spin Dynamics: Basics of Nuclear Magnetic Resonance*, 2nd ed., John Wiley &. Sons, Chichester, UK, 2008.

[13] Keeler, J. *Understanding NMR Spectroscopy*, 2nd ed., John Wiley &. Sons, Cambridge, UK, 2010.

[14] Lux, J.; Sherry, A. D. Advances in gadolinium-based MRI contrast agent designs for monitoring biological processes in vivo. *Curr. Opin. Chem. Biol.* 2018, 45: 121-130.

[15] Kim, H.; Lee, G. H.; Chang, Y. Gadolinium as an MRI contrast agent. *Future Med. Chem.* 2018, 10(6):639-661.

[16] Bertini, I.; Luchinat. C.; Parigi, G.; Ravera, E.; *NMR of Paramagnetic Molecules, Applications to Metallobiomolecules and Models*, 2nd ed., Elsevier, Amsterdam, **2017**.

[17] Pell, A.J.; Pintacuda, G.; Grey, C.P. Paramagnetic NMR in solution and the solid state. *Prog. Nucl. Magn. Reson. Spectrosc.* **2018**, In Press.

[18] Koehler, J.; Meiler, J. Expanding the utility of NMR restraints with paramagnetic compounds:Background and practical aspects. *Prog. Nucl. Magn. Reson. Spectrosc.* **2011**, 59:360–389.

[19] Guan, Y. J.; Keizers, P. H. J.; Liu, W. M.; Löhr, F.; Skinner, S. P.; Heeneman, E. A.; Schwalbe, H.; Ubbink, M.; Siegal, G. Small-molecule binding sites on proteins established by paramagnetic NMR spectroscopy. *J. Am. Chem. Soc.* **2013**, 135:5859–5868.

[20] Maltsev, S.; Hudson, S. M.; Sahu, I. D.; Liu, L.; Lorigan, G. A. Solid-state NMR ^{31}P paramagnetic relaxation enhancement membrane protein immersion depth measurements. *J. Phys. Chem. B.* **2014**,118:4370–4377.

[21] Su, Y.; Mani, R.; Hong, M. Asymmetric insertion of membrane proteins in lipid bilayers by solid-state NMR paramagnetic relaxation enhancement: a cell-penetrating Peptide example. *J. Am. Chem. Soc.* **2008**,130:8856–8864.

[22] Respondek, M.; Madl, T.; Göbl, C.; Golser, R.; Zangger, K. Mapping the orientation of helices in micelle-bound peptides by paramagnetic relaxation waves. *J. Am. Chem. Soc.* **2007**, 129:5228–5234.

[23] Luchinat, C.; Parigi, G.; Ravera, E.; Rinaldelli, M. Solid-state NMR crystallography through paramagnetic restraints. *J. Am. Chem. Soc.* **2012**, 134:5006–5009.

[24] Pintacuda, G.; John, M.;Su, X.; Otting, G. NMR Structure Determination of Protein−Ligand Complexes by Lanthanide Labeling *Acc. Chem. Res.* **2007**, 40, 206–212.

[25] Crichton, R.R. Biological Inorganic Chemistry: A New Introduction to Molecular Structure and Function, 2nd ed.; Elsevier: Oxford, **2012**.

[26] Lee, J.; Nyenhuis, D. A.; Nelson, E. A.; Cafiso, D. S.; White, J. M.; Tamm, L. K. Structure of the Ebola virus envelope protein MPER/TM domain and its interaction with the fusion loop explains their fusion activity. *PNAS* **2017,** 114 (38), E7987-E7996.

[27] Park, S. H.; Wang, V. S.; Radoicic, J.; Angelis, A. A. D.; Berkamp, S.; Opella, S. J. Paramagnetic relaxation enhancement of membrane proteins by incorporation of the metal-chelating unnatural amino acid 2-amino-3-(8-hydroxyquinolin-3-yl)propanoic acid (HQA) *J. Biomol. NMR* **2015**, 61(3–4), 185–196.

[28] Gong, Z.; Gu, X.; Guo, D.; Wang, J.; Tang, C. Protein Structural Ensembles Visualized by Solvent Paramagnetic Relaxation Enhancement *Angew. Chem. Int. Ed.* **2017**, 56 (4), 1002-1006.

[29] Ullrich, S. J.; Hölper, S.; Glaubitz, C. Paramagnetic doping of a 7TM membrane protein in lipid bilayers by Gd^{3+}-complexes for solid-state NMR spectroscopy *J. Biomol. NMR* **2014**, 58(1), 27–35.

[30] Sherry, A.D.; Caravan,P.; Lenkinski, R.E. Primer on gadolinium chemistry *J. Magn. Reson. Imaging*. **2009**, 30(6), 1240–1248.

[31] Caravan, P. Strategies for increasing the sensitivity of gadolinium based MRI contrast agents. *Chem. Soc. Rev.* **2006**, 35:512–523.

[32] Benmelouka, M.; Borel, A.; Moriggi, L.; Helm, L.; Merbach, A.E. Design of Gd(III)-Based Magnetic Resonance Imaging Contrast Agents: Static and Transient Zero-Field Splitting Contributions to the Electronic Relaxation and Their Impact on Relaxivity *J. Phys. Chem. B.* **2007**, 111, 832–840.

[33] Ishiguchi, T.; Takahashi, S. Safety of gadoterate meglumine (Gd-DOTA) as a contrast agent for magnetic resonance imaging: results of a post-marketing surveillance study in Japan. *Drugs in R&D*. **2010**,10:133–45.

[34] Serber, Z.; Keatinge-Clay, A. T.; Ledwidge, R.; Kelly, A. E.; Miller, S. M.; Dötsch, V. High-resolution macromolecular NMR spectroscopy inside living cells. *J. Am. Chem. Soc.* **2001**, 123(10):2446-2447.

[35] Sakai, T.; Tochio, H.; Tenno, T.; Ito, Y.; Kokubo, T.; Hiroaki, H.; Shirakawa, M. In-cell NMR spectroscopy of proteins inside *Xenopus laevis* oocytes. *J Biomol NMR.* **2006**, 36(3):179-188.

[36] Selenko, P.; Serber, Z.; Gadea, B.; Ruderman, J.; Wagner, G. Quantitative NMR analysis of the protein G B1 domain in *Xenopus laevis* egg extracts and intact oocytes. *Proc Natl Acad Sci USA*. **2006**, 103(32):11904-11909.

[37] Inomata, K.; Ohno, A.; Tochio, H.; Isogai, S.; Tenno, T.; Nakase, I.; Takeuchi, T.; Futaki, S.; Ito, Y.; Hiroaki, H.; Shirakawa, M. High-resolution multi-dimensional NMR spectroscopy of proteins in human cells. *Nature*. **2009**, 458(7234):106-109.

[38] Ogino, S.; Kubo, S.; Umemoto, R.; Huang, S.; Nishida, N.; Shimada, I. Observation of NMR signals from proteins introduced into living mammalian cells by reversible membrane permeabilization using a pore-forming toxin, streptolysin O. *J Am Chem Soc*. **2009**, 131(31):10834-10835.

[39] Binolfi, A.; Limatola, A.; Verzini, S.; Kosten, J.; Theillet, F. X.; Rose, H. M.; Bekei, B.; Stuiver, M.; van Rossum, M.; Selenko, P. Intracellular repair of oxidation-damaged α-synuclein fails to target C-terminal modification sites. *Nat Commun.* **2016**, 7:10251-10261.

[40] Theillet, F.X.; Binolfi, A.; Bekei, B.; Martorana, A.; Rose, H.M.; Stuiver, M.; Verzini, S.; Lorenz, D.; van Rossum, M.; Goldfarb, D.; Selenko, P. Structural disorder of monomeric α-synuclein persists in mammalian cells. *Nature*. **2016**, 530(7588):45-50.

[41] Aricescu, A. R.; Lu, W.; Jones, E. Y. A time- and cost-efficient system for high-level protein production in mammalian cells. *Acta Crystallogr D Biol Crystallogr*. **2006**, 62:1243-1250.

[42] Seiradake, E.; Zhao, Y.; Lu, W.; Aricescu, A. R.; Jones, E. Y. Production of cell surface and secreted glycoproteins in mammalian cells. *Methods Mol Biol*. **2015**, 1261:115-127.

[43] Banci, L.; Barbieri, L.; Bertini, I.; Luchinat, E.; Secci, E.; Zhao, Y.; Aricescu, A. R. Atomic-resolution monitoring of protein maturation in live human cells by NMR. *Nat Chem Biol.* **2013**, 9(5):297-299.

[44] Barbieri, L.; Luchinat, E.; Banci, L. Characterization of proteins by in-cell NMR spectroscopy in cultured mammalian cells. *Nat Protoc.* **2016**, 11(6):1101-1111.

[45] Reckel, S.; Lopez, J.J.; Löhr, F.; Glaubitz, C.; Dötsch, V. In-cell solid-state NMR as a tool to study proteins in large complexes. *Chembiochem*. **2012**, 13(4):534-537.

[46] Renault, M.; Pawsey, S.; Bos, M. P.; Koers, E. J.; Nand, D.; Tommassen-van, B. R.; Rosay, M.; Tommassen, J.; Maas, W. E.; Baldus, M. Solid-state NMR spectroscopy on cellular preparations enhanced by dynamic nuclear polarization. *Angew Chem Int Ed Engl.* **2012**, 51(12):2998-3001.

[47] Yamamoto, K.; Caporini, M. A.; Im, S. C.; Waskell, L.; Ramamoorthy, A. Cellular solid-state NMR investigation of a membrane protein using dynamic nuclear polarization. *Biochim Biophys Acta*. **2015**, 1848:342-349.

[48] Viennet, T.; Viegas, A.; Kuepper, A.; Arens, S.; Gelev, V.; Petrov, O.; Grossmann, T. N.; Heise, H.; Etzkorn, M. Selective Protein Hyperpolarization in Cell Lysates Using Targeted Dynamic Nuclear Polarization. *Angew Chem Int Ed Engl.* **2016**, 55(36):10746-50.

[49] Luchinat, E.; Banci, L. In-cell NMR: a topical review. *IUCrJ*. **2017**,4: 108–118.

[50] Rahmana, S.; Byun, Y.; Hassan, M. I.; Kim, J.; Kumar, V. Towards understanding cellular structure biology: In-cell NMR. *Biochim. Biophys. Acta, Proteins Proteomics* **2017**, 1865(5): 547-557.

[51] von Heijne, G. Membrane-protein topology. *Nat Rev Mol Cell Biol.* **2006**, 7(12):909-918.

[52] Fries, P.H.; Ferrante, G.; Belorizky, E.; Rast, S. The rotational motion and electronic relaxation of the Gd(III) aqua complex in water revisited through a full proton relaxivity study of a probe solute. *J. Chem. Phys.* **2003**, 119: 8636–8644.

[53] Sakakibara, D.; Sasaki, A.; Ikeya, T.; Hamatsu, J.; Hanashima, T.; Mishima, M.; Yoshimasu, M.; Hayashi, N.; Mikawa, T.; Wälchli, M.; Smith, B. O.; Shirakawa, M.; Güntert, P.; Ito, Y. Protein structure determination in living cells by in-cell NMR spectroscopy. *Nature* **2009**, 458:102-105.

[54] Phillips, R.; Kondev, J.; Theriot, J.; Garcia, H. *Physical Biology of the Cell*, 2nd Ed., Garland Science, New York, **2012**.

[55] Iwahara, J.; Tang, C.; Clore, M. G. Practical aspects of ^{1}H transverse paramagnetic relaxation enhancement measurements on macromolecules. *J. Magn. Reson.* **2007**, 184:185–195.

[56] Yazyev, O. V.; Helm, L.; Malkin, V.G.; Malkina, O. L. Quantum chemical investigation of hyperfine coupling constants on first coordination sphere water molecule of gadolinium(III) aqua complexes. *J. Phys. Chem. A.* **2005**,109:10997–11005.

[57] Luz, Z.; Meiboom, S. Proton relaxation in dilute solutions of cobalt(II) and nickel(II) ions in methanol and the rate of methanol exchange of the solvation sphere. *J. Chem. Phys.* **1964**, 40:2686–2692.

[58] Yazyev, O. V.; Helm, L.; Malkin, V. G.; Malkina, O. L. Quantum chemical investigation of hyperfine coupling constants on first coordination sphere water molecule of gadolinium(III) aqua complexes. *J. Phys. Chem. A.* **2005**, 109:10997–11005.

[59] Luz, Z.; Meiboom, S. Proton relaxation in dilute solutions of cobalt(II) and nickel(II) ions in methanol and the rate of methanol exchange of the solvation sphere. *J. Chem. Phys.* **1964**, 40:2686–2692.

[60] Swift, T.J.; Connick, R. E. NMR-relaxation mechanisms of ^{17}O in aqueous solutions of paramagnetic cations and the lifetime of water molecules in the first coordination sphere. *J. Chem. Phys.* **1962**, 37:307–320

[61] Benmelouka, M.; Borel, A.; Moriggi, L.; Helm, L.; Merbach, A. E. Design of Gd(III)-based magnetic resonance imaging contrast agents: static and transient zero-field splitting contributions to the electronic relaxation and their impact on relaxivity. *J. Phys. Chem. B* **2007**, 111:832–840.

[62] Banci, L.; Bertini, I.; Luchinat, C. ^{1}H NMRD studies of solutions of paramagnetic metal ions in ethyleneglycol. *Inorganica Chemica Acta*. **1985**, 100:173–181.

[63] Powell, D. H.; Gonzfilez, G.; Tissières, V.; Micskei, K.; Brücher, E.; Helm, L.; Merbach, A. E. Gd^{3+} chelates of interest in magnetic resonance imaging (MRI): studies

using ^{17}O NMR and EPR at several magnetic fields. *J. Alloys Compd.* **1994**, 207/208:20–24.

[64] Micskei, K.; Powell, D. H.; Helm, L.; Brücher, E.; Merbach, A. E. Water Exchange on $[Gd(H_2O)_8]^{3+}$ and [Gd(PDTA)(H_2O)] in Aqueous Solution : A variable-pressure, -temperature and -magnetic field ^{17}O NMR Study. *Magn. Reson. Chem.* **1993**, 31:1011–1020.

[65] Taupitz, M.; Stolzenburg, N.; Ebert, M.; Schnorr, J.; Hauptmann, R.; Kratz, H.; Hamm, B.; Wagner, S. Gadolinium-containing magnetic resonance contrast media: investigation on the possible. *Contrast Media Mol. Imaging.* **2013**, 8: 108–16.

[66] Jeong, H.; Barbe, V.; Lee, C. H.; Vallenet, D.; Yu, D. S.; Choi, S.; Couloux, A.; Lee, S.; Yoon, S. H.; Cattolico, L.; Hur, C.; Park, H.; Ségurens, B.; Kim, S. C.; Oh, T. K.; Lenski, R. E.; Studier, F. W.; Daegelen, P.; Kim, J. F. Genome sequences of *Escherichia coli* B strains REL606 and BL21(DE3). *J. Mol. Biol.* **2009**, 394, 644–652.

[67] Nishiyama, Y.; Frey, M. H.; Mukasa, S.; Utsumi, H. ^{13}C Solid-state NMR chromatography by magic angle spinning ^{1}H T_1 relaxation ordered spectroscopy. *J.Magn. Reson.* **2010**, 202, 135–139.

[68] Szeverenyi, N. M., Sullivan, M. J.; Maciel, G. E. Observation of spin exchange by two-dimensional fourier transform ^{13}C cross polarization-magic-angle spinning. *J. Magn. Reson.* **1982**, 47, 462-475.

[69] Wang, T.; Williams, J. K.; Schmidt-Rohr, K.; Hong, M. Relaxation-compensated difference spin diffusion NMR for detecting 13C-13C long-range correlations in proteins and polysaccharides. *J. Biomol. NMR* **2015**, 61, 97-107.

[70] Kern, T.; Hediger, S.; Müller, P.; Giustini, C.; Joris, B.; Bougault, C.; Vollmer, W.; Simorre, J. Toward the Characterization of Peptidoglycan Structure and Protein−Peptidoglycan Interactions by Solid-State NMR Spectroscopy. *J. Am. Chem. Soc.* **2008**, 130 (17), 5618 – 5619.

[71] Sundararaj, S.; Guo, A; Habibi-Nazhad, B.; Rouani, M.; Stothard, P.; Ellison, M.; Wishart, D. S. The CyberCell Database (CCDB): a comprehensive, self‐updating,

relational database to coordinate and facilitate in silico modeling of *Escherichia coli*. *Nucleic Acids Res.* **2004**, 32, D293 - D295.

[72] Phillips, R.; Kondev, J.; Theriot, J. *Physical Biology of the Cell*; Garland Science: New York, **2009**.

[73] Ingraham, J. L.; Maaloe, O.; Neidhaedt, F. C. Growth of the Bacteria Cell. *Sinauer Associates*, Sunderland, Massachusetts, **1983**.

[74] Bennett, B. D.; Kimball, E. H.; Gao, M.; Osterhout, R.; Van Dien, S. J.; Rabinowitz, J. D. Absolute metabolite concentrations and implied enzyme active site occupancy in *Escherichia coli*.*Nat. Chem. Biol.* **2009**, *5*, 593–599.

[75] Neidhardt, F. C. *Escherichia coli and Salmonella: Cellular and Molecular Biology,* 2nd ed.; AMS Press: Washington, **2005**; vol. 1.

[76] Lowe, I. J. ; Tse, D. Nuclear Spin-Lattice Relaxation via Paramagnetic Centers. *Phys. Rev.* **1968**, 166, 279-291.

[77] Phua, T.-T.; Beaudry, B. J.; Peterson, D. T.; Torgeson, D. R. Paramagnetic impurity effects in NMR determinations of hydrogen diffusion and electronic structure in metal hydrides. Gd^{3+} in YH_2 and $LaH_{2.25}$ *Phys. Rev. B* **1983**, 28(11), 6227-6249.

[78] Blumberg, W. E. Nuclear Spin-Lattice Relaxation Caused by Paramagnetic Impurities. *Phys. Rev.* **1960**, 119, 79- 84

[79] Sandratskii, L. M.; Kübler, J. Local Magnetic Moments of Conduction Electrons in Gadolinium. *Europhys. Lett.* 1993, 23(9), 661-666.

[80] Cai, W. Z.; Schmidth-Rohr, K.; Egger, N.; Gerharz, B.; Spiess, H. W. A solid-state n.m.r. study of microphase structure and segmental dynamics of poly(styrene-b-methylphenylsiloxane) diblock copolymers. *Polymer* **1993**, 267-276.

[81] Cheung, T. T. P. Spin Diffusion in Solids. *Encyclopedia of NMR* **2012**, 8, 4676–4682.

[82] Hazlewood, C. F.; Chang, D. C.; Nichols, B. L.; Woessner, D. E. Nuclear magnetic resonance transverse relaxation times of water protons in skeletal muscle. *Biophys. J.* **1974**;14(8):583–606.

[83] Donahue, K. M.; Weisskoff, R. M.; Chesler, D. A.; Kwong, K.K.; Bogdanov, A. A.; Mandeville, J. B.; Rosen, B. R. Improving MR quantification of regional blood volume with intravascular T_1 contrast agents: Accuracy, precision, and water exchange. *Magn. Reson. Med.* **1996**;36(6):858–867.

[84] Fick, A. On liquid diffusion. *Phil. Mag.* **1855**, 10 (4), 30 - 39.

[85] Hindman, J. C.; Svirmickas, A.; Wood, M. Relaxation processes in water. A study of the proton spin-lattice relaxation time. *J. Chem. Phys.* **1973**, 59:1517–1522.

[86] Morokuma, K.; Winick, J. R. Molecular orbital studies of hydrogen bonds: dimeric H_2O with the slater minimal basis set. *J. Chem. Phys.* **1970**, 52:1301–1306.

[87] Fogel'son, R. L.; Likhachev, E. R. Temperature dependence of viscosity. *Tech. Phys.* **2001**, 46:1056–1059.

[88] Baldwin, W. W.; Myer, R.; Powell, N.; Anderson, E.; Koch, A. L. Buoyant density of *Escherichia coli* is determined solely by the osmolarity of the culture medium. *Arch Microbiol*. **1995**, 164:155-157.

[89] Doerrler, W. T. Density Gradient enrichment of Escherichia coli conditional msbA mutants. *Appl Environ Microbiol.* **2007**, 73:7992–7996.

[90] Vishnevskaya, G. P.; Frolova, E. N.; Gataullin, A. M.; Gumerov, F. M.; Fakhrutdinov, A. R. Structural transformations and phase transitions in aqueous solutions of gadolinium nitrate in the course of freezing. *Phys. Solid State.* **2003**, 45:1322–1326.

[91] Koenig, S. H.; Epstein, M. Ambiguities in the interpretation of proton magnetic relaxation data in water solutions of Gd^{3+} ions. *J. Chem. Phys.* **1975**, 63:92279–2284.

[92] Tei, L.; Baranyai, Z.; Gaino, L.; Forgács, A.; Vágner, A.; Botta, M. Thermodynamic stability, kinetic inertness and relaxometric properties of monoamide derivatives of lanthanide(III) DOTA complexes. *Dalton Trans*. **2015**, 44:5467–78.

[93] Persson, E.; Halle, B. Cell water dynamics on multiple time scales. *Proc Natl Acad Sci*. **2008**;105:6266–6271.

[94] Qvist, J.; *a* is the distance between adjacent nuclei, μ_p is the magnetic moment of paramagnetic electron and μ_n is the magnetic moment of nuclei, E.; Mattea, C.; Halle, B. Time scales of water dynamics at biological interfaces: peptides, proteins and cells. *Faraday Discuss*. **2009**;141:131–144.

[95] van Dalen, A.; de Kruijff, B. The role of lipids in membrane insertion and translocation of bacterial proteins. *Biochim. Biophys. Acta.* **2004**,1694:97–109.

[96] Silhavy, T. J.; Kahne, D.; Walker, S. The bacterial cell envelope. *Cold Spring Harbor Perspect. Biol.* **2010**, 2:a000414.

[97] Nadaud, P. S. .; Helmus, J. J.; Kall, S. L.; Jaroniec, C. P. Paramagnetic ions enable tuning of nuclear relaxation rates and provide long-range structural restraints in solid-state NMR of proteins. *J. Am. Chem. Soc*. **2009**, 131:8108–8120.

[98] Sanders, C. R. Solid state ^{13}C NMR of unlabeled phosphatidylcholine bilayers: spectral assignments and measurement of carbon-phosphorus dipolar couplings and ^{13}C chemical shift anisotropies. *Biophys. J*. **1993**, 64:171–81.

[99] Laage, S.; Tao, Y.; McDermott, A. E. Cardiolipin interaction with subunit c of ATP synthase: solid-state NMR characterization. *Biochim Biophys Acta.* **2015**, 1848:260–265.

[100] Boettcher, J. M.; Davis-Harrison, R. L.; Clay, M. C.; Nieuwkoop, A. J.; Ohkubo, Y. Z.; Tajkhorshid, E.; Morrissey, J. H.; Rienstra, C. M. Atomic view of calcium-induced clustering of phosphatidylserine in mixed lipid bilayers. *Biochemistry.* **2011**, 50:2264–2273.

[101] Bryant, J. E.; Lecomte, J. T. J.; Lee, A. L.; Young, G. B.; Pielak, G. J. Protein dynamics in living cells. *Biochemistry*. **2005**, 44:9275–9279.

[102] Jucker, B. A.; Harms, H.; Zehnder, A. J. B. Adhesion of the positively charged bacterium Stenotrophomonas (Xanthomonas) maltophilia 70401 to glass and teflon. *J. Bacteriol.* **1996**, 178:5472–5479.

[103] Otto, K.; Elwing, H.; Hermansson, M. Effect of ionic strength on initial interactions of *Escherichia coli* with surfaces, studied on-line by a novel quartz crystal microbalance technique. *J. Bacteriol.* **1999**, 181:5210-5218.

[104] Marchanka, A.; Carlomagno, T. Rapid access to RNA resonances by proton-detected solid-state NMR at >100 kHz MAS. *eMagRes* **2014**, 3, 119–128.

[105] Schmidt-Rohr, K.; Spiess. H. *Multidimensional Solid-State NMR and Polymers*, 1st Ed., Academic Press, London, **1996**.

[106] Walker, J.; Halliday, D. *Fundamentals of physics*. 9th Ed., John Wiley & Sons, USA, **2011**.

[107] Cai, W. Z.; Schmidth-Rohr, K.; Egger, N.; Gerharz, B.; Spiess, H. W. A solid-state n.m.r. study of microphase structure and segmental dynamics of poly(styrene-b-methylphenylsiloxane) diblock copolymers. *Polymer* **1993**, 267-276.

[108] Jeong, H.; Barbe, V.; Lee, C. H.; Vallenet, D.; Yu, D. S.; Choi, S.; Couloux, A.; Lee, S.; Yoon, S. H.; Cattolico, L.; Hur, C.; Park, H.; Ségurens, B.; Kim, S. C.; Oh, T. K.; Lenski, R. E.; Studier, F. W.; Daegelen, P.; Kim, J. F. Genome sequences of *Escherichia coli* B strains REL606 and BL21(DE3). *J. Mol. Biol.* **2009**, 394, 644–652.

[109] Nagle, J. F.; Tristram-Nagle, S. Lipid bilayer structure. *Curr. Opin. Struct. Biol*. **2000**, 10,474–480.

[110] Sahoo, B.; Maruyama, K.; Edula, J.; Tougan, T.; Lin, Y.; Lee, Y. H.; Horii, T.; Fujiwara, T. Mechanistic and structural basis of bioengineered bovine Cathelicidin-5 with optimized therapeutic activity. *Scientific Reports*. **2017**, 7,44781.

[111] Fuma, S.; Takeda, H.; Miyamoto, K.; Yanagisawa, K.; Inoue, Y.; Ishii, N.; Sugai, K.; Ishii, C.; Kawabata, Z. Ecological evaluation of gadolinium toxicity compared with

other heavy metals using an aquatic microcosm. *Bull. Environ. Contam. Toxicol*. **2001**, 66:231–238.

[112] Donahue, K. M.; Weisskoff, R. M.; Burstein, D. Water diffusion and exchange as they influence contrast enhancement. *J. Magn. Reson. Imaging.* **1997**, 7:102-110.

[113] Labadie, C.; Lee, J. H.; Vétek, G.; Springer, C. S.; Relaxographic Imaging. *J. Magn. Reson. Ser. B* **1994**, 105:99-112.

[114] Åslund, I.; Nowacka, I. A.; Nilsson, M.; Topgaard, D.; Hürlimann, M. D.; Song, Y. Q.; Fantazzini, P.; Bortolotti, V. Molecular exchange between intra- and extracellular compartments in a cell suspension. *AIP Conference Proceedings.* **2008**, 79–82.

[115] Cabella, C.; Crich, S. G.; Corpillo, D.; Barge, A.; Ghirelli, C.; Bruno, E.; Lorusso, V.; Uggeri, F.; Aime, S. Cellular labeling with Gd(III) chelates: only high thermodynamic stabilities prevent the cells acting as "sponges" of Gd^{3+} ions. *Contrast Media & Molecular Imaging*. **2006**, 1:23–29.

[116] Crich, S. G.; Biancone, L.; Cantaluppi, V.; Duò, D.; Esposito, G.; Russo, S.; Camussi, G.; Aime, S. Improved route for the visualization of stem cells labeled with a Gd-/Eu-chelate as dual (MRI and fluorescence) agent. *Magn. Reson. Med.* **2004**, 51(5):938–944.

[117] Modo, M.; Mellodew, K.; Cash, D.; Fraser, S. E.; Meade, T. J.; Price, J.; Williams, SC. Mapping transplanted stem cell migration after a stroke: a serial, in vivo magnetic resonance imaging study. *NeuroImage*. **2004**, 21:311–317.

[118] Vuu, K.; Xie, J.; Mcdonald, M. A.; Bernardo, M.; Hunter, F.; Zhang, Y.; Li, K.; Bednarski, M.; Guccione, S. Gadolinium-Rhodamine Nanoparticles for Cell Labeling and Tracking via Magnetic Resonance and Optical Imaging. *Bioconjug. Chem.* **2005**, 16:995–999.Frederick C. Neidhardt *Escherichia coli and Salmonella typhimurium: Cellular and Molecular Biology Vol. 1.*; 2nd ed.; ASM Press: Washington, 1996; p. 51.

[119] Goodsell, D. S. Escherichia coli. *Biochem. Mol. Biol. Educ.***2009**, 37(6), 325 – 332.

[120] Nakae, T.; Nikaido, H. Outer membrane as a diffusion barrier in Salmonella typhimurium. Penetration of oligo- and polysaccharides into isolated outer membrane vesicles and cells with degraded peptidoglycan layer. *J. Biol. Chem.* **1975**, 250, 7359 – 7365.

[121] Dijkstra, A. J.; Keck, W. Peptidoglycan as a barrier to transenvelope transport. *J. Bacteriol.* **1996**, 178(19), 5555 – 5562.

[122] Fogelqvist, E.; Kördel, M.; Carannante, V.; Önfelt, B.; Hertz, H. M. Laboratory cryo x-ray microscopy for 3D cell imaging. *Scientific Reports* **2017**, 7: 13233-13241.

[123] Cho, S.; Jang, J.; Song, C.; Lee, H. ; Ganesan, P.; Yoon, T.; Kim, M. W.; Choi, M. C.; Ihee, H.; Heo, W. D.; Park, Y. K. Simple super-resolution live-cell imaging based on diffusion-assisted Förster resonance energy transfer. *Scientific Reports* **2013**, 3: 1208-1215.

[124] Leavesley, S. J.; Rich, T. C. Overcoming Limitations of FRET Measurements. *Part A Cytometry*. **2016**, 89A: 325-327.

[125] Irobalieva, R. N.; Martins, B.; Medalia, O. Cellular structural biology as revealed by cryo-electron tomography. *J. Cell. Sci.* **2016**, 129: 469-476

Appendix

A.1 Statistical data of *E. coli*

This study used the statistical data of *E. coli* [71-73] to simulate NMR spectrum of *E. coli* sample and analyze experimental results.

A.1.1 General properties of *E. coli*

Diameter	8×10^{-7}	m
Length	2×10^{-6}	m
Aqueous volume	7×10^{-16}	m^2
Total volume	1×10^{-15}	l
Surface area	6×10^{-12}	kg
Wet weight	1×10^{-15}	kg
Dry weight	3.0×10^{-16}	l
Volume of cytoplasm	6.7×10^{-16}	l
Volume of periplasm	6.5×10^{-17}	l
Volume of envelope	1.6×10^{-16}	l
Volume of Nuclear (Protein and DNA)	1.6×10^{-16}	l
Thickness of inner membrane	8×10^{-9}	m
Thickness of periplasm	1×10^{-8}	m
Thickness of outer membrane	$8 - 15 \times 10^{-9}$	m
Percent of protein per cell mass	16.5	%
Percent of DNA per cell mass	0.93	%
Percent of RNA per cell mass	6.12	%
Percent of water per cell mass	70.0	%

Percent of lipopolysaccharide per cell mass	1.02	%
Percent of lipid per cell mass	2.73	%
Percent of peptidoglycan per cell mass	0.75	%
Percent of glycogen per cell mass	0.75	%
Percent of ions per cell mass	0.30	%
Percent of small metabolites per cell mass	0.87	%

A.1.2 Amounts of macromolecules in *E. Coli*

Membranes	2	unit
Cell walls	1	unit
Fraction of protein in lipid bilayer	60	%
Fraction of lipid in lipid bilayer	40	%
rRNA	18,000	molecules
mRNA	4,000	molecules
tRNA	200,000	molecules
All RNA	222,000	molecules
Murein	240,000-700,000	molecules
Polysaccharides	39,000	molecules
All lipids	25,000,000	molecules
Lipopolysaccharide	600,000	molecules
Phosphatidyl glycerol	5,000,000	molecules
Phosphatidylethanolamine	18,500,000	molecules
Cardiolipin	1,200,000	molecules
LPS (10kD)	600,000	molecules
Phosphatidylserine	500,000	molecules
Porins in outer membrane	60,000	molecules
Outer membrane proteins	300,000	molecules
Lipoproteins in outer membrane	240,000	molecules
Nuclear proteins	100,000	molecules
Inner membrane proteins	200,000	molecules
Cytoplasmic proteins (exclude riboproteins)	1,000,000	molecules
Ribosomal proteins	900,000	molecules
Periplasmic proteins	80,000	molecules

All intracellular proteins	2,600,000	molecules
All proteins	3,600,000	molecules
External proteins (flag or pili)	1,000,000	molecules

A.1.3 Amounts of small molecules and ions in *E. Coli*

Small organic molecule	40-50	mM
Water molecules	23.4×10^{10}	molecules
Sodium ion	5	mM
Potassium ion	200-250	mM
Free calcium ion	100	nM
All calcium ion	6	mM
Chlorine ion	6	mM
Iron ions	18	mM
Magnesium ions	10	mM
Zinc ions	4	mM
Manganese ions	4	mM
Copper ions	4	mM
Molybdenum ions	4	mM
Glucose	0.5-1	mM
Phosphate ion	5	mM
PEP	2.8	mM
Gluc-6-Pi	0.05	mM
Pyruvate	0.9	mM
ADP	0.17	mM
ATP	1.3-7.0	mM
NADPH	0.56	mM
NADP	0.63	mM
All amino acids	1.5	mM
Free Aspartate	1.34	mM
Free Alanine	0.8	mM
Free Glutamate	0.5	mM
Free Cysteine	0.2	mM
Free Glycine	0.8	mM

Free Histidine	0.2	mM
Free Phenylalanine	0.4	mM
Free Isoleucine	0.5	mM
Free Leucine	0.7	mM
Free Lysine	0.46	mM
Free Asparagine	0.5	mM
Free Methionine	0.1	mM
Free Glutamine	0.5	mM
Free Proline	0.5	mM
Free Serine	0.7	mM
Free Arginine	0.4	mM
Free Threonine	3.49	mM
Free Tryptophan	0.2	mM
Free Valine	0.6	mM
Free Tyrosine	0.7	mM

A.1.4 Amounts of small amino acids required for producing protein in 1 g of dried cell

Alanine	488	μmol
Asparagine	229	μmol
Arginine	281	μmol
Aspartic acid	229	μmol
Glutamic acid	250	μmol
Cysteine	87	μmol
Glutamine	250	μmol
Histidine	90	μmol
Glycine	582	μmol
Isoleucine	276	μmol
Lysine	326	μmol
Leucine	428	μmo
Phenylalanine	176	μmol
Methionine	146	μmol

Proline	210	µmol
Threonine	241	µmol
Serine	205	µmol
Tyrosine	131	µmol
Tryptophan	54	µmol
Valine	402	µmol

A.2 Fortran code for analyzing paramagnetic relaxation in model *E. coli* systems under proton spin diffusion

```
      PROGRAM SpinDiffusion
      REAL D, Pi
      REAL L_ex,L_in,res
      Real x(10000),center
      REAL xsquare(10000),G(10000,10000),SD(10000,10000)
      REAL M(10000),Mx(10000),Mi(10000),Mintf(10000)
      REAL Mo_ex,Mo_in,Mo_intf,T_ex,T_in,T_interf
      REAL time, Tstep,t
      REAL dMx, dMi, dMintf, dx, dt
      INTEGER Nx,I,J,K,L, Nt
      INTEGER endIN,Interf,begEX
C     ------------------------------------------------------------------------
C      1. Declaration of Constants
C     ------------------------------------------------------------------------
      PARAMETER (PI=3.14159265)
C     ------------------------------------------------------------------------
C      2. Input Data
C     ------------------------------------------------------------------------
      OPEN(1,FILE='input.in')
      read(1,*)D                              ! Diffusivity
      read(1,*)dx                             !(dx)nm
      read(1,*)Mo_ex
      read(1,*)Mo_in
      read(1,*)L_ex                            ! nm
```

```
      read(1,*)L_in                                  ! nm
      read(1,*)T_ex                                  ! ms
      read(1,*)T_in                                  ! ms
      read(1,*)time                                  ! ms
      read(1,*)dt                                    ! (dt)ms
      CLOSE(1)
C     ------------------------------------------------------------------------
C      3. Precalculation
C     ------------------------------------------------------------------------
C
      Nx=(((2*L_ex)+(2*L_in))/dx)+1
      Nt=time/dt
C
      Interf = ((2*L_in)/dx)+1          !Tnterface between intracellular and extracelular domain
      endIN=Interf-1                  ! Ending point of intracellular domain
      begEX=Interf+1                   ! beginning point of extracellular domain
C
      DO 100 I=1,Nx,1
        M(I)=0.00
 100   CONTINUE
C
      T_intf= ((Mo_ex+Mo_in)*T_ex*T_in)/((Mo_ex*T_in)+(Mo_in*T_ex))
C
      Mo_intf = 1.00
C
      center=-(2*L_in)
```

```
      x(1)=center
C
      DO 200 I=2,Nx,1
        x(I)= x(I-1)+dx
 200   CONTINUE
C
      FourD = 4.00*D
      FourDPi=4.00*D*PI
      Time=time/dt
C     ------------------------------------------------------------------------
C       4. Spin Diffusion
C     ------------------------------------------------------------------------
C
      OPEN(1,FILE='output.dat',STATUS='REPLACE',ACTION='WRITE')
      write(1,*) '     '
      write(1,'(a,F20.2,a)') 'Diffusivity (D):             ',D,' nm^2.m
     &s^-1'
      write(1,'(a,F20.2,a)') 'Total time :                 ',time,
     & ' ms'
      write(1,'(a,F20.2,a)') 'Time step(dt) :              ',dt,' ms
     & '
      write(1,'(a,F20.2,a)') 'Resolution(dx) :             ',dx,' nm'
      write(1,'(a,F20.2,a)') 'Extracellular magnetization :',Mo_ex
      write(1,'(a,F20.2,a)') 'Intracellular magnetization :',Mo_in
      write(1,'(a,F20.2,a)') 'Extracellular depth :        ',L_ex,' nm'
      write(1,'(a,F20.2,a)') 'Intracellular depth :        ',L_in,' nm'
```

```
      write(1,'(a,F20.2,a)') 'Extracellular T1 :           ',T_ex,' ms'
      write(1,'(a,F20.2,a)') 'Intracellular T1 :           ',T_in,' ms'
      write(1,*) '     '
      write(1,'(a20,5000F20.2)')'t(ms)/x(nm)',(x(I),I=1,Nx)
CC
      t=1.00
      DO 300 I=1,Nt,1
C
C Intracellular
      DO 400 K=1,endIN,1
        DO 410 J=1,Nx,1
          IF(D.EQ.0.00)THEN
            IF(J.EQ.K)THEN
              G(K,J)=M(K)+((Mo_in-M(K))/T_in)
            ELSE
              G(K,J)=0.00
            ENDIF
          ELSE
            xsquare(J)= (x(J)-center-(dx*(K-1)))**2
            G(K,J)= (exp((-(xsquare(J)))/(FourD*dt)))
            G(K,J)= G(K,J)/(sqrt(FourDPi*dt))
            G(K,J)= G(K,J)*(M(K)+((Mo_in-M(K))/T_in))
          ENDIF
 410      CONTINUE
 400   CONTINUE
C
```

```
C interface
C
      DO 500  J=1,Nx,1
        IF(D.EQ.0.00)THEN
          IF(J.EQ.Interf)THEN
            G(Interf,J)=M(Interf)+((Mo_INTF-M(Interf))/T_intf)
          ELSE
            G(Interf,J)=0.00
          ENDIF
        ELSE
          xsquare(J)= (x(J)-center-(dx*(Interf-1)))**2
          G(Interf,J)= (exp((-(xsquare(J)))/(FourD*dt)))
          G(Interf,J)=G(Interf,J)/(sqrt(FourDPi*dt))
          G(Interf,J)=G(Interf,J)*(M(Interf)+((Mo_in-M(Interf))/T_int
     & f))
        ENDIF
 500   CONTINUE
C
C Extracellular part
C
      DO 600 K=begEX,Nx,1
        DO 610 J=1,Nx,1
          IF(D.EQ.0.00)THEN
            IF(J.EQ.K)THEN
              G(K,J)=M(K)+((Mo_ex-M(K))/T_ex)
            ELSE
```

```
            G(K,J)=0.00
          ENDIF
        ELSE
          xsquare(J)= (x(J)-center-(dx*(K-1)))**2
          G(K,J)= (exp((-(xsquare(J)))/(FourD*dt)))
          G(K,J)= G(K,J)/(sqrt(FourDPi*dt))
          G(K,J)= G(K,J)*(M(K)+((Mo_ex-M(K))/T_ex))
        ENDIF
610     CONTINUE
600   CONTINUE
C
      DO 700 J=1,Nx,1
        M(J)=0.00
          DO 710 K=1,Nx,1
            M(J)=M(J)+G(K,J)
710         CONTINUE
700   CONTINUE
C
      write(1,'(1F20.8,5000E20.8)')t,(M(J),J=1,Nx)
      t=t+dt
300   CONTINUE
C
      CLOSE(1,STATUS='KEEP')
C
      write(*,*) 'FINISHED!!!!!'
      write(*,*) 'The result is in output.dat'
```

```
C
      STOP
      END
```